

POLITECNICO DI TORINO

Master's Degree in Civil Engineering



Master's Degree Thesis

**Tailings Dam Collapse and Propagation Modelling: A Study Case
in Brazil**

Supervisors

Prof. Claudio Scavia

Prof. Marina Pirulli

Dr. Alessandro Leonardi

Candidate

Larissa Santoro Dias Macedo

November 2020

Abstract

Tailings Dams are structures constructed to store the waste of mining activities. Nonetheless, its collapse is a recurring phenomenon, due to the lack of control and monitoring of the material deposition and the stability conditions of the reservoir. In this context, the Brumadinho tailings dam failure occurred in January of 2019, in Brazil, causing around 270 casualties, destroying residential and administrative buildings, native vegetation, agricultural fields; and polluting water resources. The damage extent of the phenomenon can be back-calculated from numerical analyses, using rheology laws, which can describe the behavior of the flowing material. In this thesis, it was employed the Voellmy and Bingham methodologies for modeling the runout, and they are expressed as a function of some intrinsic parameters, such as the basal friction angle and the turbulence coefficient, for the former, and the yield stress and plastic viscosity, for the latter. It is important to perform a calibration of these values such that the real phenomenon is accurately reproduced. However, if a predictive analysis is performed to analyze the potential of failure, known values of similar events could be used and adapted to the case under study. Using this methodology, it is possible to reproduce the path followed by the flow, the velocity profile, and the flow depth; and to analyze who and what was affected by the runout. More importantly, even if this study was a post-failure analysis, the techniques discussed here can be used in a monitoring study to evaluate the hazard posed by the rupture of tailings dam and the consequences it would cause.

Keywords: Tailings dam, static liquefaction, numerical modeling, rheology, runout.

Acknowledgments

Firstly, I would like to express my gratitude to my parents who made it possible for me to study abroad, at Politecnico di Torino, and who always supported me in my decisions and my willingness to explore the world outside my home.

Then, I wish to thank my friends in Turin, from the group “Prod em Turim”, who have been my family during this period in Italy, and especially to Karina, for being my best friend outside and inside the Politecnico classrooms, the person who always supported me and gave me strength when everything seemed too hard.

Additionally, I would like to thank Dr. Alessandro Leonardi, Andrea Pasqua, and Giulia La Porta, who gave me the necessary support and knowledge to do the work presented here.

I wish to thank also the University of Campinas, which provided the required material used in the analyses presented in this thesis.

Table of Contents

1.	Introduction to Tailings Dams and Discussion about the Collapse of Brumadinho	1
1.1	Tailings Dams: Construction, operation, and water influence	1
1.2	Córrego do Feijão Mine: Characterization of the tailings dam	6
1.3	The collapse of the Brumadinho tailings dam: Possible Causes and Consequences	10
2.	Methodology.....	21
2.1	Triggering Analysis and the Limit Equilibrium Method	21
2.2	Analytical and Numerical Modeling of Runout and the RASH 3D.....	23
I.	Landslide Flows: Definitions and Classification	23
II.	Numerical Models for the Runout Analysis.....	27
III.	Rheological Laws to describe the behavior of the flow	31
3.	Classification of the Tailings Flow of Brumadinho Dam Collapse.....	35
3.1	Takahashi Classification (2014).....	35
3.2	Varnes (1978) and Cruden and Varnes (1976) Classifications	36
3.3	Hungr Classification (2001).....	37
4.	Analysis of the Runout with RASH 3D.....	42
I.	Determination of Height: Method I – Volume and Area Analysis	43
II.	Determination of Height: Method II – Slip Surface Analysis.....	44
4.1	Results and Discussion.....	52
I.	Voellmy Rheology: Method I – Volume and Area analysis.....	53
II.	Voellmy Results: Method II – Slip Surface Analysis	58
III.	Bingham Rheology: Method I – Volume and Area analysis.....	61
IV.	Bingham Rheology: Method II – Slip Surface Analysis	66
V.	Summary of the Results and Further Analyses	68
5.	Conclusions	79
6.	Bibliography.....	81

List of Figures

Figure 1 - Hydraulic separation through hydrocyclones (Fleurisson & Cojean, 2016).....	1
Figure 2 - Spigotting technique (Adapted from Thomé & Passini, 2018).....	2
Figure 3 - Hydraulic segregation techniques (Thomé & Passini, 2018).....	2
Figure 4 - Upstream Heightening dam (Fleurisson & Cojean, 2016).....	2
Figure 5 - Liquefaction and the loss of adhesion among the particles due to the excessive water pore-pressure (adapted from Araujo & Ledezma, 2020).	3
Figure 6 - Water control in tailing dams (Rodríguez Pacheco, 2019).	4
Figure 7 - a) Piping, b) Overtopping (Rodríguez Pacheco, 2019).	6
Figure 8 – Position of the Córrego do Feijão Mine and the Dam I (Google Earth, 2018).	6
Figure 9 - Cross-section of Dam I (Schnaid et al., 2013).	7
Figure 10 - Tailings Disposal System (adapted from Silva, 2010).....	8
Figure 11 - Internal drainage system (adapted from ANA - Agência Nacional das Águas, 2016).	8
Figure 12 - Deep Horizontal Drain (<i>Dreno Horizontal Profundo - Drilling</i> , n.d.).....	9
Figure 13 - Damage extension of dam breaching (Google Earth, 2019).	10
Figure 14 - Satellite monitoring of the dam movement and real-time result from the ground-based radar interferometry (<i>CPI: Rompimento da Barragem de Brumadinho</i> , 2019).	12
Figure 15 - Satellite images showing superficial water in the reservoir, in June of 2017 and 2018, respectively (D. M. Pereira et al., 2019).	12
Figure 16 - Satellite image showing the rupture crest in March of 2019 (adapted from Google Earth, 2019).....	12
Figure 17 - TVDI distribution on January 14, 2019 (Lan et al., 2019).....	13
Figure 18 - TVDI distribution on January 30, 2019 (Lan et al., 2019).....	14
Figure 19 - Aerial images of the analysis of water influence, in July 2011(<i>BRUMADINHO ENGINEERING HISTORY – World Mine Tailings Failures - from 1915</i> , n.d.).	14
Figure 20 - Aerial images of the analysis of water influence, in July 2018 (<i>BRUMADINHO ENGINEERING HISTORY – World Mine Tailings Failures - from 1915</i> , n.d.).	15
Figure 21 – The most critical cross-section of the dam, according to the LEM analysis (Vale & TUV SUD, 2018).	15
Figure 22 - Analysis of stability by LEM under undrained conditions (Vale & TUV SUD, 2018).	17
Figure 23 - The land cover of the area covered by the Tailings (adapted from L. F. Pereira et al., 2019).	18
Figure 24 - Highlighted the region of the Lower Paraobeba, where the tailings were concentrated one year after the event, and where the tailings reached the river (adapted from D. M. Pereira et al., 2019).....	19
Figure 25 - Vertical slices scheme with the acting forces (Zhu, 2008).	21
Figure 26 - Textural composition of the material in different types of flows.....	25
Figure 27 - Modelling of a flow as a homogeneous apparent fluid, with velocity profile dependent on the chosen rheology (Hungr, 1995).	29
Figure 28 - Blocks representing the fluid and the forces acting on each block.	30
Figure 29 - Curve representing the Bingham model (adapted from Leonardi, 2015).	34
Figure 30 - Common rheologies for fluids.	34
Figure 31 - Travel distance of the tailing flow in Brumadinho.	35

Figure 32 - Slope map of the area that covers the runout.	38
Figure 33 - Textural composition of the runout.	39
Figure 34 - Final Classification of the runout in Brumadinho.	40
Figure 35 - Digital Elevation Model of the terrain and the contour of the damage extent.	42
Figure 36 - Part of the DEM converted into points.	42
Figure 37 - Scheme of the coordinates and height h of the flow (adapted from Kritikos & Davies, 2015).	43
Figure 38 - a. Area of the detachment obtained using Google Earth; b. points in the detachment are for which the value of height was assigned.	44
Figure 39 - Model for LEM analysis on Slide.	45
Figure 40 - Model for LEM analysis on Slide in detail.	45
Figure 41 - Slip surfaces obtained from the Slide analysis.	47
Figure 42- a),b),c) Images of the moment of the collapse, highlighting the first rupture areas in the slope, d) Indication of the place of rupture in the bottom of the dam (Youtube, 2019).	48
Figure 43 - Indication of the place of rupture at the bottom of the dam in the model.	48
Figure 44 - Verification of possible rupture crests.	49
Figure 45 - Primary and secondary instabilities of tailings dam (adapted from Lumbroso et al., 2020).	49
Figure 46 - Images of the moment of failure of Brumadinho dam (Youtube, 2019).	50
Figure 47 - Vertical Slices from LEM analysis.	50
Figure 48 - Detachment area derived from the slices of Slide analysis.	51
Figure 49 - Real flow after the collapse (Youtube, 2019).	54
Figure 50 - Results of Voellmy Calibration (method I).	55
Figure 51 - Results of simulation with Voellmy Rheology (method I), $\phi = 0.4^\circ$ and $\xi = 2000$ m/s ²	56
Figure 52 - Position of the flow at t:2500s for Voellmy simulation (method I) (Google Earth, 2019).	57
Figure 53 - Map of velocities with Voellmy Rheology (method I), $\phi = 0.4^\circ$ and $\xi = 2000$ m/s ² , t=12000s.	58
Figure 54 - Results of Voellmy calibration (method II).	59
Figure 55 - Results of simulation with Voellmy Rheology (method II), $\phi = 0.4^\circ$ and $\xi = 2000$ m/s ²	60
Figure 56 - Map of velocities with Voellmy Rheology (method II), $\phi = 0.18^\circ$ and $\xi = 2000$ m/s ² , t=12000s.	61
Figure 57 - Results of simulation with Bingham Rheology (method I), $\tau_y=50$ Pa and $\mu_0=250$ Pas.	64
Figure 58 - Map of velocities with Bingham Rheology (method I), $\tau_y=50$ Pa and $\mu_0=250$ Pas, t=12000s.	66
Figure 59 - Results of simulation with Bingham Rheology (method II), $\tau_y=50$ Pa and $\mu_0=250$ Pas.	67
Figure 60 - Map of velocities with Bingham Rheology (method II), $\tau_y=50$ Pa and $\mu_0=250$ Pas, t=12000s.	68
Figure 61 - Comparison between the different simulations in terms of shape and maximum height (m), 1- Voellmy (method I), 2 – Voellmy (method II), 3 – Bingham (method I), 4 – Bingham (method II).	69

Figure 62 - Comparison between the different simulations in terms of velocity (m/s), 1- Voellmy (method I), 2 – Voellmy (method II), 3 – Bingham (method I), 4 – Bingham (method II).	70
Figure 63 - Voellmy branches.....	71
Figure 64 - Analysis of Voellmy branch I.	71
Figure 65 – Analysis of Voellmy branch II.	72
Figure 66 - Representation of the points below the threshold for Voellmy simulation.....	72
Figure 67 - Analysis of Voellmy extra points.....	72
Figure 68 - Bingham overflow.....	73
Figure 69 - Analysis of Bingham overflow.	73
Figure 70 - Comparison between Voellmy and Bingham flows in 3D, for the first method...	74
Figure 71 - Comparison between Voellmy and Bingham velocities, for the first method.	74
Figure 72 - 3D representation of the runout I.	75
Figure 73 - 3D representation of the runout II.	75
Figure 74 - 3D representation of the runout III.....	75
Figure 75 - Final shape of Voellmy (method I) simulation plotted on Google Earth.....	76
Figure 76 - Final shape of Bingham (method I) simulation plotted on Google Earth.	76
Figure 77 - Final shape of Voellmy (method II) simulation plotted on Google Earth.	77
Figure 78 - Final shape of Bingham (method II) simulation plotted on Google Earth.....	77
Figure 79 - Comparison between the detachment area and the Voellmy simulations.....	78

List of Tables

Table 1 - Characterisation of the Land cover in the area covered by the tailings (based on L. F. Pereira et al., 2019).....	18
Table 2 – Classification of the mass movements according to their magnitude and mobility (Takahashi, 2014)	23
Table 3 - Varnes classification (1978) (Hungr et al., 2001)	24
Table 4 - Cruden and Varnes Classification (1996) (Hungr et al., 2001).....	24
Table 5 - Hungr classification of landslides of the flow type (Hungr et al., 2001)	26
Table 6 - Takahashi's Classification of the Brumadinho runout.....	36
Table 7 - Varnes, and Cruden and Varnes Classifications of the Brumadinho runout.....	37
Table 8 - Hungr Classification of the Brumadinho runout	39
Table 9 - Material properties for undrained conditions (adapted from Vale & TUV SUD, 2018).	46
Table 10 - Results from Slide analysis.	47
Table 11 – Representative values of Bingham model (adapted from Pastor et al., 2004).....	63

List of Acronyms

TVDI – Temperature Vegetation Dryness Index

CPTU – Piezocone Penetration Test

DAN – Dynamic Analysis

LEM – Limit Equilibrium Method

1. Introduction to Tailings Dams and Discussion about the Collapse of Brumadinho

1.1 Tailings Dams: Construction, operation, and water influence

Tailings are formed by the waste of the ore's mechanical and chemical processing to extract the desired economic product from the mine resource. Their components are commonly mixed into a slurry, which is carried by pipes (Fleurisson & Cojean, 2016), until disposal in settling ponds, with the material retained by impoundments. However, before launching it in the settling ponds, the water present in the material can be recovered and used in the mining process, decreasing the demand for hydric resources and the susceptibility to accidents due to liquefaction (Thomé & Passini, 2018).

The hydraulic separation can be done using hydrocyclones, which also enables the division of the tailings into fine and coarse particles (more commonly sand). The excess water and the coarse particles are launched downstream and the fine material with remaining water is launched upstream the dyke (Figure 1) (Thomé & Passini, 2018).

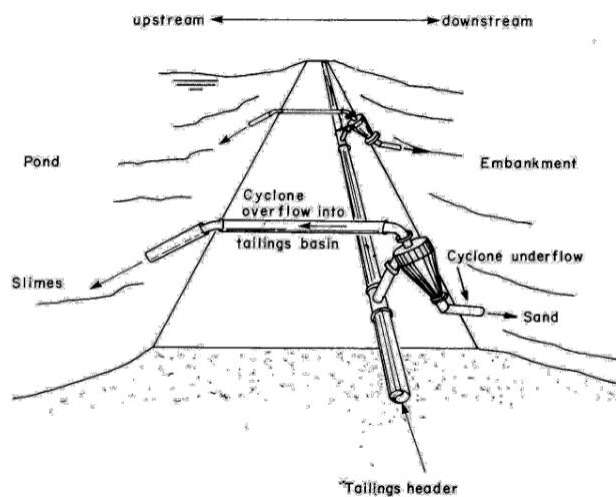


Figure 1 - Hydraulic separation through hydrocyclones (Fleurisson & Cojean, 2016).

Another technique is the spigotting, where all the material is disposed upstream the dyke (Figure 2). Due to different settling velocities, the coarse particles accumulate near the discharge points, forming beaches that work as a retention shell (Martin, 2002), meanwhile, the fines are carried by the water flow and deposit on the ponds (Thomé & Passini, 2018).

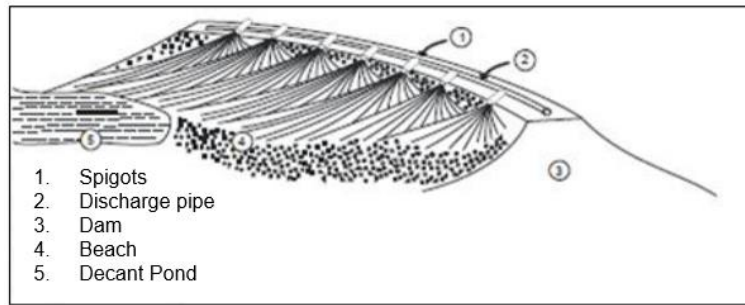


Figure 2 - Spigotting technique (Adapted from Thomé & Passini, 2018).

The last method to be mentioned is the one where the disposal is done with spray-bars, and in this technique, the main goal is to reduce the pressure of the tailings launch, and, consequently, to decrease the dragging of the particles and to improve the hydraulic separation. For this aim, tubes with holes along its extension are positioned longitudinally on the beach to capture the tailings released from the main pipe and redistribute it (Thomé & Passini, 2018). The three methods discussed above are illustrated in Figure 3.

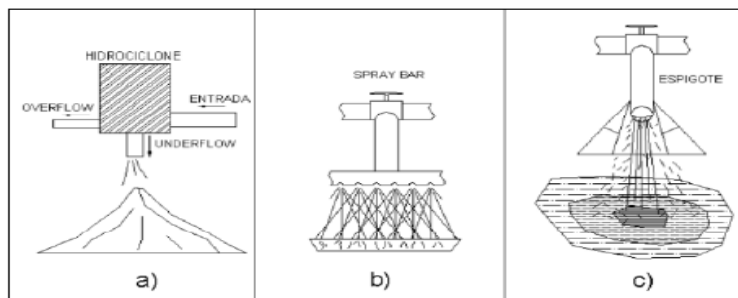


Figure 3 - Hydraulic segregation techniques (Thomé & Passini, 2018).

Initially, only the starter dyke is constructed, and when the need for more volume capacity takes place, the so-called heightening dykes are built (Figure 4). Different procedures can be used for this process, according to the shift of the axis of the dam. Among them, there is the upstream method that consists of the construction of the new dykes over the beaches formed in the decantation after discharge, moving the crest of the dam upstream (Thomé & Passini, 2018).

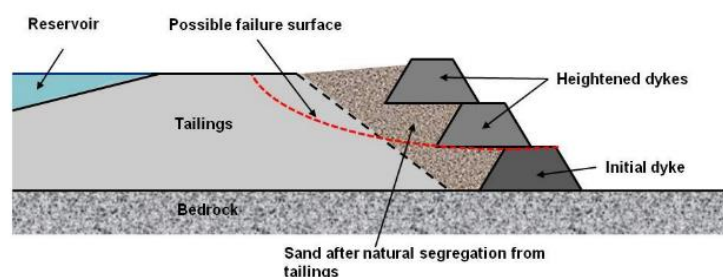


Figure 4 - Upstream Heightening dam (Fleurisson & Cojean, 2016).

In this way, the dam is built using as a foundation the tailings that settled on the beach, so the volume of material in the construction is reduced, which decreases the cost and increases the procedure velocity. Due to these conditions, this is one of the most used techniques for heightening, even though the resultant safety is lower since the sediments on the beach are not compacted. This condition may originate differential settlements and hydraulic segregation (associated with the granulometric distribution and water flow), and, consequently, the formation of liquefaction regions (Lima Bevilaqua, 2019). Besides that, the higher the final height of the impoundment, the more the potential sliding surface is placed in the fine elements of the pond, significantly decreasing the safety factor (Fleurisson & Cojean, 2016).

The dams constructed with the upstream method have a greater probability of failing, given poor maintenance, errors in the design, and/or structural failure. Among several possible causes of failure, the most common is due to static liquefaction, in which the material starts to behave as a liquid, due to an applied stress (Kossoff et al., 2014). This stress causes a compression force in the grains of tailings, reducing the volume of voids (Lima Bevilaqua, 2019), thereby the material must be contractive. In contractive conditions, there is a reduction of the pore volume due to the outflow of water that fills up the void spaces of granular material (Rodríguez Pacheco, 2019).

Due to the low permeability of tailings and at undrained conditions, the water is not able to percolate, so this compressive stress is also transmitted to the fluid, and, consequently, the pore pressures increase (Lima Bevilaqua, 2019) (Rodríguez Pacheco, 2019). When the pore pressure reaches a critical level and the intergranular stresses are annulled (reduction of effective stresses), the soil behavior becomes viscous liquid (**Erro! Fonte de referência não encontrada.**) (Araujo & Ledezma, 2020).

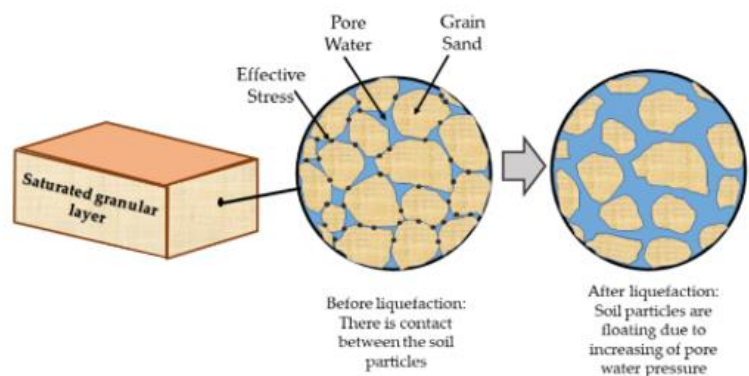


Figure 5 - Liquefaction and the loss of adhesion among the particles due to the excessive water pore-pressure (adapted from Araujo & Ledezma, 2020).

The liquefaction of tailings occurs when the tailings are contractive, saturated more than 80%, and the effective stress σ' is null. According to Terzaghi's principle (Equation 1), this corresponds to the situation when the pore pressure u is equal to the total stress σ (Rodríguez Pacheco, 2019).

$$\sigma = \sigma' + u \quad (1)$$

Moreover, the shear stress resistance of soils is given by Equation 2:

$$\tau = (\sigma - u) \cdot \tan\phi + c \quad (2)$$

Where τ is the shear strength, ϕ is the internal friction angle and c is the cohesion. The last two are characteristic parameters related to the type of material, and for tailings, the internal friction angle varies from 18 to 38 and the cohesion is zero. Thus, when the pore pressure increases, the shear strength decreases, until a value where geotechnical stability is lost, and the safety factor is lower than one. This can be caused by a dynamic or quasi-static load, being the last one related to excessive dam rising rate, increase in the water table due to rainfalls, injection of water due to failures in the drainage system, among other reasons (Rodríguez Pacheco, 2019).

As mentioned above, some problems related to water may affect the stability of the system, therefore, water control during the construction is fundamental. It is necessary to assess and reduce as much as possible the water flow inside the dam and in the foundation. Water can originate from the slurry and the environment, through rainfalls, run-offs coming from the upper catchment (Fleurisson & Cojean, 2016), the underground, or from a capillary rise. The water coming from rainfall partly infiltrates the beach and the rest flows as a surface run-off until reaching the ponds. Also, evaporation occurs and induces the capillary rise coming from the phreatic surface (Rodríguez Pacheco, 2019). Figure 6 summarizes the phenomena related to water that affect the operation of tailings dam.

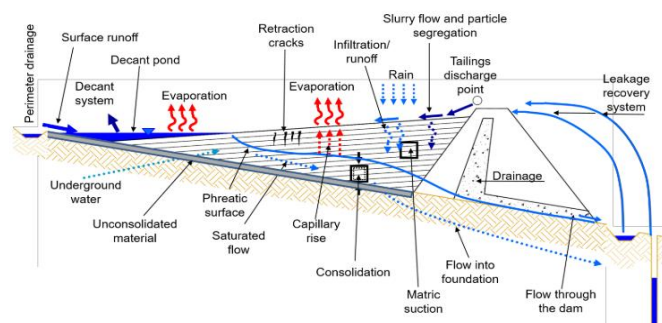


Figure 6 - Water control in tailing dams (Rodríguez Pacheco, 2019).

Moreover, to avoid problems with stability due to water pore-pressure effects, the initial dyke, which constitutes the toe of the final dam, must allow the drainage of possible seepage water inside the system. This preventive action can be done by placing an upstream underdrainage system under the initial dyke, and if necessary in the heightening ones, which are responsible for the water table drawdown (Fleurisson & Cojean, 2016).

Some considerations must be given to the foundation material, which may also cause the failure of the system. If a structurally weak material with low permeability is used, the pore-pressure tends to increase, and then, the shear strength is reduced (Equation 2). On the other hand, if permeability is too high, water flow can be formed making the foundation vulnerable to piping failure (Kossoff et al., 2014).

If the drainage system is not efficient, the water flow can cause internal erosion, related to the motion of particles and the formation of empty tubes in the ground. This situation may contribute to collapses and lateral landslides, characterizing the above-mentioned piping (Lima Bevilaqua, 2019). This phenomenon occurs when the erosion resistance is overcome, the soil nature is dispersive, and the critical stress (resistance to effective stress) and critical hydraulic load (amount of energy required to initiate the erosion due to seepage flow) are achieved (Rodríguez Pacheco, 2019).

Moreover, it is required to assess and control the water level in the settling pond to prevent the occurrence of water overtopping, which may cause crest erosion and dam breaching. To avoid seepage, the level of the water table must be as low as possible from the top of the impoundment, which is often formed by coarser material with higher permeability (Fleurisson & Cojean, 2016). Additionally, the level of the phreatic line is an important factor for the dam stability since the pore-pressure increases with higher levels of the water table. Failure can occur if the width of the beach is too short and the ponds are close to the dam crest, which increases the hydraulic gradient (Rodríguez Pacheco, 2019). Figure 7 describes the phenomena mentioned above.

Nevertheless, in many failure cases in history, the causes were related to a combination of factors. The previously discussed events related to water can be associated with meteorological causes (e.g. intense rainfalls), structural problems, slope instability, bad management and operation, among others (Rico et al., 2008).

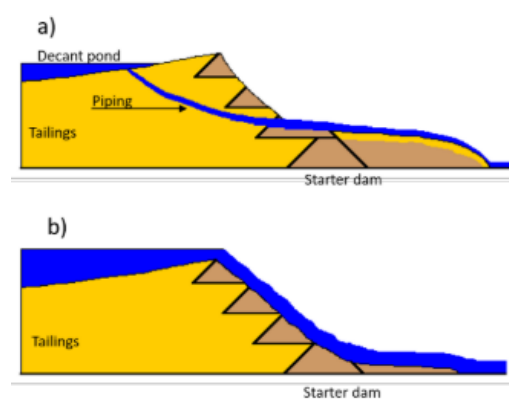


Figure 7 - a) Piping, b) Overtopping (Rodríguez Pacheco, 2019).

1.2 Córrego do Feijão Mine: Characterization of the tailings dam

The mine called Córrego do Feijão (Figure 8), located in Brumadinho, Minas Gerais, Brazil, was part of a mining complex composed by the dam I and other 12 structures, currently a property of the company Vale S.A., whose main activities were the iron ore extraction and distribution, tailings disposal, sediments retention, water flow control and water collection (G1 Notícias, 2019).

The construction of Dam I, for tailings disposal, was initiated in 1976 when the starter dam was built, with a maximum height of 18 m (Lima Bevilaqua, 2019), over a rocky soil with good bearing capacity and low permeability (Illipronti Laurino et al., 2020). The dykes resultant from the raises have as a foundation the tailings beaches, and in the abutments, they are supported by residual or saprolitic soil (Vale & TUV SUD, 2018).



Figure 8 – Position of the Córrego do Feijão Mine and the Dam I (Google Earth, 2018).

As the volume of production and, consequently, of tailings increased, the upstream method was the main choice to enhance the capacity of the dam, and nine more raising lifts were added to the structure in 14 stages, built using compacted soils or compacted tailings (Figure 9). Finally, the last dike was constructed in 2013 and the total height of the dam reached 86 m (Lima Bevilaqua, 2019).

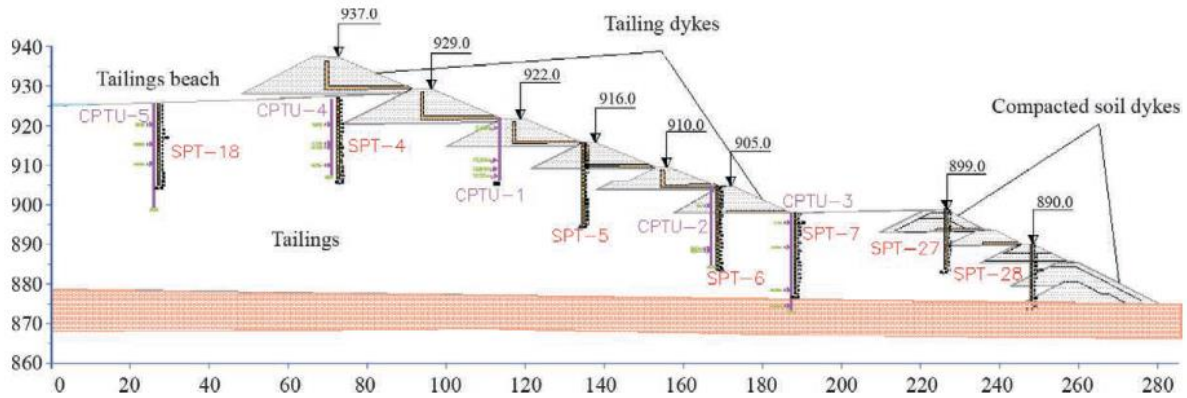


Figure 9 - Cross-section of Dam I (Schnaid et al., 2013).

Between 1976 and 2005, the disposal of the tailings was performed using the spigotting technique, and problems occurred due to the distance between the points of material release, which was about 100 m. In this way, the formed beach was not uniform, with regions of good compressibility and drainage close to the release points, and worse conditions between them. Consequently, this operation caused the formation of non-uniform disposal of the tailings, with the presence of layers with different compaction values (Silva, 2010).

After 2006, the spigotting technique was substituted with the spray-bars (Figure 10), which operated alternately among 3 divisions, with 3 to 4 bars each. In this way, it was expected to form more uniform and homogeneous tailings deposits in the reservoir, providing adequate hydraulic segregation. Moreover, the alternated operation would be able to favor the drying of the release tailings and, consequently, their decantation, which contributes to the increase of their resistance (Silva, 2010).

The tailings constituted of uniform fine silty sand, with, approximately, 4% of clay, 28% of silt, 56% of fine sand, 8% of medium sand, 3% of coarse sand, and 1% of gravel. Although the high concentration of sand, some strata presented low plasticity, with liquid limit $w_L \leq 35\%$ (Schnaid et al., 2013). The compaction of the material was heterogeneous, varying from soft to compact, and the permeability coefficient was in the range of 10^{-5} a 10^{-4} cm/s (Vale & TUV SUD, 2018).

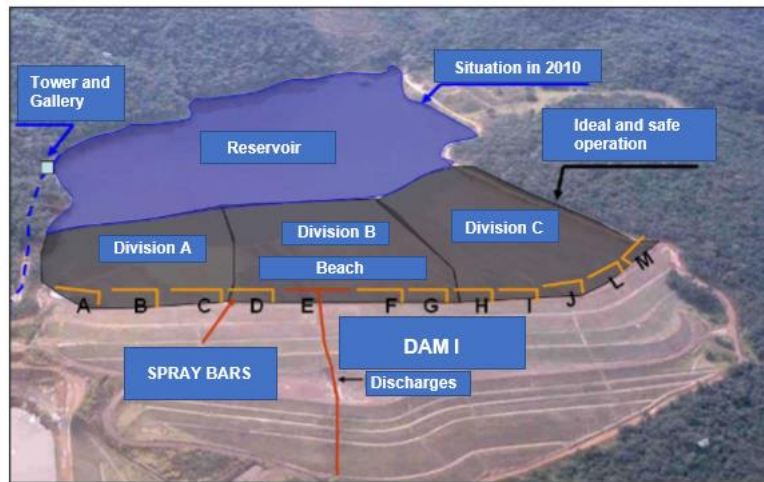


Figure 10 - Tailings Disposal System (adapted from Silva, 2010).

Regarding the internal drainage of the system, there is not much information concerning the first dykes, but the executive projects indicate the construction of blanket drains, made of sinter feed, and longitudinal tubes, for the second and fourth heightening. For the remaining ones, As-Built projects were consulted and, according to it, blanket drains and chimney drains were used for the fifth to ninth heightening, constituted by sinter feed or sand, and for the last one, only a blanket drain made of sand was installed (Vale & TUV SUD, 2018). This drainage system can be observed in Figure 9.

For the outlet of the draining system, perforated PVC tubes were designed (raises 5, 6,7, and 8), toe drains covered by geosynthetic material (raises 9 and 10), and a cut-off trench of 2 m (raise 8) (Vale & TUV SUD, 2018). Some of the structures mentioned above, which constituted the drainage system, are illustrated in Figure 11. Furthermore, the superficial drainage is made of concrete channels on the berms that direct the flow downstream.

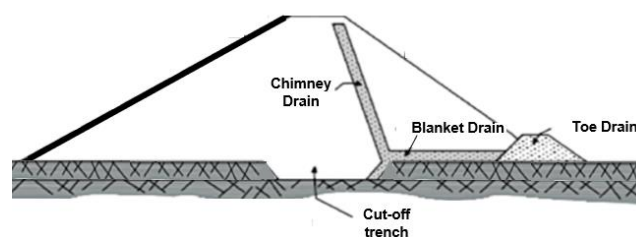


Figure 11 - Internal drainage system (adapted from ANA - Agência Nacional das Águas, 2016).

The monitoring of the dam was done through periodic reading of Sandpipe or Casagrande piezometers, water level indicators, inclinometers, and measures of water flow. Then, the

monitoring data was compared to the previously established levels of safety: attention, alert, and emergency (Illipronti Laurino et al., 2020).

From the year 2017, the company owning the complex decided to install deep horizontal drains (Figure 12), after a reunion of international specialists, where it was alerted that the factor of safety was 1.06 (*CPI: Rompimento da Barragem de Brumadinho*, 2019), and it was necessary to drawdown the water table to achieve stability (Jornal Estado de Minas Gerais & Parreiras, 2019). These drains are installed in boreholes with a horizontal axis and small inclination to allow the water flow by gravity; they are constituted by tubes and filters, which retain the particles during the water movement. They reduce the water pore-pressure by collecting the water from the infiltration of the water table (*CPI: Rompimento da Barragem de Brumadinho*, 2019).

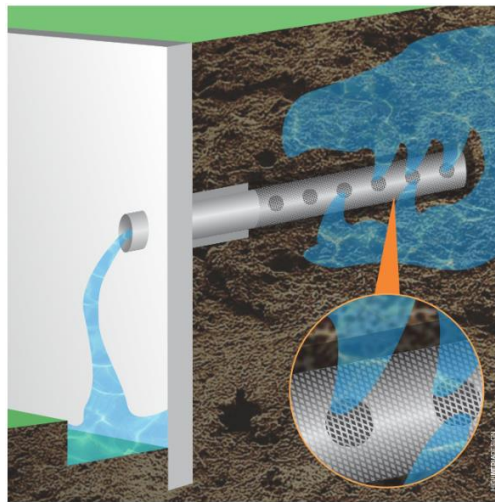


Figure 12 - Deep Horizontal Drain (*Dreno Horizontal Profundo - Drilling*, n.d.).

The procedure to install the drains was, nevertheless, poorly executed and did not enhance the safety factor of the impoundment. On the contrary, an incident occurred on June 2018, during the installation of drain 15 (in a planned total amount of 30), when an excess of water pressure during the drilling caused hydraulic fracturing and, consequently, pipping, when solid material was dragged to the downstream side of the dam (*CPI: Rompimento da Barragem de Brumadinho*, 2019).

Vale decided to interrupt these interventions and after looking for other solutions, they carried out a project for deep wells, but there was no time to implement it (Jornal Estado de Minas Gerais & Parreiras, 2019). However, in the final investigations, the incident with the drains was disregarded as a possible contribution to the failure, as well as the drilling of new boreholes

for the installation of piezometers (*BRUMADINHO ENGINEERING HISTORY – World Mine Tailings Failures - from 1915, n.d.*).

1.3 The collapse of the Brumadinho tailings dam: Possible Causes and Consequences

The tailings dam I collapsed on January 25th, 2019 at 12:28, triggering a flow with an initial velocity close to 80 km/h, which, in seconds, reached the company installations, such as the railway and the bays for the ore distribution and, subsequently, the administrative center with the offices and the lunchroom for the employees (G1 NOTÍCIAS, 2019).

These constructions were located, approximately, 1 km downstream of the dam (CPI: Rompimento da Barragem de Brumadinho, 2019). Residential and administrative buildings, infrastructures, and farms were affected or destroyed, and after three hours, approximately, the flow reached the river Paraopeba, about 9 km away, as illustrated in Figure 13 (G1 NOTÍCIAS, 2019). The tragedy caused between 270 and 310 casualties, dead or missing. Post-failure studies indicate that if a warning had been released 15 minutes before the collapse, the number of deaths would have been reduced to zero, or if released at least at the moment of the collapse, many lives could have been saved. However, the warning system did not work (Lumbroso et al., 2020).

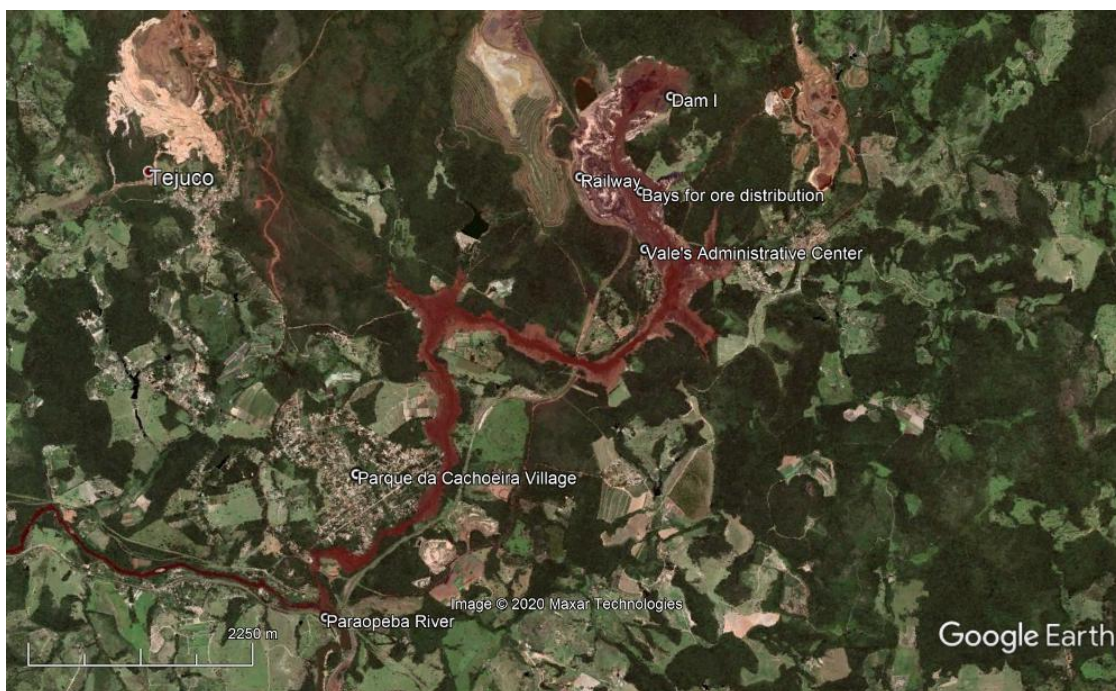


Figure 13 - Damage extension of dam breaching (Google Earth, 2019).

Studies commissioned by Vale S.A. confirmed that the dam rupture was caused by static liquefaction, releasing 75% of the volume capacity of the impoundment before the collapse,

which corresponds to 9.7 million m³. This value was obtained via analysis of satellite images and comparison of the volume before and after the breaching (G1, 2019). This volume was formed by water, mud and solid material from the dam, which took about 5 minutes to leave completely the breaching zone and the maximum mudflow discharge was of 90,000 m³/s, according to post-failure modeling of the phenomenon (Lumbroso et al., 2020).

As stated by the report published almost one year after the collapse, some triggering factors could have contributed to the dam instability, such as quick loading due to the heightening construction or tailings launch, quick cyclic loading or fatigue caused by detonations, unloading due to raising of level water or movement, internal erosion, human interaction, localized loss of resistance due to underground source of water, loss of suction and resistance in unsaturated zones above the water level and creep (G1, 2019).

Additionally, the technicians pointed to insufficient internal drainage of the system, which culminated in the high water level close to the dam and the saturation of a significant part of the tailings, which caused high shear stresses inside the dam, mainly in its toe. Concerning the causes, there was no relation to seismic movements or explosions, which could provoke quick loads. Moreover, it was mentioned the elevated precipitation levels during the rainy season and the high iron content, resulting in water accumulation, heavy tailings, and cementation of the particles, what would make them very fragile in undrained condition (HuffPost Brasil, 2019).

It was considered as a leading cause of the breaching a faulty design of the dam, whose toe had blocked a creek that was used to drain groundwater, a fact that culminated in constant rising water level inside the dam. Moreover, the abrupt failure can be associated with creep rupture, triggered by even an irrelevant small strain (*BRUMADINHO ENGINEERING HISTORY – World Mine Tailings Failures - from 1915*, n.d.).

Data from satellite monitoring indicated movement and deformation of the downstream side of the dam in the analysis right before the collapse (Figure 14). These results matched with deformations detected from a ground-based radar interferometry, located near the railway, which pointed to a reduction of the amplitude of the reflected wave in a certain area. This could be related to the variation of humidity or level of compaction (*CPI: Rompimento da Barragem de Brumadinho*, 2019).

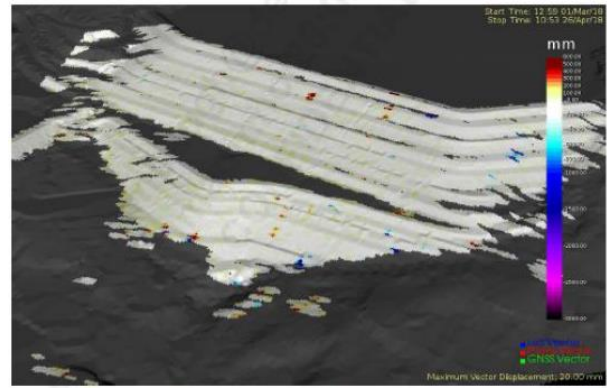
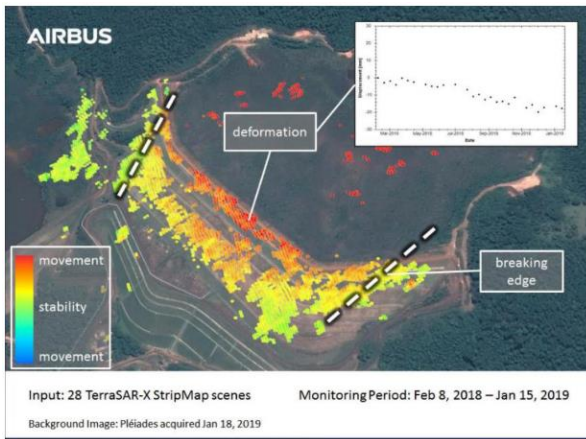


Figure 14 - Satellite monitoring of the dam movement and real-time result from the ground-based radar interferometry (CPI: *Rompimento da Barragem de Brumadinho*, 2019).

Some hypotheses about problems in the drainage system can be raised while observing satellite images of the dam months before the collapse (Figure 15). The existence of superficial water on the backside of the dam (after inactivation) can be observed, which is very close to the rupture crest (Figure 16) (D. M. Pereira et al., 2019).



Figure 15 - Satellite images showing superficial water in the reservoir, in June of 2017 and 2018, respectively (D. M. Pereira et al., 2019).



Figure 16 - Satellite image showing the rupture crest in March of 2019 (adapted from Google Earth, 2019).

Another study evaluated the Temperature Vegetation Dryness Index (TVDI) before and after the collapse, using Landsat-8 data. This parameter is correlated to the soil moisture, in the way that the lower the value of TVDI, the higher is the soil moisture, and consequently, the soil is more likely to suffer from liquefaction. According to the analysis, the TVDI at the dam body was relatively high, but the region close to the vegetation boundary and another about 199 m from the dam crest had TVDI either negative or between 0 and 0.2, indicating high soil moisture (Figure 17) (Lan et al., 2019).

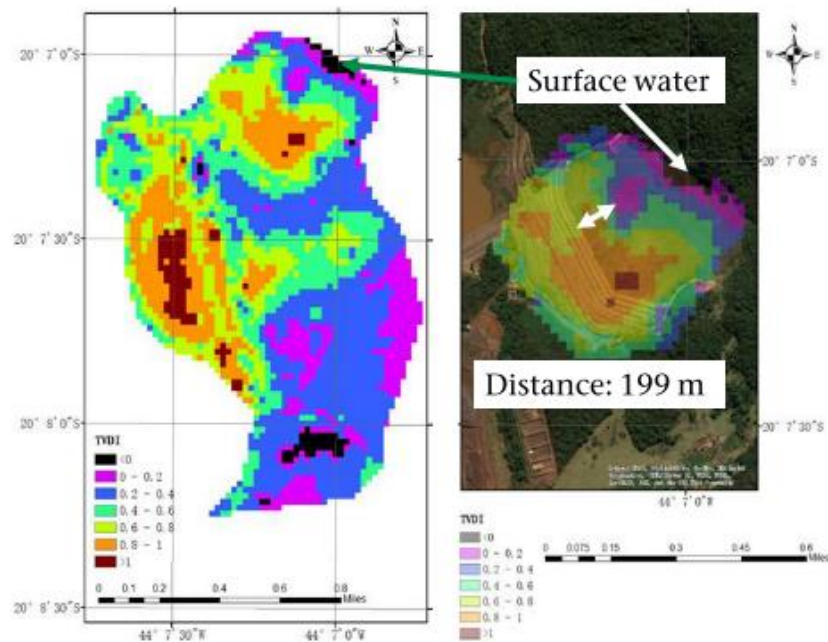


Figure 17 - TVDI distribution on January 14, 2019 (Lan et al., 2019).

The same analysis was performed after the collapse, and it showed the surface, the sub-soil, and the water in the tailings dam exposed, with a large area of negative values, confirming the high level of soil moisture (Figure 18). Moreover, this area had no precipitation in January, directing the attention to the insufficient drainage and the possibility of water accumulation (Lan et al., 2019).

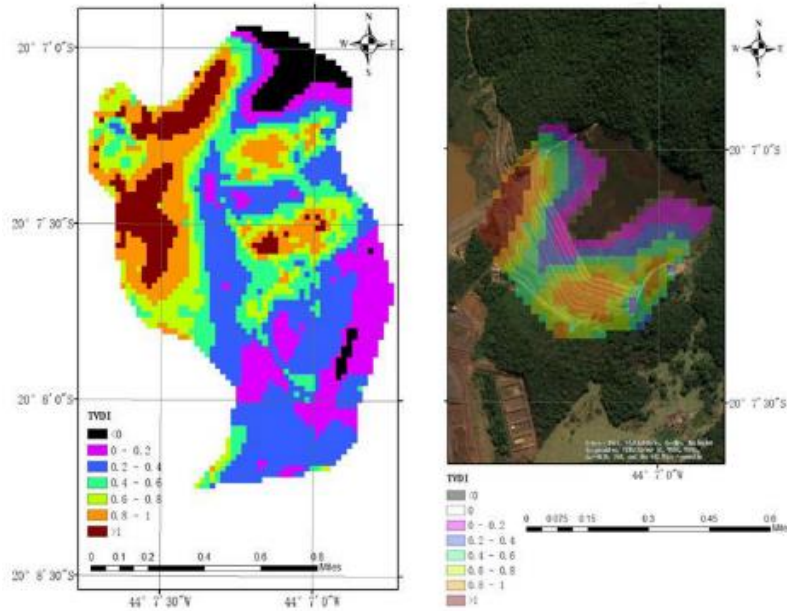


Figure 18 - TVDI distribution on January 30, 2019 (Lan et al., 2019).

A study about the dam I stability was carried out by Frederico Lopes Freire, who analyzed aerial images of the structure. He pointed out the saturation increase due to constant natural drainage within the impoundment, whose origin probably derives from higher elevation points and the dense forest behind it. In Figure 19, it is possible to visualize the tailings pond, and the arrows indicate the flow of water, drained outside the dam at the elevations 912 m and 913 m (*BRUMADINHO ENGINEERING HISTORY – World Mine Tailings Failures - from 1915, n.d.*).

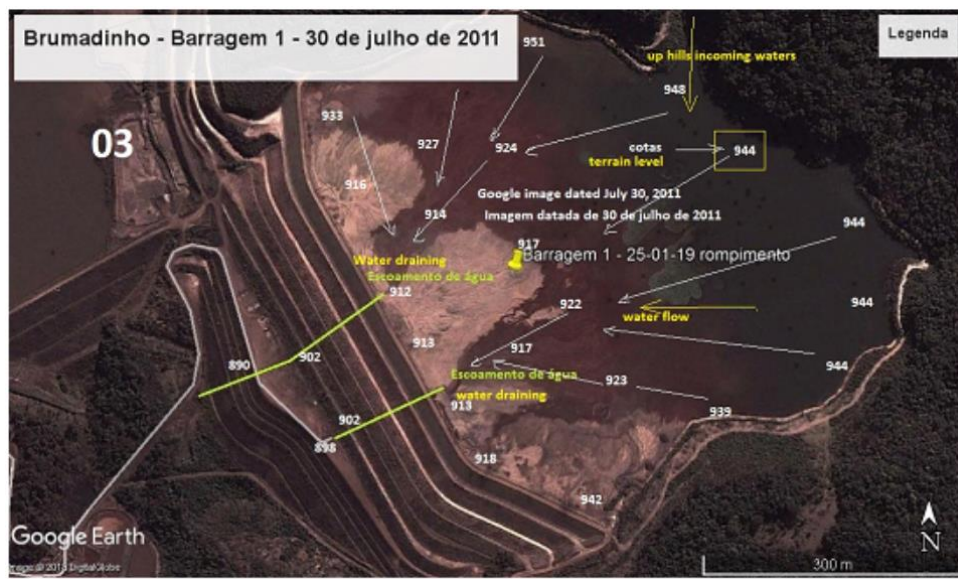


Figure 19 - Aerial images of the analysis of water influence, in July 2011 (*BRUMADINHO ENGINEERING HISTORY – World Mine Tailings Failures - from 1915, n.d.*).

Figure 20 shows the same image after some years, when the dam was already inactive. In this context, the arrows point to the middle of the reservoir, and the water is not more collected by the drains, causing an increase of the humidity stain. Moreover, it was noted a top alignment deformation on the left side of the dam (indicated by the white square) (*BRUMADINHO ENGINEERING HISTORY – World Mine Tailings Failures - from 1915, n.d.*).



Figure 20 - Aerial images of the analysis of water influence, in July 2018 (*BRUMADINHO ENGINEERING HISTORY – World Mine Tailings Failures - from 1915, n.d.*).

Another study was performed, in 2018, by a company hired by Vale to monitor dam I. It was done the stability analysis of the system, and it was computed the factor of safety and the circular slip surface, using the Limit Equilibrium Method. They analyzed some sections of the dam, and they considered the drained and undrained conditions for the calculation. The most critical cross-section is illustrated in Figure 21, with a red dashed line indicating its position in the aerial image (Vale & TUV SUD, 2018).

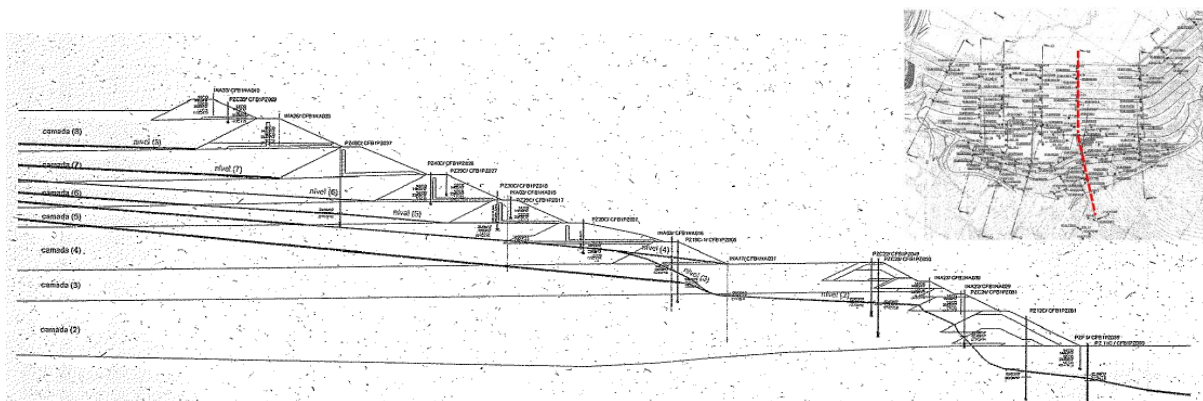


Figure 21 – The most critical cross-section of the dam, according to the LEM analysis (Vale & TUV SUD, 2018).

The piezometric condition adopted was interpreted considering not only piezometers but also the results of Piezocone Penetration Tests (CPTU) since they identified the presence of perched water tables below lenses of fine material. Then, layers of tailings were defined, through the verification of CPTU studies, which are illustrated in Figure 21, and each of these layers is assigned to a different piezometric level (Vale & TUV SUD, 2018) (Bonatto, 2019).

According to the investigations conducted by the “Superintendência Regional do Trabalho de Minas Gerais (SRT-MG)”, the inspectors concluded that the fine material was launched inappropriately. This may be related to what has been discussed previously about the launching technique consisted of the spigotting system, which resulted in non-uniform beaches. As a result, there was an accumulation of infiltration water above deposits of fines, and due to its low permeability, instead of infiltrating in the deepest layers of the reservoir, the water moved towards the front part of the structure, close to the dykes. In this way, the perched water tables were formed (Jornal Estado de Minas Gerais & Parreiras, 2019).

Regarding the geotechnical parameters, for the drained condition, they considered the unit weight, the effective cohesion, and the effective friction angle; meanwhile, for the undrained condition, the saturated materials subjected to liquefaction are characterized by their effective undrained peak resistance ($su/\sigma'v_0$) and the remaining materials, by their effective drained resistance (c', ϕ') (Vale & TUV SUD, 2018). The static slope failure occurs when the imposed stress from the permanent loading is higher than the peak of the curve obtained from the effective shear stress – shear strain relationship (Rodríguez Pacheco, 2019).

In the drained condition, the lower value of the factor of safety was $FS=1.60$, which is greater than the minimum established by the Brazilian codes as $FS=1.50$. In this case, the critical slip surface develops in the lower part of the dam (first to third raises), showing that those dykes control the stability. Nonetheless, for the undrained situation, the critical factor of safety was $FS=1.09$, the critical surface develops along the saturated tailings, involving their maximum possible volume, and the analysis shows that the upper part of the dam is more critical (Figure 22) (Vale & TUV SUD, 2018).

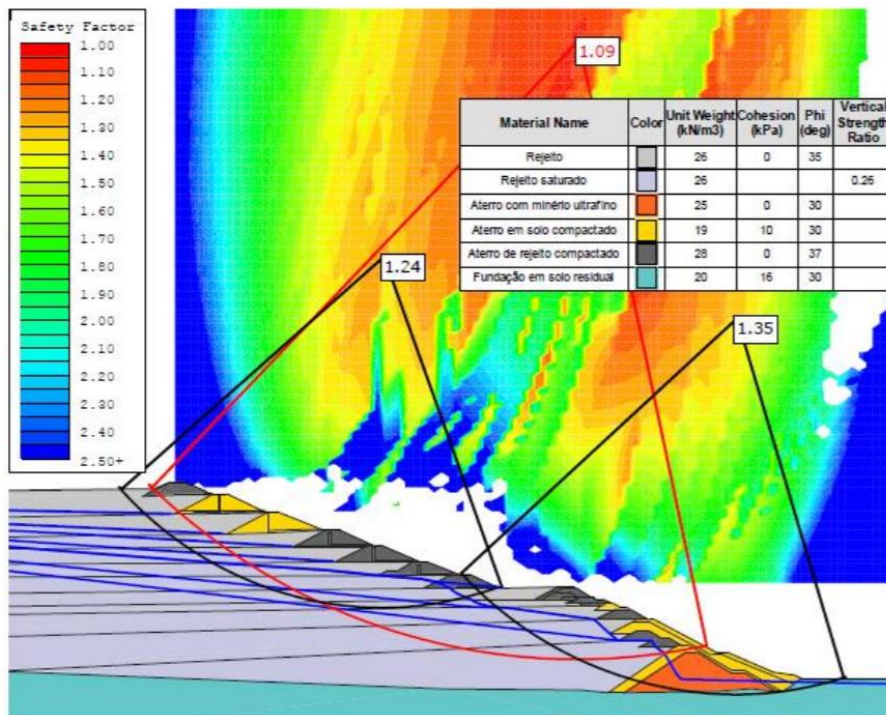


Figure 22 - Analysis of stability by LEM under undrained conditions (Vale & TUV SUD, 2018).

The ruptures of tailings dams result in severe damage in the environment and socioeconomic relations, leading to changes in the land cover, contamination and damage of ecosystems, casualties, and problems related to the health, welfare, and economic livelihood of the population affected (L. F. Pereira et al., 2019).

Regarding the land cover (Figure 23), 297.28 ha were covered by the tailings, where 193 structures have been compromised, being 41% corporative, and 59% residential homes. Furthermore, in the affected area, 51% corresponded to native vegetation (mostly preserved and part in intermediary stages of conservation), 19% to anthropic activities, and 13% to farming activities (Table 1). The remaining part was occupied by the dam and superficial water. The region is composed mainly of low and flatlands, surrounding the watercourses (L. F. Pereira et al., 2019).

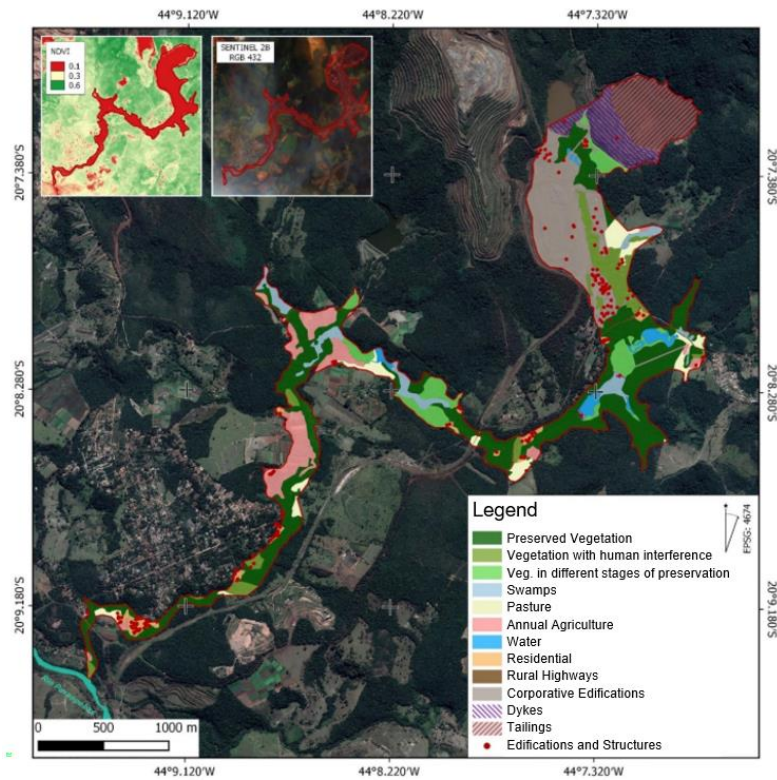


Figure 23 - The land cover of the area covered by the Tailings (adapted from L. F. Pereira et al., 2019).

Table 1 - Characterisation of the Land cover in the area covered by the tailings (based on L. F. Pereira et al., 2019)

Type of Land Cover	Area (ha)	Percentage in Area (%)
Preserved Vegetation	98.18	33.0
Vegetation with human interference	19.94	6.7
Vegetation in different stages of preservation	19.91	6.7
Swamps	12.94	4.4
Pasture	14.16	4.8
Annual Agriculture	23.30	7.8
Water	6.12	2.1
Residential	7.03	2.4
Rural Highways	1.35	0.5
Corporative Edifications	49.95	16.8
Dykes	18.33	6.2
Tailings	26.05	8.8
Total	297.26	100

In addition to affecting these areas in the Córrego do Feijão Valley, the flow reached the main river of the region, the Paraopeba river, where it has deposited a great part of the sediments transported, changing the streamflow and the number of sediments flowing along its path (Andrade et al., 2019), preventing the collection and treatment of water and causing the death of the river fishes (Romão et al., 2019).

In the days following the rupture, the tailings caused the increase of turbidity, which culminated in the total interruption of the use of water and the increase of particles in suspension. This caused the reduction of the passage of sunlight for photosynthetic activities that affected the aquatic ecosystem and contributed to the silting of the river. Moreover, the quantity of manganese detected overcame the maximum value observed in the historic series (Soares et al., 2019).

According to researchers from the Fundação SOS Mata Atlântica, one year after the tragedy, the river has still not recovered, and the water continues to be inappropriate for use, in all its extension downstream Brumadinho. They observed several points along the river path and noted that the tailings are concentrated in the lower Paraopeba (upper circle in Figure 24), moreover, none of the points presented good or great quality. The ecosystem of the basin has been altered and some species have disappeared, even if the level of oxygen was satisfactory. Regarding this, they relate it to the intense concentration of heavy metals since the analysis detected the presence of iron, manganese, and copper in levels above the maximum limits fixed in legislation (Notícias UOL, 2020).

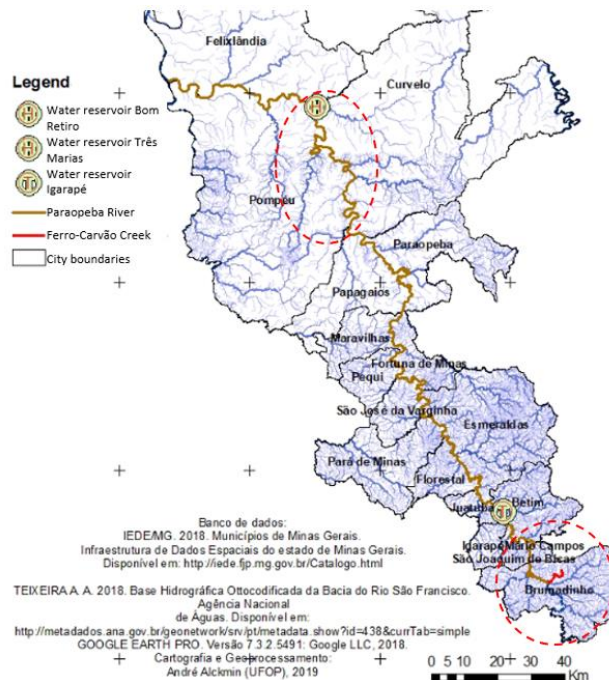


Figure 24 - Highlighted the region of the Lower Paraopeba, where the tailings were concentrated one year after the event, and where the tailings reached the river (adapted from D. M. Pereira et al., 2019).

To recover the conditions of the river, the company Vale created a treatment station in the junction of the river and the Ferro-Carvão Creek, where the tailings reached Paraopeba (close to Brumadinho, in the lower part of the map in Figure 24). Besides that, the riverbed is being

dredged for the removal of the sediments. The researchers, previously mentioned, stated that the turbidity in this point of intervention has decreased, but not the quantity of heavy metals (Notícias UOL, 2020).

2. Methodology

2.1 Triggering Analysis and the Limit Equilibrium Method

The triggering phenomenon is briefly discussed since its analysis is required in one section of this thesis. Therefore, this part is not the main goal of the present work, and only the main concepts used are described below.

The stability of the dam slope is studied using the Limit Equilibrium Method (LEM), which is one of the main methods to derive the safety factor of a slope. It consists of dividing the soil mass into some vertical or horizontal slices composing the slip surface, with constant or variable width, and, for each of them, determine the equilibrium in terms of forces and/or moments (Figure 25) (Agam et al., 2016).

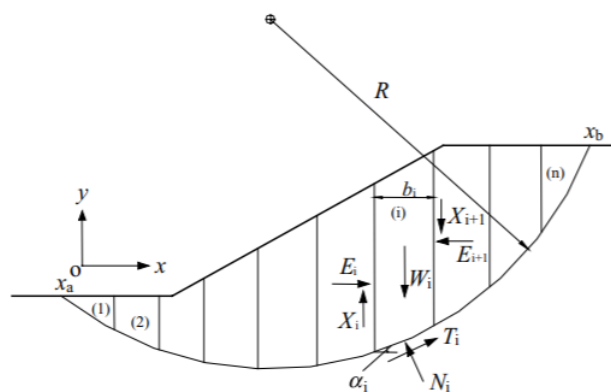


Figure 25 - Vertical slices scheme with the acting forces (Zhu, 2008).

In Figure 25, the forces acting on the slice with a width b_i and angle α_i of the base are the following (Zhu, 2008):

W_i : Weight;

E_i and E_{i+1} : Horizontal interslice forces;

X_i and X_{i+1} : Vertical interslice forces;

N_i : Normal force at the base;

T_i : Shear resistance at the base;

u_i : pore pressure at the base (not represented in the drawing).

There are different approaches, given by many authors about how to define the safety factor, however, to give a general idea, it can be mentioned the Simplified Bishop method, which says that the safety factor is given by the ratio of total strength available on the slip surface to the total shear strength mobilized (Agam et al., 2016). Thus, the main idea of this stability analysis regards the relationship between resisting and soliciting forces acting on the slices.

For the Simplified Bishop method, the vertical forces equilibrium and moment equilibrium on the center of the slip surface are satisfied, but the equilibrium of the horizontal forces is not applied. Besides that, the vertical interslice forces are neglected. Therefore, this is a non-rigorous method, however, it provides values of safety factor coherent with values resultant from more rigorous methods (Zhu, 2008).

For the calculation of the safety factor, besides the equilibrium equations, the Mohr-Coulomb failure criterion and the principle of effective stress are considered. The vertical forces and the momentum equilibrium are better described by Zhu (2008), however, the equation for the safety factor determination is illustrated below:

$$FS = \frac{\sum_{i=1}^n [(W_i - u_i b_i) \tan \phi'_i + c'_i b_i] / (\cos \alpha_i + \sin \alpha_i \tan \phi'_i)}{\sum_{i=1}^n W_i \sin \alpha_i} \quad (6)$$

Where ϕ'_i is the effective internal friction angle and c'_i is the effective cohesion.

Spencer's method is based on Bishop's simplified method and it considers the resultant of a pair of interslice forces, given by Q, as described by Agam et al. (2016). Equations 7 and 8 need to be solved to obtain the safety factor:

1. Considering that the external forces are in equilibrium and the interslice shear and normal forces are parallel:

$$\sum Q = 0 \quad (7)$$

2. Considering that the sum of the moments about the center of rotation is null:

$$\sum [Q \cos (\alpha - \theta)] = 0 \quad (8)$$

Where α is the slope of base of slice and θ is the slope of resultant Q of pair of interslice forces.

These analytical methods are used by some numerical modeling softwares to obtain the most critical slip surface and the correspondent minimum safety factor of the slope to be analyzed.

In this thesis, it is used the software RocScience Slide, and the procedure performed for the analysis is described in the next section.

2.2 Analytical and Numerical Modeling of Runout and the RASH 3D

I. Landslide Flows: Definitions and Classification

When analyzing the runout originated by a landslide, the first procedure to be done is to perform a classification of the material and of some aspects regarding its movement. Different terms and methods can be used for this classification, and some of them are discussed below.

Debris flow can be defined, according to Takahashi, as one type of massive subaerial sediment motion or transportation, a phenomenon that can be motivated by gravity or fluid dynamic forces, where in the first case, the movement is “*en masse*”, treated as a whole without distinguishing its parts and in the second it behaves as an individual particle motion. Particularly, the debris flow is characterized as a mixture of water and sediments, which flows as a continuous fluid due to gravity, and it has large mobility in reason of the large and saturated voids filled by water or slurry (Takahashi, 2014).

Additionally, a flow-like landslide usually is originated by a slide, after a rupture of the surface, and it continues to move along great distances with distributed velocity profiles. Meanwhile, the landslide source volume can be defined as the volume between the sliding surface and the ground surface before the rupture, i.e. the first volume of material that slides and originates the further flow (Hungr et al., 2001).

These mass movements may give rise to disasters and the magnitude of the damage can vary regarding the characteristics of the motion. Thereby, different types of phenomena were classified according to their destructive power, based on a standard derived from events in the past (Table 2) (Takahashi, 2014).

Table 2 – Classification of the mass movements according to their magnitude and mobility (Takahashi, 2014)

Phenomena	Magnitude (m ³)	Velocity (m/s)	Arrival distance (km)	Equivalent friction coefficient
Landslide	10~10 ⁶	10 ⁻⁶ ~10	< 0.3*	> 0.5**
Landslip	2 × 10 ⁵ **	-	0.7**	0.25**
Debris flow	10 ³ ~10 ⁶	20~0.5	0.2~10	0.3~0.05
Debris avalanche	10 ⁷ ~10 ¹⁰	10~10 ²	< 30	0.3~0.05
Pyroclastic flow	10 ⁴ ~10 ¹¹	10~50	< 60	0.4~0.2

*Landslip smaller than $1.5 \times 10^4 \text{m}^3$, **Las Colinas, El Salvador, 2001.

Observing Table 2, it is possible to note the higher fluidity of debris flow, debris avalanches, and pyroclastic flows, characterized by higher velocities, greater distances reached, and smaller equivalent friction coefficients, in comparison to landslides and landslips, which are consisted of dry earth blocks (Takahashi, 2014).

Many other classifications and reviews have been published by different authors, including a revision made by Hungr in 2001, who has taken as starter point the classifications of Varnes in 1978 (Table 3) and its later modification proposed by Cruden and Varnes in 1996 (Table 4). The first one is based on the movement mechanisms and the material type, the second adds the velocity of the movement as a key aspect (Hungr et al., 2001).

Table 3 - Varnes classification (1978) (Hungr et al., 2001)

Rate of movement	Bedrock	Debris (<80% Sand and Finer)	Earth (>80% Sand and Finer)
Rapid and higher (>1.5 m/day)	Rock flow (creep, slope sagging)	Debris flow Debris avalanche	Wet sand and silt flow Rapid earth flow Loess flow Dry sand flow
Less than rapid (<1.5 m/day)		Solifluction Soil creep Block stream	Earth flow

Table 4 - Cruden and Varnes Classification (1996) (Hungr et al., 2001)

Velocity Class	Description	Velocity (m/sec)	Typical Velocity
7	Extremely Rapid	5	5 m/sec
6	Very Rapid	5×10^{-2}	3 m/min
5	Rapid	5×10^{-4}	1.8 m/hr
4	Moderate	5×10^{-6}	13 m/month
3	Slow	5×10^{-8}	1.6 m/year
2	Very Slow	5×10^{-10}	16 mm/year
1	Extremely Slow		

As stated by Varnes, the material type distinction is based on the percentage content of coarse material, where “Earth” has less than 20% of gravel and coarser clasts, with grain diameter greater than 2 mm, and “Debris” has a higher concentration of that material type. Nonetheless, it is not simple to apply these classifications due to the difficulty of estimating the average grain-size distribution, as a consequence of lateral and vertical non-homogeneity, the difficulty of access, and lack of exposures. Additionally, the coarse material content may not affect, significantly, the mechanical behavior of the flow (Hungr et al., 2001).

Regarding these limitations, Hungr proposed a new classification, focusing on genetic concepts and the context of each landslide, instead of a simple grain size distribution. The different classes can be assessed by geomorphological analyses, field observations, and laboratory tests. The materials can be grouped in different types regarding the origin and composition, and as an example, there are the sorted anthropogenic deposits, such as mine tailings, which are related to the texture or genetic label of the soil involved, such as sand, clay, loess or talus (Hungr et al., 2001).

Based on Hungr and others, debris flow can be described as unsorted material with low plasticity, which could have been produced by unsorted anthropogenic waste, such as mine spoil, while earth flows are resultant of the process of weathering of clayey colluvium, which if liquid or semi-liquid, can characterize a mudflow instead. Analyzing the composition of the material in some events in the past (Figure 26), it is possible to observe some differences between these types of flow (Hungr et al., 2001).

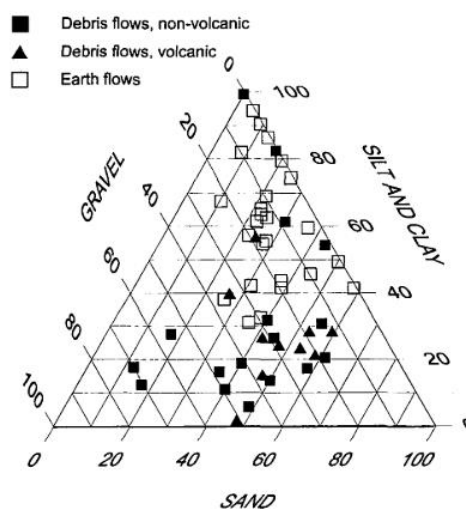


Figure 26 - Textural composition of the material in different types of flows.

Debris flows usually contain non-plastic or weakly plastic material and less than 30% of silt and fines, which sets it apart from earth flows, which has from 10% to 70% clay content. On the other hand, mudflows cannot be distinguished from earth flows based on the textural composition, but it can be in other terms like velocity and water content. Hence the importance of considering the context of each landslide. These new types of material were joined with key aspects for the definition of the landslide, and they were summarized in table 5 (Hungri et al., 2001).

Table 5 - Hungri classification of landslides of the flow type (Hungri et al., 2001)

Material	Water content¹	Special condition	Velocity	Name
Silt, sand, gravel, debris (talus)	Dry, moist or saturated	-no excess pore pressure, -limited volume	Various	Non-liquified sand (silt, gravel, debris) flow
Silt, sand, debris, weak rock ²	Saturated at rupture surface content	-liquefiable material, ³ -constant water	Ex. Rapid	Sand (silt, debris, rock) Flow slide
Sensitive clay	At or above liquid limit	-liquefaction in situ, ³ -constant water content ⁴	Ex. Rapid	Clay flow slide
Peat	Saturated	-excess pore pressure	Slow to very rapid	Peat flow
Clay or earth	Near plastic limit	-slow movements, -plug flow (sliding)	< Rapid	Earth flow

¹ Water content of material in the vicinity of the rupture surface at the time of failure.

² Highly porous, weak rock (examples: weak chalk, weathered tuff, pumice).

³ The presence of full or partial in situ liquefaction of the source material of the flow slide may be observed or implied.

⁴ Relative to in situ source material.

Debris	Saturated	-established channel, ⁵ -increased water content	Ex. Rapid	Debris flow
Mud	At or above liquid limit	-fine-grained debris flow	> Very Rapid	Mudflow
Debris	Free water present	-flood ⁶	Ex. Rapid	Debris flood
Debris	Partly or fully saturated	-no established channel, ⁵ -relatively shallow, steep source	Ex. Rapid	Debris avalanche
Fragmented rock	Various, mainly dry	-intact rock at source, -large volume ⁷	Ex. rapid	Rock avalanche

II. Numerical Models for the Runout Analysis

In reason of the potential damage caused by rapid landslides, some continuum dynamic models have been developed to predict the hazardous area extent from a possible risk situation of a landslide. Employing these models, it is possible to analyze the landslide runout and to obtain useful information about the flow velocity, depth, and areal distribution of the phenomenon (Sauthier et al., 2015).

These properties can be predicted by different numerical models, proposed by many authors. However, they all derive from some assumptions and equations to describe the flow movement. These equations are briefly illustrated below, and the assumptions made are discussed together with the models' description.

The motion can be analyzed by the equation of conservation of mass (Equation 9) and the equation for the momentum (equation 12) (Pirulli, 2010).

⁵ Presence or absence of a defined channel over a large part of the path, and an established deposition landform (fan). Debris flow is a recurrent phenomenon within its path, while debris avalanche is not.

⁶ Peak Discharge of the same order as that of a major flood or an accidental flood. Significant tractive forces of free flowing water. Presence of floating debris.

⁷ Volume greater than 10000 m³ approximately. Mass flow, contrasting with fragmental rock fall.

$$\frac{\delta \rho}{\delta t} + \nabla \cdot (\rho v_i) = 0 \quad (9)$$

Where v_i corresponds to the velocity vector in x, y, z directions, ρ is the mass density and:

$$\nabla \cdot (\rho v_i) = \frac{\delta \rho v_x}{\delta x} + \frac{\delta \rho v_y}{\delta y} + \frac{\delta \rho v_z}{\delta z} \quad (10)$$

Due to the incompressibility of the fluid, the mass density ρ is constant and Equation 9 becomes:

$$\nabla \cdot v_i = 0 \quad (11)$$

Meanwhile, the equation of momentum is the following, considering gravity and pressure forces in the fluid.

$$\rho \left(\frac{\delta v_i}{\delta t} + v_i \cdot \nabla v_i \right) = -\nabla \cdot \sigma + \rho g \quad (12)$$

Where σ is the Cauchy stress tensor, and g is the vector of gravitational acceleration.

Considering the hypothesis of shallow water, these previous equations can be integrated in depth to obtain the depth-averaged equations of motion (Equations 13) (Pirulli, 2010).

$$\left\{ \begin{array}{l} \frac{\delta h}{\delta t} + \frac{\delta(\overline{v_x}h)}{\delta x} + \frac{\delta(\overline{v_y}h)}{\delta y} = 0 \\ \rho \left(\frac{\delta(\overline{v_x}h)}{\delta t} + \frac{\delta(\overline{v_x^2}h)}{\delta x} + \frac{\delta(\overline{v_x v_y}h)}{\delta y} \right) = -\frac{\delta(\overline{\sigma_{xx}}h)}{\delta x} - \tau_{zx} + \rho g_x h \\ \rho \left(\frac{\delta(\overline{v_y}h)}{\delta t} + \frac{\delta(\overline{v_y v_x}h)}{\delta y} + \frac{\delta(\overline{v_y^2}h)}{\delta x} \right) = -\frac{\delta(\overline{\sigma_{yy}}h)}{\delta y} - \tau_{zy} + \rho g_y h \end{array} \right. \quad (13)$$

Where $\overline{v_x}$ and $\overline{v_y}$ correspond to the depth-averaged flow velocities in x, y directions, h is the flow depth, $\overline{\sigma_{xx}}$ and $\overline{\sigma_{yy}}$ are the depth-averaged normal stresses, and g_x and g_y are the projection of the gravity vector (Pirulli, 2010). Furthermore, τ_{zx} and τ_{zy} are the shear resistance stresses, or the basal shear resistance T , which is the term related to the complex rheology of the granular material (Pirulli, 2005).

The use of a continuum approach makes the solid-fluid mixture to be considered as a homogeneous continuum, whose rheological properties are similar to the real behavior of the flow (Pirulli, 2010). This is related to the assumption that the depth and length of the flowing

mass are large compared to the dimensions of a typical particle composing the granular material (Pirulli, 2005).

The flowing material is composed of a liquid phase, made up of water and finer grain fractions, and a solid phase composed of coarser grain fractions. Thus, two different approaches can be considered when modeling the flow: a two-phase model, which treats separately the solids and the interstitial fluid, and a single-phase model (Fraccarollo & Papa, 2000), which consider the behavior of the entire fluid-solid mixture (Pirulli et al., 2017). The single-phase model is often used for modeling muddy debris flows, meanwhile, the two-phase model is more common to be used for modeling granular or clay-poor debris flows (Remaître et al., 2005).

Hungr proposed a model called Dynamic Analysis (DAN), where he substitutes the real moving mass with an equivalent fluid (Figure 27), with similar bulk properties, such as external shape and mean velocity. The constitutive behavior can be determined by the Back-Analysis of a real case (Hungr, 1995).

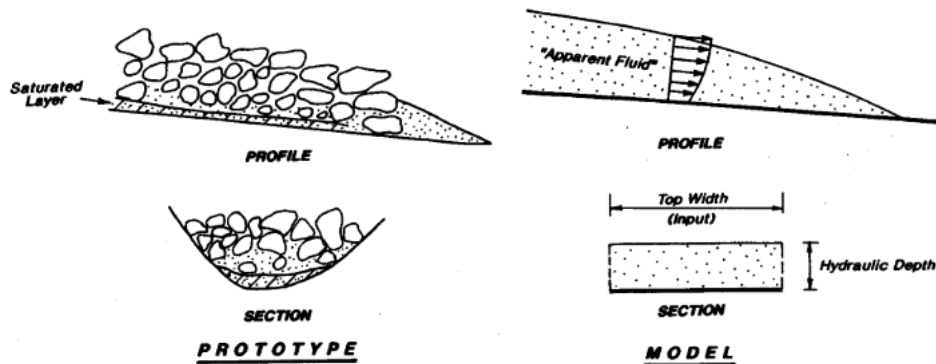


Figure 27 - Modelling of a flow as a homogeneous apparent fluid, with velocity profile dependent on the chosen rheology (Hungr, 1995).

Briefly, the fluid is divided into blocks contacting each other, free to deform and represented by a moving mesh and Lagrangian curvilinear reference frame. The forces acting on each boundary block are the tangential component of weight, the tangential internal pressure resultant P , and the basal flow resisting force T (Figure 28). The flow resistance term T and the velocity-depth distribution profile depend on the rheology of the material and they are a function of other parameters of the flow, due to the assumption that the shear stress on tangential planes increases linearly with normal depth (Hungr, 1995).

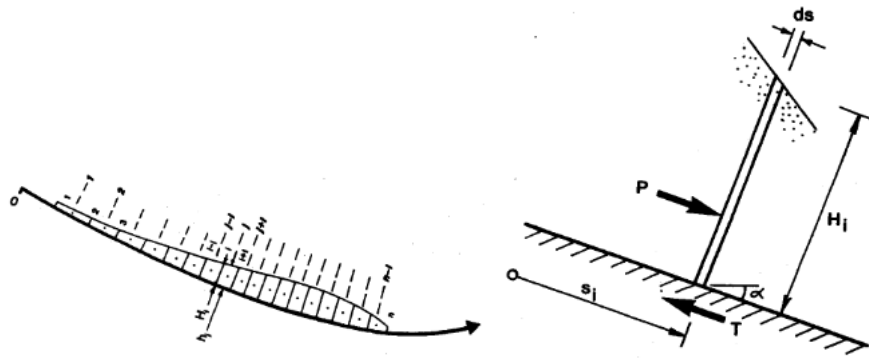


Figure 28 - Blocks representing the fluid and the forces acting on each block.

Besides Hungr, many authors have proposed models to study the debris flows, and more generally, granular flows. Among those, there is the analysis made by Savage and Hutter for the simulation of granular flows on a gentle slope, with the material considered as an incompressible continuum. In both models, it is assumed that the density of the granular flow is constant, the effects of sidewall and erosion are not considered, and the granular material remains shallow during flow. As a consequence of these hypotheses, the velocity profile is perpendicular to the flow direction and assumed to be uniform, and, the interaction between the granular material and the bed can be described by the Coulomb Frictional Law, with constant friction coefficient (Fei et al., 2012).

As hungr did in his DAN model, Savage and Hutter considered a system of depth-averaged differential equations for shallow-water (Leonardi, 2015), in a one-dimensional framing and belonging to continuum mechanics (Pirulli, 2010). The consideration of a shallow water flow means that the flow depth is small compared to the length of the channel. The one-dimensional models well describe the channeled flows and the contribution of shear stress on the rigid boundary is obtained in analogy with the case of a uniform flow having the same depth and mean velocity (Fraccarollo & Papa, 2000).

Some other hypotheses incorporated by the models are that the volume mass is volume-preserving, cohesionless, incompressible, and both the deforming mass and the sliding basal surface obey the Mohr-Coulomb yield criterion, characterized by internal (ϕ) and bed (φ) friction angles, respectively (Pirulli, 2005).

These models well simulate the granular flow in gentle slopes, but the assumptions above mentioned and the consideration of the uniform distribution of the grains simplify the problem in a way that limits its applicability. Generally, granular flows are constituted by various sizes of particles, which may lead to segregation (Fei et al., 2012), where large grains tend to move

towards the surface and the small ones tend to accumulate in the bottom. This phenomenon originates regions with different solid concentration, culminating in different regimes within the flow (Leonardi, 2015).

Finally, the RASH 3D code uses a continuum mechanics approach and it is based on a single-phase integrated solution of the Saint Venant equations considering shallow water flow, as discussed above for the other models. Therefore, the behavior of the moving mass can be described using the depth-averaged balance equations of mass and momentum (Equations 13) (Sauthier et al., 2015).

Moreover, as in the DAN model from Hungr, the heterogeneous mass is replaced by an incompressible equivalent fluid (Figure 27), and the rheology of the material is described by the basal shear resistance T (Figure 28), developed in the interface between the moving mass and the slide surface. However, differing from the last-mentioned models, the RASH 3D uses an Eulerian reference frame (Sauthier et al., 2015), which is fixed in the space, contrary to the Lagrangian, which origin is moving attached to the moving mass (Pirulli, 2005).

Even if the Lagrangian reference frame makes it possible to analyze internal strain of the moving mass, due to stretching in the path, the Eulerian allows to have a detailed overview of the displacement and the general behavior of the mass, and it is less computational demanding (Pirulli, 2005). Besides that, the apparent fluid is represented by a triangular mesh, whose behavior is analyzed using a finite volume approach (Sauthier et al., 2015).

III. Rheological Laws to describe the behavior of the flow

After the selection of the numerical model to reproduce the phenomenon under analysis, it is necessary to define the rheological law to describe the evolution of the flow.

The rheology considered is the key element to determine the behavior of the landslide, making it possible to obtain its velocity, degree of longitudinal spreading, and the distribution of deposits along the path. Each rheology is characterized by a different constitutive relationship and some parameters (Pirulli, 2005).

The rheological parameters used in the numerical models can be previously measured and used as an input or, they can be determined by calibration through the processes of back-analysis. In the first case, the landslide dynamics are described by constitutive relationships, which are a function of intrinsic properties of the material, measured by independent methods. This

process can be extremely challenging due to the complexity or impossibility of measuring properties during landslide runout flows, and these properties may also change along the path (McDougall et al., 2008).

On the other hand, in the calibration-based approach, the parameters are determined by an iterative process of trial-and-error, where the values are adjusted until the simulation can match what occurred in full-scale prototype events. Commonly, this method uses as a reference the travel distance, velocities, and the extent and depth of the deposits. The same constitutive relationships of the first method can be used in the calibration process (McDougall et al., 2008).

Among the Rheologies presented by Hungr to describe the motion, three are going to be discussed here: 1) Frictional Flow, where T is a function of the effective normal stress on the base of the flow, exclusively; 2) Voellmy Fluid, where T is a function of the basal friction φ and turbulence term ξ , given in dimensions of acceleration; 3) Bingham Flow, where T is a function of the flow depth, velocity, constant yield strength τ_y , and Bingham viscosity μ (Hungr, 1995). Nonetheless, it is necessary to consider that the debris flow may change from one regime to another during the runout (Pirulli, 2010).

Depending on the velocities and on the granulometry characterizing the flow, its nature can be laminar or turbulent, the latter more appropriate for higher velocities and coarse-grained debris flows or granular debris flows, influenced by grain collisions. However, this simple regime distinguishing is not enough for describing the entire motion, and it is necessary to add a friction term to analyze the cessation of the movement. Thus, the Frictional Rheology can be accounted for by obtaining the value of resisting shear stress, which is dependent on the normal stress only, and it is given by equation 3 (Pirulli, 2010).

$$\tau_{zi} = (\rho \cdot g_z \cdot h \cdot \tan\varphi) \cdot \text{sgn}(\bar{v}_i) \quad \text{for } i = x, y \quad (3)$$

Where ρ is the bulk density of the material, g_z is the normal projection to the slope of the gravity acceleration, h is the height of the flowing mass, \bar{v}_i are the depth-averaged velocity in x and y direction and φ is the bulk basal friction angle (Pirulli, 2010). Besides, the sgn is a function that defines the sign of the velocity vector \bar{v}_i , and it is related to the basal friction angle φ and the angle α , representing the topography of the sliding surface (Figure 28). If $\tan\varphi < \tan\alpha$, the fluid never stops on the inclined plane and the $\text{sgn}(\bar{v}_i) = -1$; in the opposite case, the fluid may stop and the values of the Coulomb friction law are not continuous, being

necessary to impose some criterion depending on the force balance, when the fluid stops (Mangeney et al., 2000).

The Voellmy rheology instead is characterized by two resistive force contributions, one related to the shear force that is proportional to the normal force and another related to viscosity, in which the drag is proportional to the velocity squared (Quan Luna et al., 2013). It adds to the frictional rheology a turbulent term related to all the resistance factors influenced by velocity. The resisting shear stress is given by equation 4 (Pirulli, 2010).

$$\tau_{zi} = - \left(\rho \cdot g_z \cdot h \cdot \tan\varphi + \frac{\rho g \bar{v}_i}{\xi} \right) \cdot \text{sgn}(\bar{v}_i) \quad \text{for } i = x, y \quad (4)$$

The main parameters of a Voellmy fluid are the Coulomb basal friction coefficient μ , which describes the stopping mechanism, and the turbulence coefficient ξ (m/s^2), which accounts for velocity-dependent friction losses. These constants are dependent on the flow properties and the roughness of the flow surface (Quan Luna et al., 2013) (Pirulli et al., 2017).

Schaerer suggests the following values of the turbulence coefficient according to the flow surface and based on field observations (M. Donnelly & L. Barger, 1977):

- Smooth snow cover, no trees: 1200-1800 m/s^2
- Average, open mountain slope: 500-750 m/s^2
- Average gully: 400-600 m/s^2
- Slope with Boulder, trees, forests: 150-300 m/s^2

According to Jeyapalan et al., 1983, the majority of the studies of tailings deposits indicates that the flow will be laminar in nature and the behavior of the liquified tailings can be described by the Bingham rheology, which is characterized by yield stress and viscous flow characteristics once the yielding is reached (Pirulli, 2017). In fact, rheological flows are characterized by the dependence of viscosity on the strain rates within the fluid (Lumbroso et al., 2020).

The Bingham fluid presents plastic and viscous behavior, which is characterized as a rigid material below a threshold yield strength, and as viscous material above this limit value (Pirulli et al., 2017). The parameters describing the rheology are the yield stress (τ_y), the minimum shear stress to induce shearing in the fluid, and the plastic viscosity (μ_0), which is the

inclination given by the curve relating the shear stress τ and the shear rate $\dot{\gamma}$ tensors (Figure 29), defined by equation 5 (Leonardi, 2015).

$$\begin{cases} \dot{\gamma} = 0 & \text{for } \tau < \tau_y \\ \tau = \tau_y + \mu_0 \cdot \dot{\gamma} & \text{for } \tau > \tau_y \end{cases} \quad (5)$$

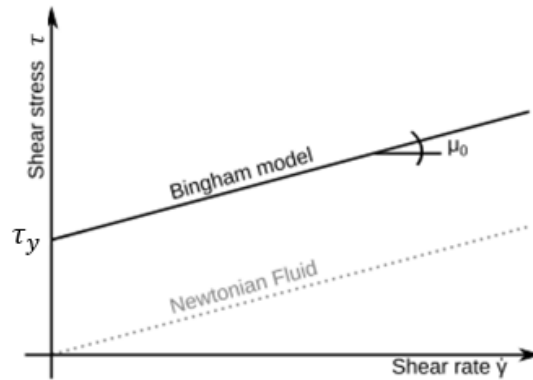


Figure 29 - Curve representing the Bingham model (adapted from Leonardi, 2015).

Moreover, the fluid can be classified as a function of viscosity μ as Newtonian, for which viscosity is constant, regardless of temperature and pressure values; and as Non-Newtonian, with viscosity varying according to quantities related to shear stress (or squared velocity, these terms are inversely proportional) and time. The latter characterizes all the rheologies discussed previously. If the viscosity decreases as the shear strain rate increases, the fluid is Pseudo-Plastic, if it increases, it is Dilatant. In Bingham rheology, when the yield shear strength is null, the fluid becomes Newtonian (Figure 30) (Pirulli, 2005).

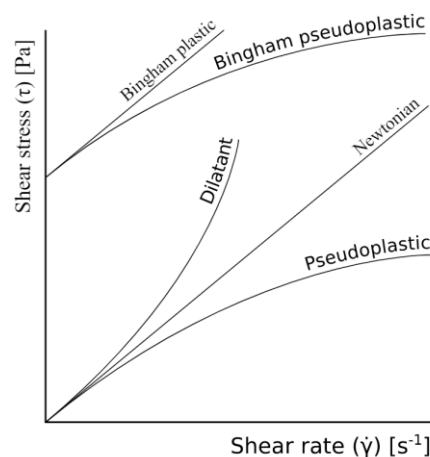


Figure 30 - Common rheologies for fluids.

3. Classification of the Tailings Flow of Brumadinho Dam Collapse

The flow originated after the collapse of the tailings dam in Brumadinho can be classified using the different methods described in section I. Each one of them can be evaluated separately, and after, the results can be compared to achieve a final classification of the material.

3.1 Takahashi Classification (2014)

This classification is described in

Table 2, and it is based on some properties concerning the destructive power of the flow, such as the magnitude, the velocity, the arrival distance, and the equivalent friction coefficient.

- Magnitude

The dam total capacity before the breaching was about 12 million m³, and, as stated before, the volume release after the collapse reached 9.7 million m³. Therefore, the magnitude of the phenomenon is in the range of 10⁷ m³, characterizing a debris avalanche.

- Velocity

The velocity registered in the subsequent moments after the collapse was close to 80 km/h, and it lost pace along the path until it reached the river Paraopeba. There is no further information published about the velocity of the runout, however, based on the range of the initial velocity (approximately 20 m/s), the flow may be started as a debris avalanche and during the path, it has become a debris flow or it has been a debris flow the entire phenomenon.

- Arrival distance

According to satellite images and digital maps of the extension and shape of the runout, the travel distance was about 8.6 km along the path (white line) or about 5.7 km if crossed a straight line (yellow line), from the position of the dam until the Paraopeba river (Figure 31).



Figure 31 - Travel distance of the tailing flow in Brumadinho.

In this way, the arrival distance can be considered in the range of 10 km, approximately, and then, the runout can be classified as a debris flow.

- Equivalent friction coefficient

There are no available data in the literature about the equivalent friction coefficient.

Finally, Table 6 summarizes the Takahashi classification according to the factors under analysis.

Table 6 - Takahashi's Classification of the Brumadinho runout

	Magnitude (m³)	Velocity (m/s)	Arrival distance (km)	Equivalent friction coefficient
Phenomenon	10 ⁷ m ³ : Debris avalanche	Initially 20 m/sec: Debris avalanche or debris flow	About 9 km: Debris flow	-

Thus, the runout probably started as a debris avalanche, due to the volume released (approximately 10⁷ m³), and the initial velocity (about 20 m/s), while along the path, it has been altered to debris flow, according to the reduction of velocity and the arrival distance (about 10 km).

3.2 Varnes (1978) and Cruden and Varnes (1976) Classifications

These classification methods are organized in Table 3 and

Table 4, and they are related to the material and velocity of the moving mass.

- Material

This factor is analyzed based on the concentration of sand and fine material in the mass, nonetheless, these quantities are difficult to estimate in the conditions of a landslide hazard. As a usual composition, tailings, resultant of mining waste, are composed of mixtures of crushed rock and fluids from the mining processes (Pirulli et al., 2017), with low permeability and cohesionless.

Nonetheless, the geotechnical characterization of the tailings has been done some years before the collapse, and the material was defined as a uniform fine silty sand with 99% of sand and

fine material. In this way, the flow is in the category of Earth, with a concentration of sand and fines higher than 80%.

- Velocity

Considering what has been discussed about velocity in the previous classification, the rate of movement was higher than 1.5m/day, characterizing wet sand and silt flow, rapid earth flow, loess flow, or dry sand flow. According to the latter modification proposed in 1996, the moving mass is in the velocity class 7, classified as extremely rapid.

Afterward, Table 7 summarizes what has been discussed in this classification method.

Then, the moving mass, according to Varnes and Cruden and Varnes’s methods, can be characterized as an extremely rapid phenomenon, which is inside the earth category regarding the material, and not debris, as concluded by the previous classification, which did not take into account the constitutive material of the mass.

Table 7 - Varnes, and Cruden and Varnes Classifications of the Brumadinho runout

	Rate of movement	Material	Typical Velocity
Phenomenon	Rapid and higher (>1.5m/day)	Wet sand and silt flow Rapid earth flow Loess flow Dry sand flow	5 m/sec – extremely rapid

3.3 Hungr Classification (2001)

Based on the classification of Varnes and Cruden and Varnes only, Hungr developed a new one, considering new key aspects, as described in Table 5. These new factors involve genetic concepts and the context of each phenomenon, such as material, water content, special condition, and velocity.

- Velocity

From the previous classification, it is already known that the movement of the mass is characterized as extremely rapid. Then, categories outside this range are excluded.

- Water content

This key aspect does not contain specific and exact data concerning it, as well, however, the studies pointed that the dam collapsed due to static liquefaction, a phenomenon that occurs with a level of saturation higher than 80%. Then, the mass may be considered saturated.

- Material and special condition

Considering the information available and discussed in the previous classification, the material may be addressed in the class containing silt, sand, debris, weak rock, which is characterized by an extremely rapid velocity. The flow slide resultant from this material involves excess pore-pressure or liquefaction of the landslide source, and sorted or unsorted loose man-made fills such as mine tailings fall in this category. Even if the flow slide may be largely unsaturated and appear dry, the liquefaction can occur in a confined thin saturated basal layer. (Hungr et al., 2001).

Moreover, this phenomenon culminates in runouts with high velocity and long lengths even in gentle slopes, which is a distinguishing aspect. Then, for a better analysis, it can be verified the slope map of the terrain in the area that covers the runout (Figure 32). The slope of the terrain is measured in degrees and it is organized in different classes, represented by graduated colors. As can be seen, a great part of the area is covered by very flat slopes, mostly lower than 10 degrees, and with a maximum slope of 23 degrees. Even then, the runout reached almost 9 km of the path from the dam position until it reached the Paraopeba river.

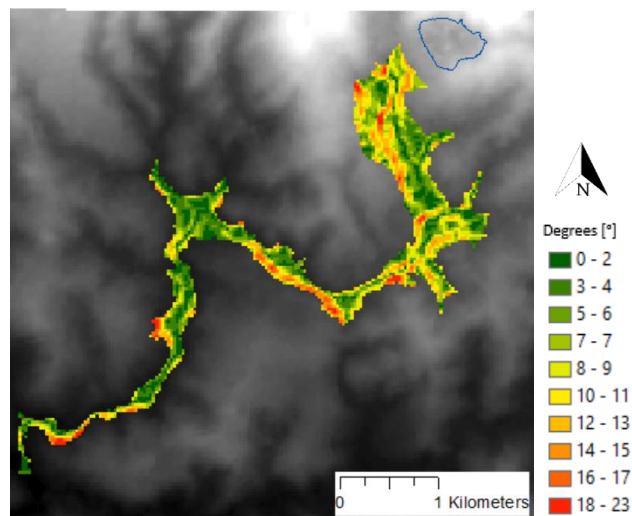


Figure 32 - Slope map of the area that covers the runout.

The runout can also be compared to past events, in terms of the textural composition of the material, using the Ternary diagram of Figure 26. Drawing the lines according to the material

composition: 32% of silt and clay, 67% of sand, and 1% of gravel, it is found the position representing the runout material. As it can be seen in Figure 33, mainly earth flows are characterized by very low gravel content as in the case of the Brumadinho runout, on the other hand, the runout presents a lower amount of fine material in comparison to most of the earth flows, being more similar to debris flows. In any case, the variability is too high to take into consideration only the granulometry of the materials.

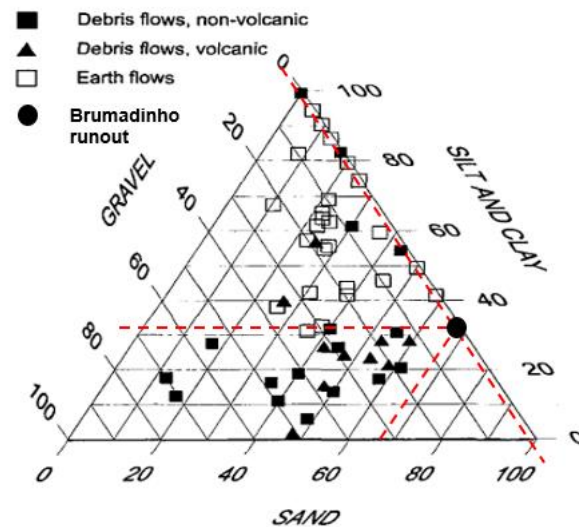


Figure 33 - Textural composition of the runout.

Moreover, it is interesting to note that liquefaction may also develop in debris flows, but this phenomenon does not occur spontaneously at the source, but during the motion along the path, with modification of the source material or entrance of new materials (Hungri et al., 2001). In the case of Brumadinho, it is known that the liquefaction occurred in the source material and it originates the flow.

Finally, Table 8 summarizes what has been discussed.

Table 8 - Hungri Classification of the Brumadinho runout

	Material	Special condition	Velocity
Phenomenon: Sand (silt, debris, rock) Flow slide	Silt, sand, debris, weak rock	-liquefiable material, -constant water	Extremely rapid

In conclusion, according to Hungri classification, the runout is characterized by a Sand-silty-fine flow, regarding its textural granulometric composition; its origin, related to the liquefiable

source material; and the context of the landslide, which was extremely rapid even in a gentle slope terrain.

Finally, considering all the methods discussed above, it is possible to join the results in a final classification, which describes the general idea about the type of runout (Figure 34).

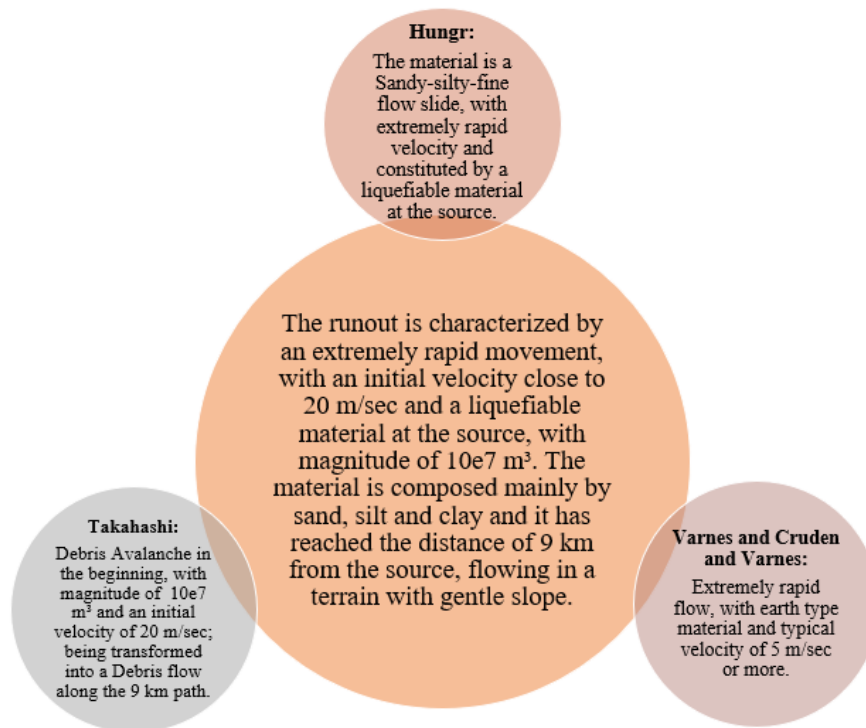


Figure 34 - Final Classification of the runout in Brumadinho.

Even if Takahashi's classification resulted in a flow constituted by debris, what has been found out as wrong in the following methods, some key aspects that define the flow have been discussed, such as the magnitude of the moving mass, in the range of 10^7 m^3 , the range of velocity with an initial value of 20 m/s, decreasing along the path, and the arrival distance of approximately 9 km.

Then, in Varnes's Classification, the material has been included as an important factor to the definition of the flow, and due to its composition of 99% of sand and fines, the possibility of debris has been excluded, according to this method. Moreover, with the latter modification proposed by Cruden and Varnes, the flow has been classified in class 7 of velocity, which means it was an extremely rapid movement.

Finally, with the classification proposed by Hungr, the method of Cruden and Varnes has been improved, considering not only the granulometric distribution of the mass but the origin and

the context involving the flow phenomena. Then, the occurrence has been classified as a sand-silty-fine flow slide, originated by a liquefiable material that with an increasing of saturation and pore-pressure culminate in the flow slide, flowing in gentle slope terrain for almost 9 km, until it reached the Paraopeba river.

4. Analysis of the Runout with RASH 3D

For the analysis of the flow originated by the dam I collapse, it was used the code RASH 3D to obtain the change in position of certain points after some intervals of time and the velocity of the movement. The mentioned points belong to a study area surrounding the phenomenon, and their position is given by coordinates x,y,z , i.e. the planar coordinates and the elevation. The initial values, corresponding to the situation before the collapse, is obtained using a Digital Elevation Model (DEM) (Figure 35) of the area of interest, with a spatial resolution of 30 meters.

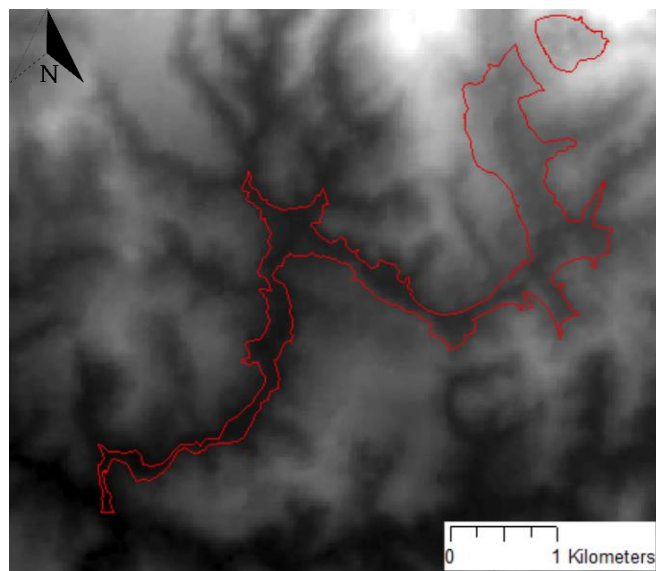


Figure 35 - Digital Elevation Model of the terrain and the contour of the damage extent.

The points and their initial coordinates are determined using the software Arcmap, where each cell of the raster, i.e. the DEM, is converted into a point. These points are positioned in the center of each cell and they carry the information about position (x, y, z) correspondent to the cell that originates them, as exemplified in Figure 36.

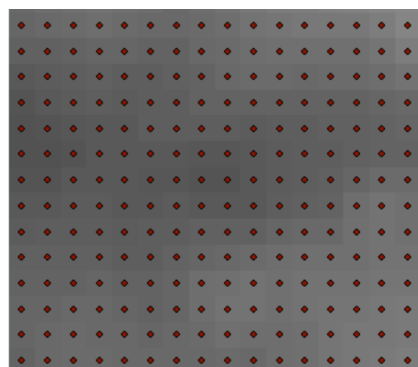


Figure 36 - Part of the DEM converted into points.

Besides the coordinates x, y, z , it is required to determine the value of height h , which corresponds to the height of the moving mass, given initially by the position of the sliding surface (Figure 37). There is no available DEM post-failure, as the one considered previously, so this value of height is not known, and, therefore, two different methods are chosen to determine it.

The first one is a simplistic approach, in which it is considered the volume of material and the area of the dam to extract the height, given as a constant value for all the points. In the second method, it is determined the slip surface of the dam slope, using the Limit Equilibrium Method in a numerical analysis, which resulted in different values of height along the surface.

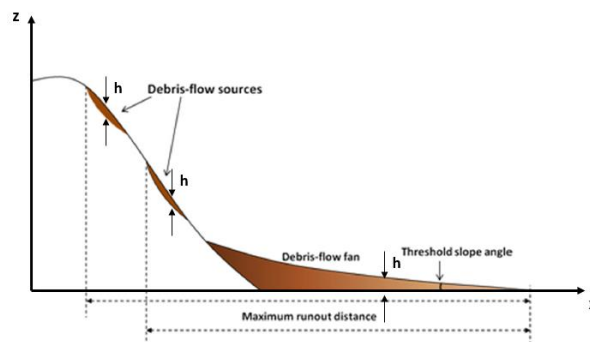


Figure 37 - Scheme of the coordinates and height h of the flow (adapted from Kritikos & Davies, 2015).

I. Determination of Height: Method I – Volume and Area Analysis

In the first attempt to determine the height, it is obtained a simplified representative value using a volume/area calculation, where it was defined the area and the volume of the detachment, and consequently the height of the moving mass. The area of the detachment was considered as the area of the top of the dam (Figure 38a), equal to 230,114 m², which is associated with a released volume of 9.7 million m³, resulting in the value H of 42.2 m (Equation 14). This value is considered constant and it is applied to all the points inside the detachment area (Figure 38b).

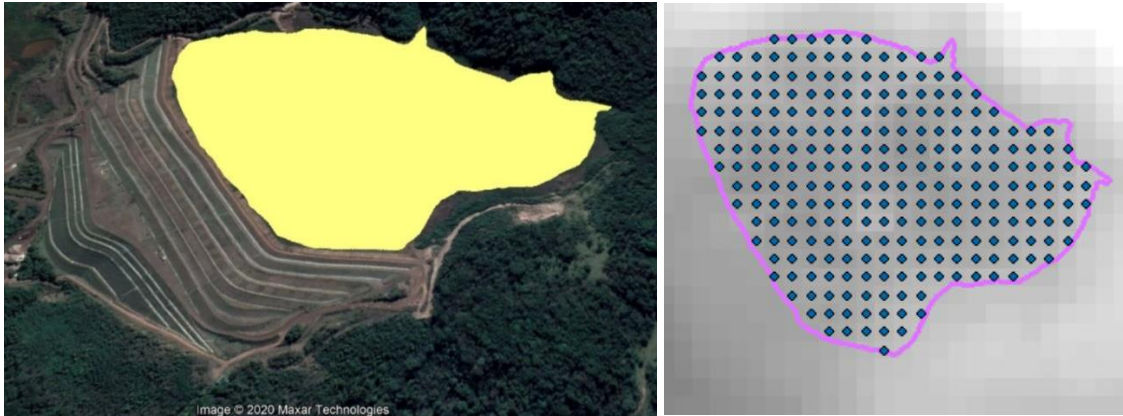


Figure 38 - a. Area of the detachment obtained using Google Earth; b. points in the detachment are for which the value of height was assigned.

$$Height = \frac{Volume}{Area} = \frac{9.7 \cdot 10^6}{230,114} = 42.2 \text{ m} \quad (14)$$

In this case, the volume of the released material was already known, since it is a post-failure analysis. However, the total volume of the dam could be used in predictive analysis, since in liquefaction of tailings, most of the material tends to become unstable, so it would be more conservative and in favor of safety to consider a release of 100% of the material.

II. Determination of Height: Method II – Slip Surface Analysis

In the second approach, the height is derived from the slip surface of the dam, obtained employing a numerical analysis in the software Slide 2. For this aim, it is used the Limit Equilibrium Method (LEM), where the potential slip surface associated with the minimum factor of safety is determined (RocScience, 2016). As discussed before, this same technique was used in predictive analysis to verify the stability of the dam.

The first thing to be done is to define the model that represents the medium that is going to be analyzed, and for that, it is used as a basis the model illustrated in Figure 22, which represents the most solicited cross-section found in the analysis of the stability study performed before the collapse. The final model is illustrated in Figure 39.

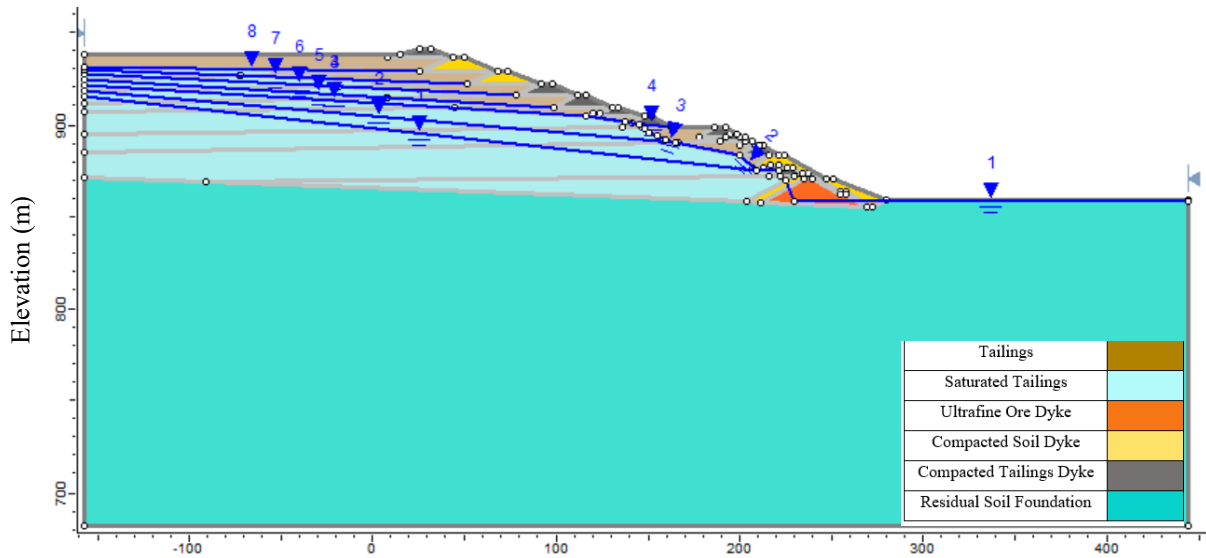


Figure 39 - Model for LEM analysis on Slide.

As discussed before, in Section 1.3, the inappropriate material deposition inside the dam created perched layers of clay material, resulting in a total of 8 layers, where each one is assigned to a different piezometric level. Moreover, the dykes are assigned to the piezometric level of the layer where they are located. In each layer, above the piezometric line, the material is considered as unsaturated tailings (brown), and below it, as saturated tailings (light blue) (Figure 40).

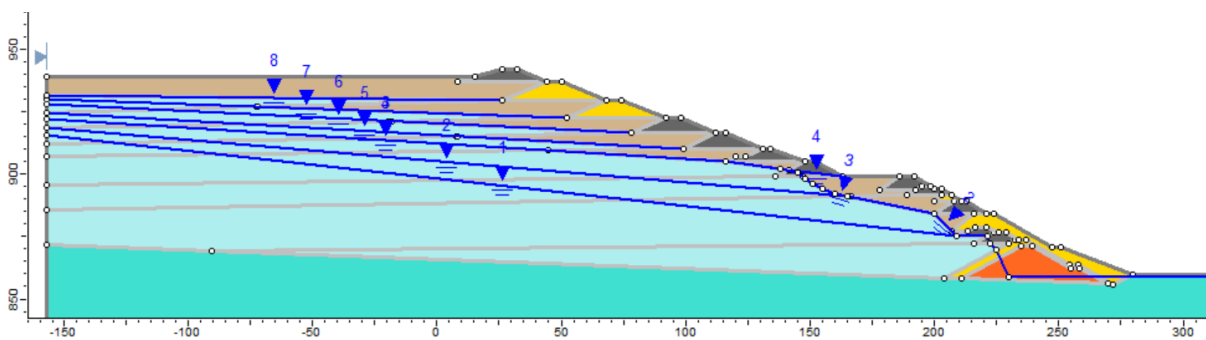


Figure 40 - Model for LEM analysis on Slide in detail.

Then, it is necessary to determine the material properties, such as the unit weight and the strength parameters: cohesion and friction angle. These values are obtained from the same study used for the model, and they were determined for the undrained condition, suitable to represent the state of the materials subjected to a possible occurrence of liquefaction. These values are shown in Table 9.

Table 9 - Material properties for undrained conditions (adapted from Vale & TUV SUD, 2018).

Material	Model's color	γ (KN/m ³)	ϕ' (degrees)	c' (KPa)	$Su/\sigma'v0$ Peak
Tailings		26	35	0	
Saturated Tailings		26			0.26
Ultrafine Ore Dyke		25	30	0	
Compacted Soil Dyke		19	30	10	
Compacted Tailings Dyke		28	37	0	
Residual Soil Foundation		20	30	16	

Usually, circular surfaces are applicable in scenarios with homogeneous slopes or simple multi-material slopes. On the other hand, some complex slopes may have almost circular slip surfaces, so this analysis is always recommended, at least, to initially identify a possible position of the surface (RocScience, 2016).

Non-circular surfaces are expected in more complex situations, in models with thin weak layers or anisotropic materials (RocScience, 2016). The Brumadinho dam is composed of tailings, which material composition is nearly regular, however, there was the formation of the perched layers that modifies the scenario under analysis. In this way, it is convenient to test both circular and non-circular slip surfaces searches and verify the results.

In Slide, there are different methods to “search” for the different slip surfaces in the slope and define the most critical one, which gives the smaller safety factor. There are methods for both circular and non-circular surfaces, using different techniques, and it is interesting to test some of them. When different methods result in a similar surface, it is a good indication that this is the critical surface.

It was considered all the search methods available for circular slip surfaces, and the two most recommended for non-circular surfaces, with which is obtained the global minimum slip surface. The Monte Carlo optimization is used to refine the search and find surfaces with an even lower factor of safety. Moreover, the approach used to obtain the surfaces was Spencer’s, which is recommended for both circular and non-circular analysis (RocScience, 2016). Figure 41 illustrates the slip surfaces obtained in the analysis, and Table 10 describes the data related to each one of them.

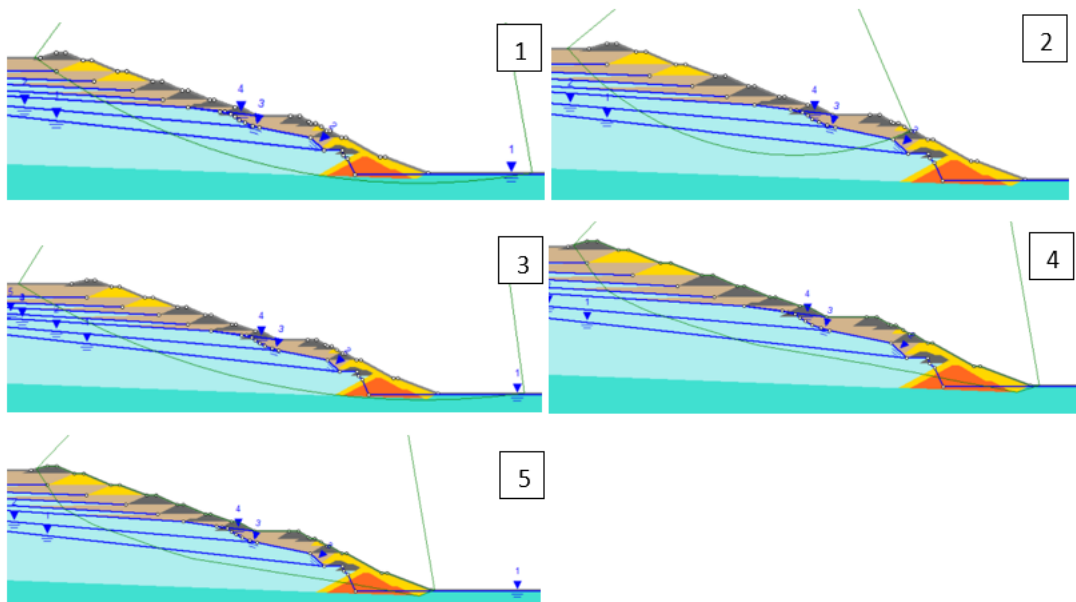


Figure 41 - Slip surfaces obtained from the Slide analysis.

Table 10 - Results from Slide analysis.

Slip Surface	Type	Search Method	LEM Approach	Safety Factor FS
1	Circular	Auto refine search	Spencer	1.189
2	Circular	Grid search	Spencer	1.187
3	Circular	Slope search	Spencer	1.177
4	Non-circular	Cuckoo search with Monte Carlo optimization	Spencer	1.036
5	Non-circular	Simulated annealing search with Monte Carlo optimization	Spencer	1.038

Observing the images in Figure 41, it is possible to note some similarities between the surfaces, regardless of the one found with the Grid Search. The Auto refined and Slope searches resulted in a similar critical surface, which involves the entire dam, and the safety factor of 1.19. The Cuckoo and Simulated Annealing searches found almost identical surfaces, also involving the entire dam, with a safety factor of 1.04.

A difference that could be pointed is that the circular surfaces cross the foundation below the starter dyke, and the non-circular ones cross the starter dyke and they end on the toe of the dam. Furthermore, in the slope search, the surface begins in the tailings, more distant from the last heightened dyke, differently in comparison to the others.

Observing the video that recorded the moment of the dam breaching, it is possible to observe that the collapse started at the top of the dam, which began to move and lower its level. Some seconds after, the effects appeared in the lower part of the dam, close to the starter dyke (Figure 42).

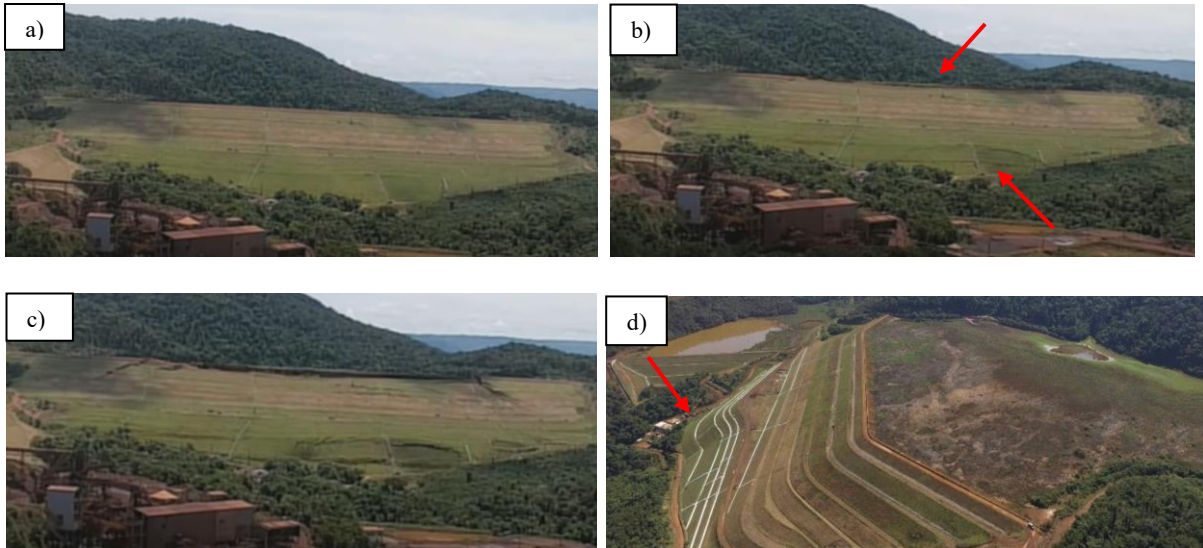


Figure 42- a),b),c) Images of the moment of the collapse, highlighting the first rupture areas in the slope, d) Indication of the place of rupture in the bottom of the dam (Youtube, 2019).

According to the images above, the collapse in the bottom part occurred, approximately, in the region pointed by the arrow in Figure 42d, which in the model corresponds to the area indicated in Figure 43.

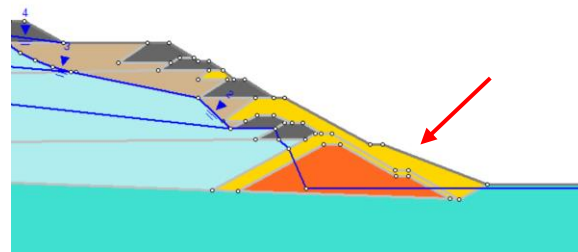


Figure 43 - Indication of the place of rupture at the bottom of the dam in the model.

These observations confirm the hypothesis that the slip surface involves all the dam, with limits in the upper part of the system and the lower part, very close to the level of the terrain. Analyzing the aerial image of the dam right after the collapse, it is possible to assume some areas where the rupture probably occurred.

Figure 44 shows the rupture distant from the last dyke, located in the middle of the tailings, between 240 and 340 meters from the crest of the dam. In this scenario, a larger amount of saturated tailings is involved by the slip surface, which makes sense in terms of liquefaction occurrence. However, in the results from the numerical analysis, the slip surfaces are very close to the crest of the dykes, and for example, in the slope search, the distance between the slip surface the dyke's crest is about 50 meters.

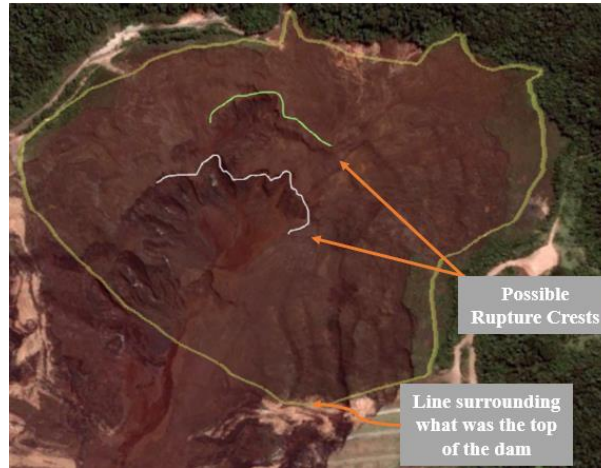


Figure 44 - Verification of possible rupture crests.

What could explain this difference is how tailings instability evolves in the process of failure. Probably, there was an initial slide correspondent to the slip surface obtained on the software, and, after some time, secondary instabilities may have occurred, when a new slip movement was formed carrying more material. This phenomenon is illustrated in Figure 45, where the surfaces represented are not the real ones and they are only used to explain the concept discussed here.

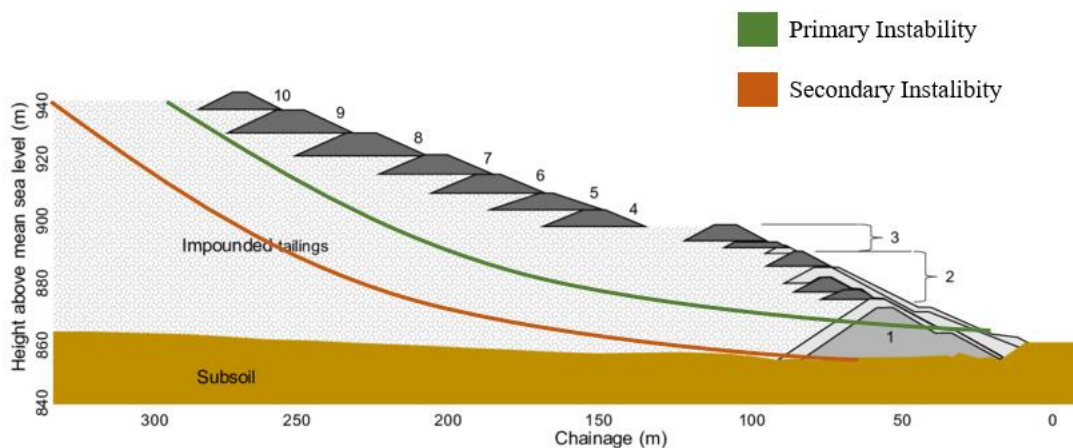


Figure 45 - Primary and secondary instabilities of tailings dam (adapted from Lumbroso et al., 2020).

In fact, the investigations carried after the failure pointed that the first failure occurred close to the crest of the dam, but it was followed by progressive failures, involving the whole dam structure and releasing more volume of tailings (Lumbroso et al., 2020). Watching the videos recorded in the moment of the collapse, it is observed that after the initial failure, the material keeps detaching from the main structure, as illustrated in Figure 46.



Figure 46 - Images of the moment of failure of Brumadinho dam (Youtube, 2019).

Considering all of this information, it was chosen the slip surface number 3 (Slope search method) to derive the values of height used in RASH3D, since is the only one that starts in the tailings in liquefaction and it involves all the dam, even if the safety factor was not the lowest value found, being prioritized the shape of the curve. The vertical slices of the stability analysis are illustrated in Figure 47, and from each of them is considered an average value of height.

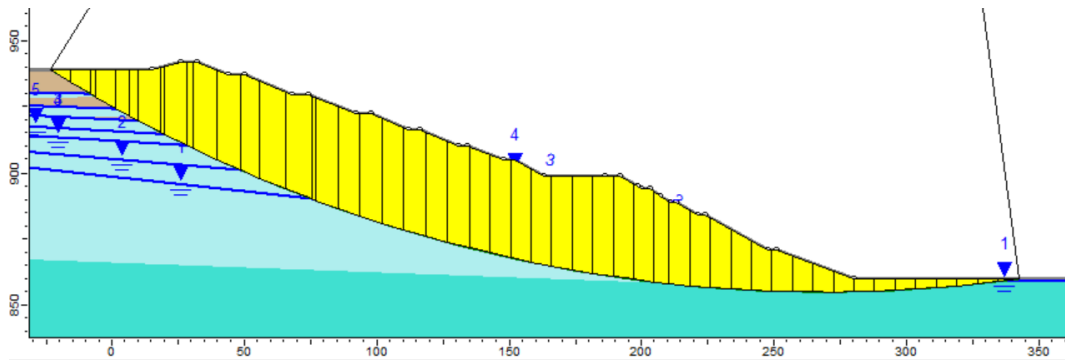


Figure 47 - Vertical Slices from LEM analysis.

These slices are drawn in the plan view, determining a detachment area, and the points inside the slices are assigned with the corresponding value of height (Figure 48). As discussed before, the values of height are not constant for the entire slope, as in the first method, but they vary along the surface according to the slices.

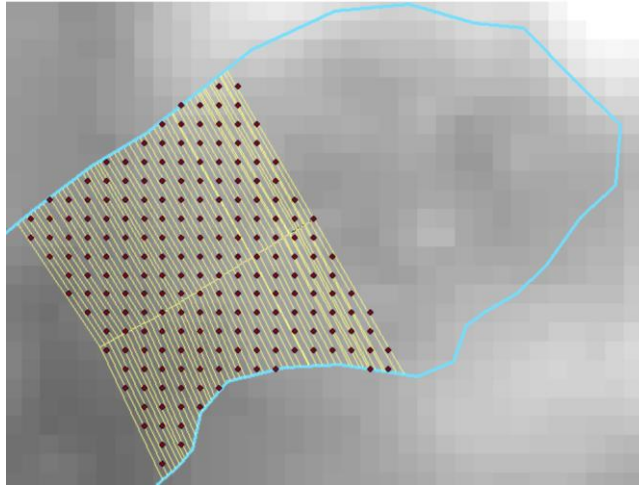
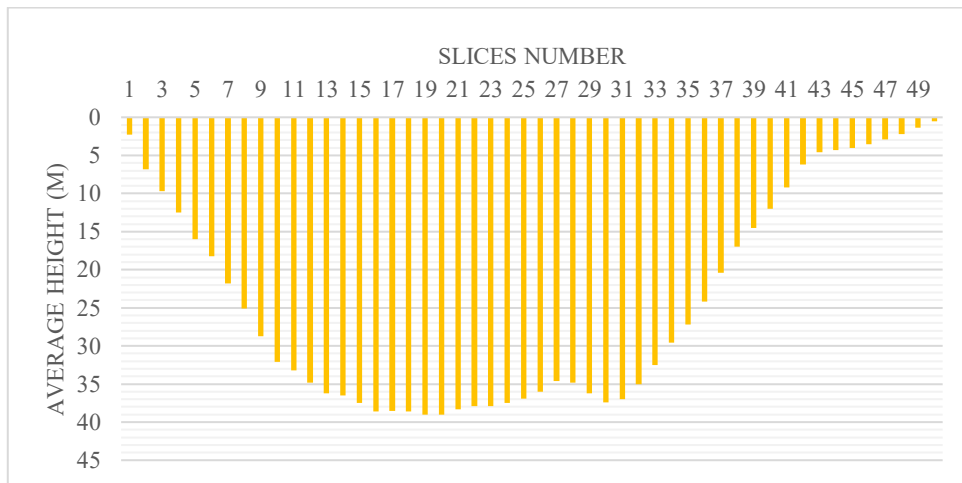


Figure 48 - Detachment area derived from the slices of Slide analysis.

In this case, the maximum value of height was 39 meters and the minimum, 0.5 meters. Graphic 1 summarizes all the values of average height considered for the 50 vertical slices resultant from the LEM analysis on Slide.

Graphic 1 - Values of height derived from the vertical slices of LEM on Slide.



The correspondent released volume is obtained by taking the area between the slip surface and the surface of the dam and multiplying it by an average width, giving a value of, approximately, 4 million m³ (almost 60% of reduction in volume). Therefore, even if this approach is more robust since it considers a numerical analysis to obtain the slip surface, it is not possible to reproduce the occurrence of a secondary instability as discussed previously. Then, for this specific problem, it is observed a significative underestimation of the released volume, being less reliable in comparison to the previous method.

The most important point to consider from the Slide analysis, which is a prediction of what could happen in reality, is that in the condition where the tailings reach their maximum peak

undrained resistance, the safety factor becomes almost 1, with the slip surface involving a large portion of the saturated tailings, mostly in the bottom part. Then, even if the results are not reproducing the entire phenomenon correctly, it is a good indication that instability may occur in some way, given certain conditions of the materials involved.

To summarize and conclude this topic, the input data for the RASH3D code are given by the initial coordinates x , y , z , h of the points, the duration of the analysis, the intervals of time to be analyzed, and the parameters corresponding to the chosen rheology. These parameters are unknown and must be determined by a calibration process of trial and error until the results are reasonable and similar to what happened in reality.

The results will be compared to the known data such as the shape of the damage extent, the duration of the phenomenon, and the maximum velocity reached at the beginning of the collapse. According to official reports about the occurrence, the collapse started at 12:28:30", when the B1 dam formed giant waves of tailings with an initial velocity close to 22 m/s and lost pace during the flow. Finally, it has reached the river Paraobeba at 15:50.

4.1 Results and Discussion

The analyses are performed using RASH 3D code, with which is possible to test different rheologies, such as frictional and Voellmy, whose intrinsic parameters are the basal friction angle (φ), for both, and the turbulence coefficient (ξ), for the latter only; and also Bingham, whose parameters are the yield stress (τ_y) and the plastic viscosity (μ_0).

However, after performing the simulations for the frictional rheology, the results were not good and did not match the occurrence in any aspect, so they are not going to be discussed here. This may be related to the fact that this rheology only considers the resisting contribution from the normal force at the base, being a bit simplistic in comparison to other rheologies.

Then, for Voellmy and Bingham, different values of parameters were used until the simulation properly matched the real phenomenon, in a calibration process. The first registration time was 0.00 seconds, the last was 12,000 seconds (the phenomenon lasted 12,150 seconds or 3 hours and 22 minutes), and the interval between registrations was 500 seconds.

The results are described below, at different intervals of time, and each point of the flow is classified according to their maximum height (H_{max}), in meters, during the runout; it was used a total of 10 classes, distinguished by graduated colors. Moreover, a threshold value of height

was selected for the representation of results, equal to 0.01m, so only points with a height greater than this value are going to be shown. This is used since RASH3D tends to enlarge the runout using points with very small heights, so a minimum value can be chosen to visualize the most significant points representing the runout movement.

I. Voellmy Rheology: Method I – Volume and Area analysis

For the Voellmy rheology, it is necessary to verify different values of the basal friction angle and the turbulence coefficient to find out which quantities better describe the phenomenon. Therefore, it is analyzed the individual influence of each of these parameters on the material behavior, varying them, separately, until the movement is properly reproduced.

Concerning the basal friction angle, it is possible to obtain a first idea of the range of values that can be used by verifying the slope map of the terrain, in degrees, since the Coulomb basal friction angle should be lower than the terrain slope to allow sliding. This map was already shown in Figure 32, where it is observed that, inside the flow path, low values of slope degree (represented by green colors) are predominant in the terrain.

It is possible to determine the maximum, minimum, and average values, and the distribution along the area of study.

- Minimum: 0
- Maximum: 23.27°
- Average: 6.84°
- Standard Deviation: 4.07°

Therefore, the first attempts may consider values of basal friction angle close to $6.84^\circ - 4.07^\circ = 2.77^\circ$, and, depending on the results, this value can be increased or decreased.

Running the simulations, it was observed that only very low values of basal friction angle ($\varphi < 1.0^\circ$) led to satisfactory results, which followed a similar path in comparison to reality. For higher values of this parameter, the flow stops very distantly from the final position it should reach. So, reducing the basal friction angle, the reached distance is greater for the same interval of time. The very small values of friction angle indicate that the friction between the tailings and the terrain is practically null, so the runout would depend only on the turbulence coefficient.

As a matter of fact, using a null value of friction angle, the runout follows its path correctly, but it reaches the final position in an interval of time smaller than the real one: $t=2000s$, when it should be around $t=12000s$. Therefore, the value of friction is fixed at 0.4° in order to adjust the duration of the phenomenon.

This specific situation can be related to the nature of liquified tailings, whose friction mobilization is very low. In fact, for the transmission of Coulomb friction stress, it is required a large enough solid concentration to ensure that the particles are always in contact, even if their relative positions change in time (Pirulli et al., 2017). Looking at the video that recorded the collapse and part of the runout movement, it is observed that the flow is very liquid (Figure 49).



Figure 49 - Real flow after the collapse (Youtube, 2019).

In terms of turbulence coefficient, a wide range of values was tested, from 1000 to 2000 m/s^2 , as used for other phenomena modeling, such as the Stava Valley case (Pirulli et al., 2017). It was observed that the path is practically the same for each of them, and the main influence is on the velocity of the material. The greater the turbulence coefficient, the greater are the velocities. All the results discussed in these last paragraphs are illustrated in Figure 50.

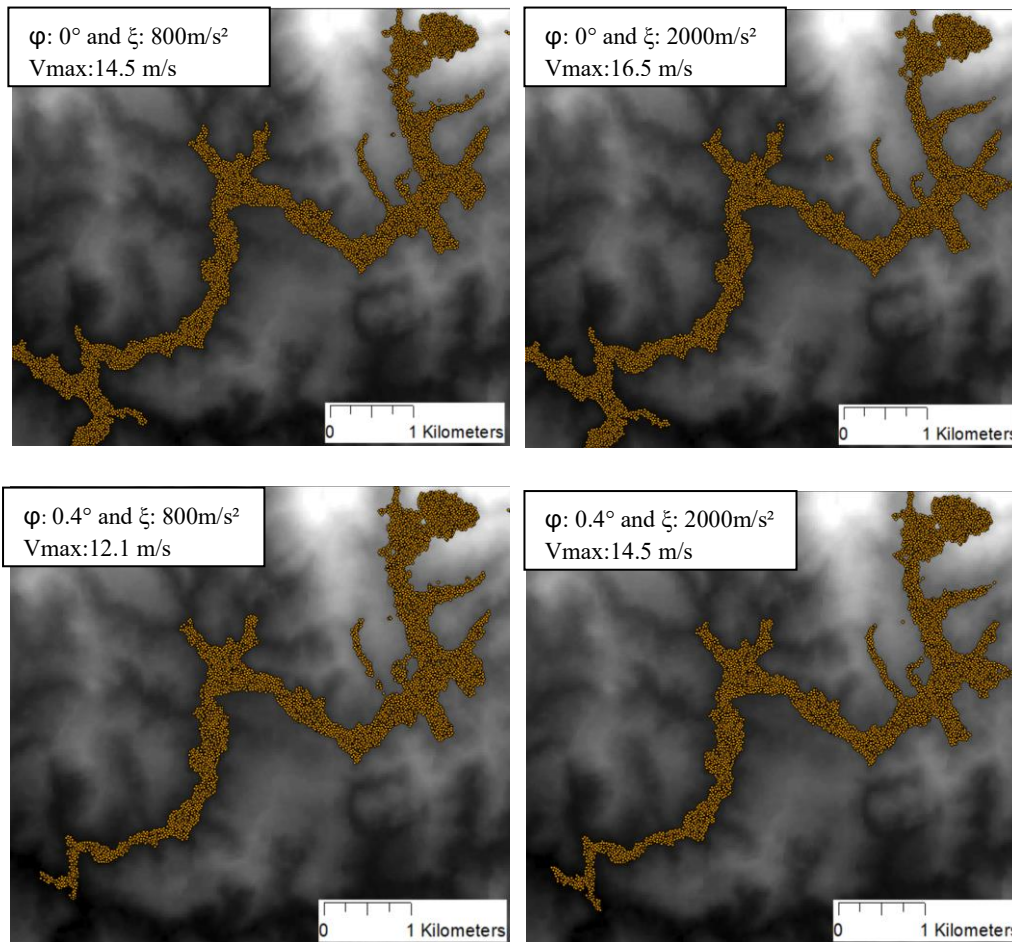


Figure 50 - Results of Voellmy Calibration (method I).

Finally, the simulation that better fits the phenomenon is chosen as the one with $\varphi: 0.4^\circ$ and $\xi: 2000\text{m/s}^2$, since it shows a greater value of maximum velocity $V_{\text{max}}: 14.5 \text{ m/s}$ and the duration is similar to the real one. Even if this simulation has a greater value of velocity, it is yet quite smaller in comparison to the maximum value, reported in the news, around 22 m/s . However, since this value has no scientific support or more accurate data about it, the velocity profile is not going to be used for the comparison with the real phenomenon. The development of the flow over the terrain is illustrated in Figure 51 at different intervals of time.

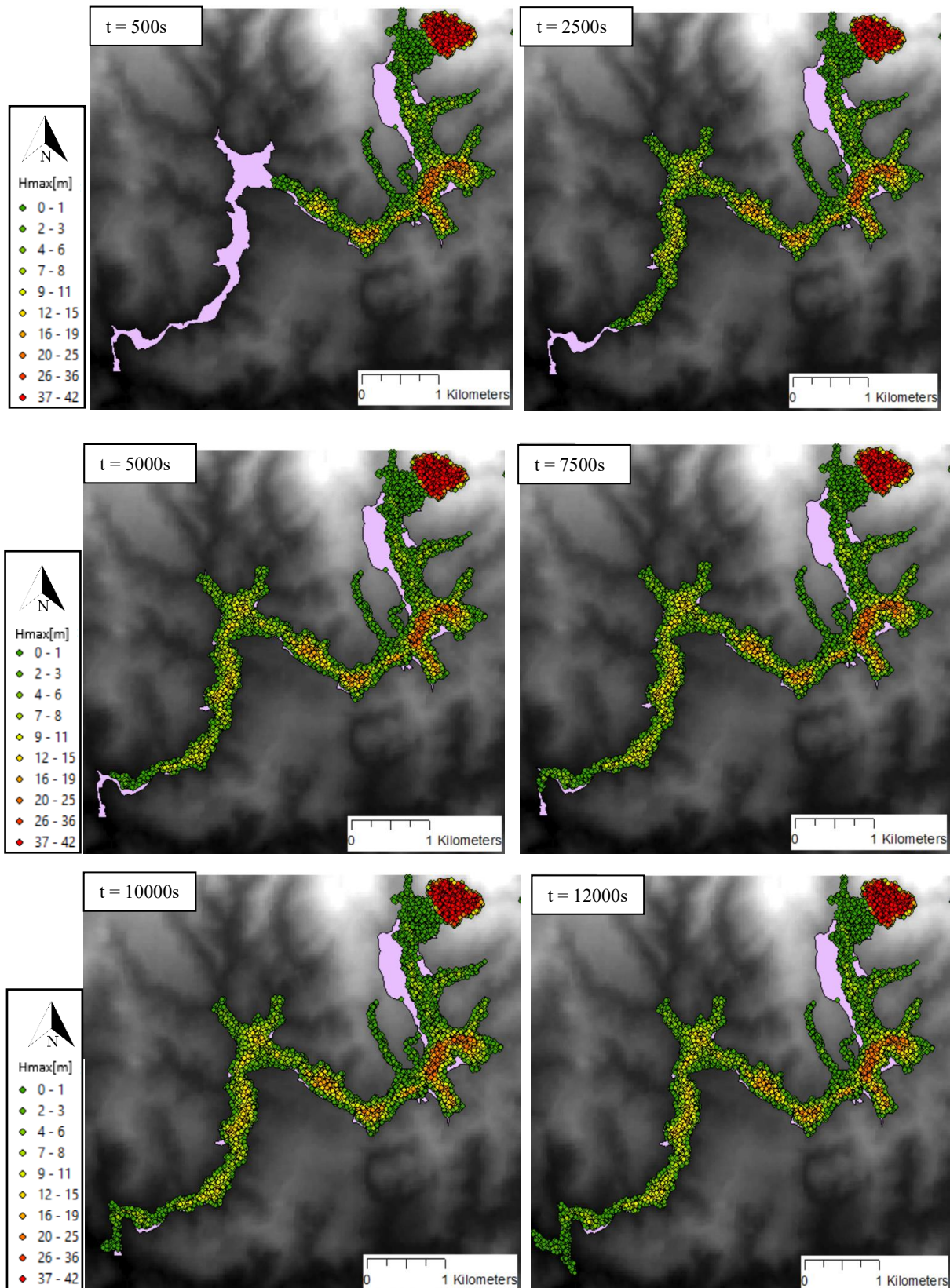


Figure 51 - Results of simulation with Voellmy Rheology (method I), $\varphi = 0.4^\circ$ and $\xi = 2000 \text{ m/s}^2$.

In this simulation, between t:10000 and t:12000 seconds, the flow reaches the river Paraopeba, completing the trajectory. In terms of shape, it can be observed that the simulation resembles

the real path, and the areas that are not covered by the points are correspondent to a maximum height below the threshold. The maximum depth of the runout along the path was about 24 m, in the region where orange to red points are observed, close to the first main curve.

Observing the evolution of the runout through time in the simulation, it is noted that a great distance is reached at only $t:2500s$ (or 42 min) and the flow completes its path along the remaining time. The satellite image of the area (Figure 52) shows that at this time interval the flow reached the Village of Brumadinho with a settlement there, and this change of the terrain occupation could have influenced the flow dynamics.



Figure 52 - Position of the flow at $t:2500s$ for Voellmy simulation (method I) (Google Earth, 2019).

In this way, it is possible to assume that the velocity of the points decreased drastically after this moment, nonetheless, this reduction is not perceptible in the velocity map of Figure 53. Looking at the velocity map created with the results of the simulation, some regions are observed with higher velocities, indicated by the arrows. On the other hand, in the last part of the path, there is a more homogeneous distribution of velocities with values lower than 5.5 m/s, located after the dashed line.

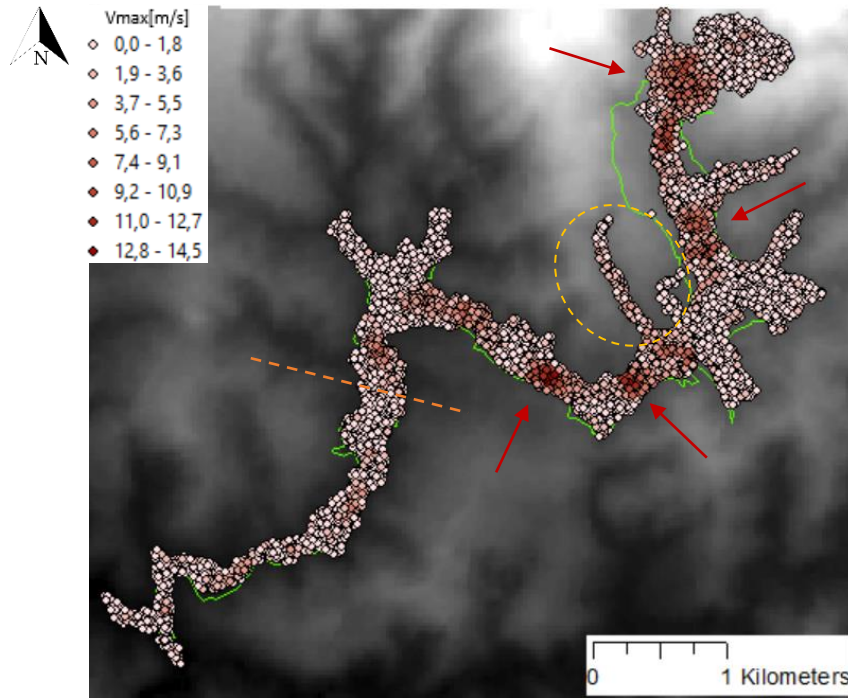


Figure 53 - Map of velocities with Voellmy Rheology (method I), $\varphi = 0.4^\circ$ and $\xi = 2000 \text{ m/s}^2$, $t=12000\text{s}$.

One observation that can be made is the creation of branches that do not exist in reality, which are highlighted by the circle in Figure 53. This element is connected to points with a maximum height below the threshold, and it could have been formed due to the influence of a possible gully in the topography.

II. Voellmy Results: Method II – Slip Surface Analysis

For this new analysis, the same calibration process was performed, starting from values similar to the ones found in the previous simulation. When the same values of parameters were applied, the runout does not complete its path in the final interval of time, which makes sense since, in this case, the volume is largely reduced (Figure 54).

As discussed before, the friction between the terrain and the flow material is practically null, and the turbulence coefficient is the parameter with a real physical value governing the phenomenon. Since in this method the position where the flow stops is not relevant, due to the volume reduction, it is used the same parameters as the previous simulation to analyze its behavior.

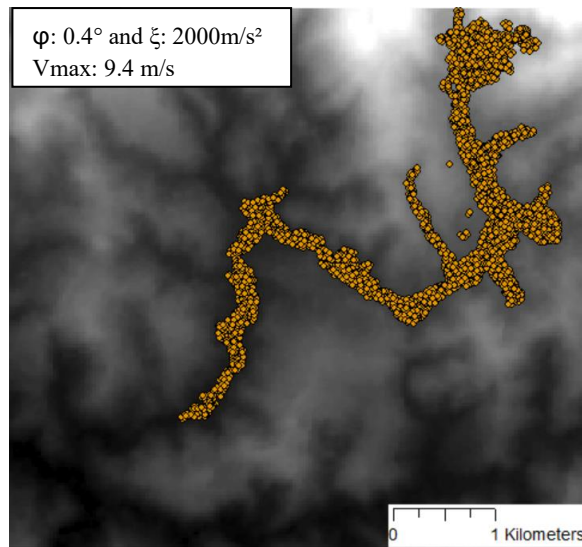


Figure 54 - Results of Voellmy calibration (method II).

It is interesting to observe that even with a significant reduction of the volume, the runout reached a great distance in the simulation with method II, stopping close to the Brumadinho Village. Therefore, even if the volume is underestimated, the damage caused by the outflow is still remarkable.

The results of the simulation time after time are shown in Figure 55.

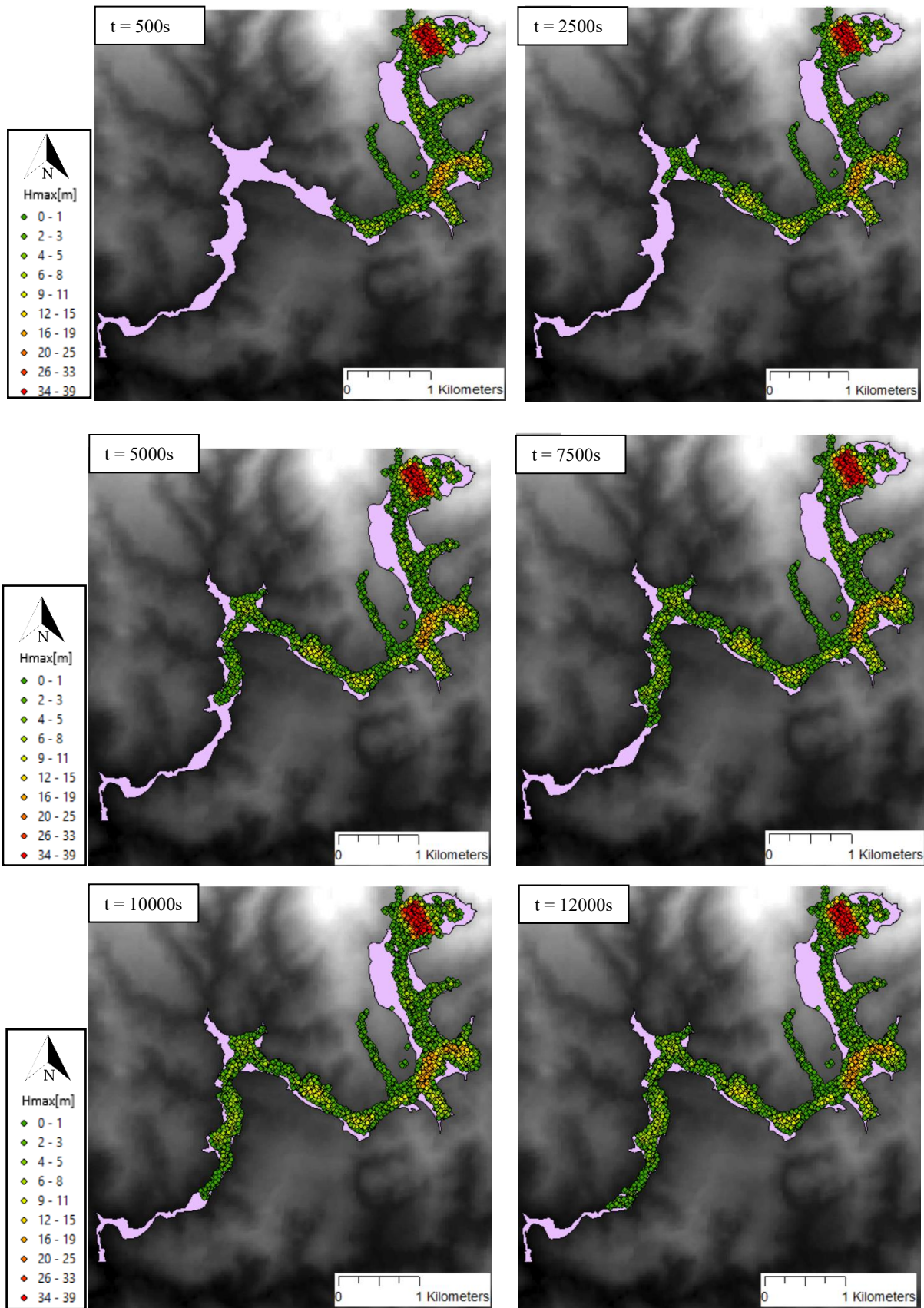


Figure 55 - Results of simulation with Voellmy Rheology (method II), $\varphi = 0.4^\circ$ and $\xi = 2000 \text{ m/s}^2$.

In terms of shape, the result is very similar to the ones obtained in the simulation for the first method, but one main difference is the position of the first detachment area, which is away from the top of the dam, considered before. This happens because the slip surface starts close to the dykes, and it is positioned below them, embracing a reduced portion of the area of the tailings. The maximum values of height were about 16 to 19 m, near the first main curve, in the same position defined by method I.

Moreover, for the earlier intervals of time, the distance reached by the flow is smaller in comparison to the previous case. This fact can be associated with the reduction of volume and of the maximum velocity of the simulation, which is 9.4 m/s. Looking at Figure 56, it is observed some regions with higher values of velocity.

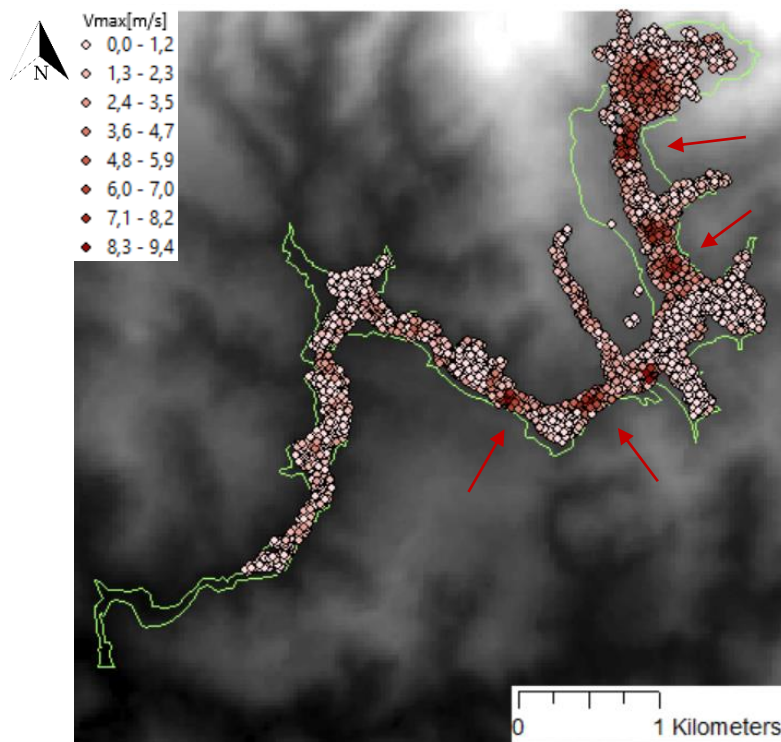


Figure 56 - Map of velocities with Voellmy Rheology (method II), $\varphi = 0.18^\circ$ and $\xi = 2000 \text{ m/s}^2$, $t=12000\text{s}$.

III. Bingham Rheology: Method I – Volume and Area analysis

After obtaining the flow path using Voellmy rheology, the Bingham rheology is applied to compare the results and verify which model better describes the phenomena.

The parameters are the yield stress (τ_y) and the plastic viscosity (μ_0), which have been altered several times until reaching values that result in a behavior more similar to reality. Each of

these values has been modified separately in order to check their individual influence in the flow. Then, it was observed that as the yield stress is reduced, the distance reached by the flow and its velocity are higher. On the other hand, if the plastic viscosity is increased, the shape of the flow, in the beginning, is better but the velocity is reduced.

In general, it was noted that the shape of the flow in the area close to the detachment is very large (more points with a maximum height above the threshold) and even if it gets thinner with an increase of plastic viscosity, the velocity reduces a lot, becoming much smaller than the maximum values registered at the beginning of the collapse. Moreover, for high values of yield stress, the flow does not reach the end of the path, stopping before it.

Thus, there was an attempt to balance the influence of both parameters to achieve a result considering the shape of the flow and the velocity, and the calibration process resulted in the following values for the Bingham parameters: $\tau_y = 50$ Pa and $\mu_0 = 250$ Pa.s. So, in this case, it is possible to state that both parameters have physical meaning, contributing to the runout behavior.

In fact, Bingham is a more rigorous method, meanwhile Voellmy is more empirical and it works better for a certain scale of the phenomenon, in a way that results are probably affected by the great volume released in the Brumadinho failure.

Some other tailings dam failure modeling, such as the Stava Valley case, in Italy, used much higher values of yield stress, around 1000 to 2000 Pa (Pirulli et al., 2017). However, if these values were used in the simulation, the distance reached by the flow would be extremely low, and the path would stop close to the detachment area. Therefore, the yield stress, i.e. the minimum value of shear stress that induces shear strains, for this case specifically needs to be reduced.

These values used for Stava Valley failure were based on an analysis of a gypsum tailings impoundment in Texas, and, in that case, the volume released was about 100,000 m³, which reached a height of 11 m when the collapse occurred, and followed a total distance of 300 m with an average velocity of 2.5 to 5 m/s. Besides that, the runout was modeled in a total interval of time of 120 seconds (Pastor et al., 2004). Thus, the scale of this phenomenon is much more reduced if compared to the Brumadinho case. Some authors have identified different representative values for the Bingham model, as introduced in Table 11.

Table 11 – Representative values of Bingham model (adapted from Pastor et al., 2004)

Author	τ_y (Pa)	μ_0 (Pa.s)
Jan	100-160	40-60
Johnson	60,170-500	45
Sharp and Nobles		20-60
Pierson	130-240	210-810
Jin and Fread (Anhui Debris dam)	38	2.1
(Aberfan)	4,794	958
(Rudd Creek)	956	958

Observing Table 11, it is possible to conclude that there is a very wide range of values that can describe the runout movement, and they can vary according to the different scenarios behind the phenomena. For the RASH3D computation, as discussed before, the input data regarding the scenario studied is the topography of the terrain and the height of the detachment. In this way, the chosen rheology, and its parameters combined with the input data (scenario) must represent the expected runout, in that case of post-failure analysis.

The calibration of the parameters only depends on the initial information given about the phenomenon, i.e. the topography and the detachment height, and on the expected results, i.e. shape, velocity, and duration of the runout. Even with a great value of height detachment and volume released, if the yield stress is too high, the runout reached distance is too small, therefore if greater distances are expected for the flow, this parameter needs to be decreased.

On the other hand, the plastic viscosity gives the inclination of the curve relating the shear stress and the shear rate (Figure 29). For the tailings in Texas, the value of viscosity was about 50 Pa.s, whereas, for Brumadinho, the calibration resulted in a viscosity of 250 Pa.s, so the inclination of the curve is greater. If smaller values of viscosity were used the flow duration to reach the final distance was smaller than expected.

Nonetheless, for Aberfan failure, the plastic viscosity was almost 1000 Pa.s (Pastor et al., 2004), with a travel distance of 600 m, velocities observed between 4.5 to 9 m/s, and the slope of terrain was about 12° (Dutto et al., 2017). If such a high value were used, the flow would stop before the expected point. In that case, it is interesting to observe that the slope of terrain was much greater than the ones observed in Brumadinho, and for gentle slopes, a big value of viscosity would make the flow to reach smaller distances.

The results for Bingham rheology using method 1 are illustrated in Figure 57.

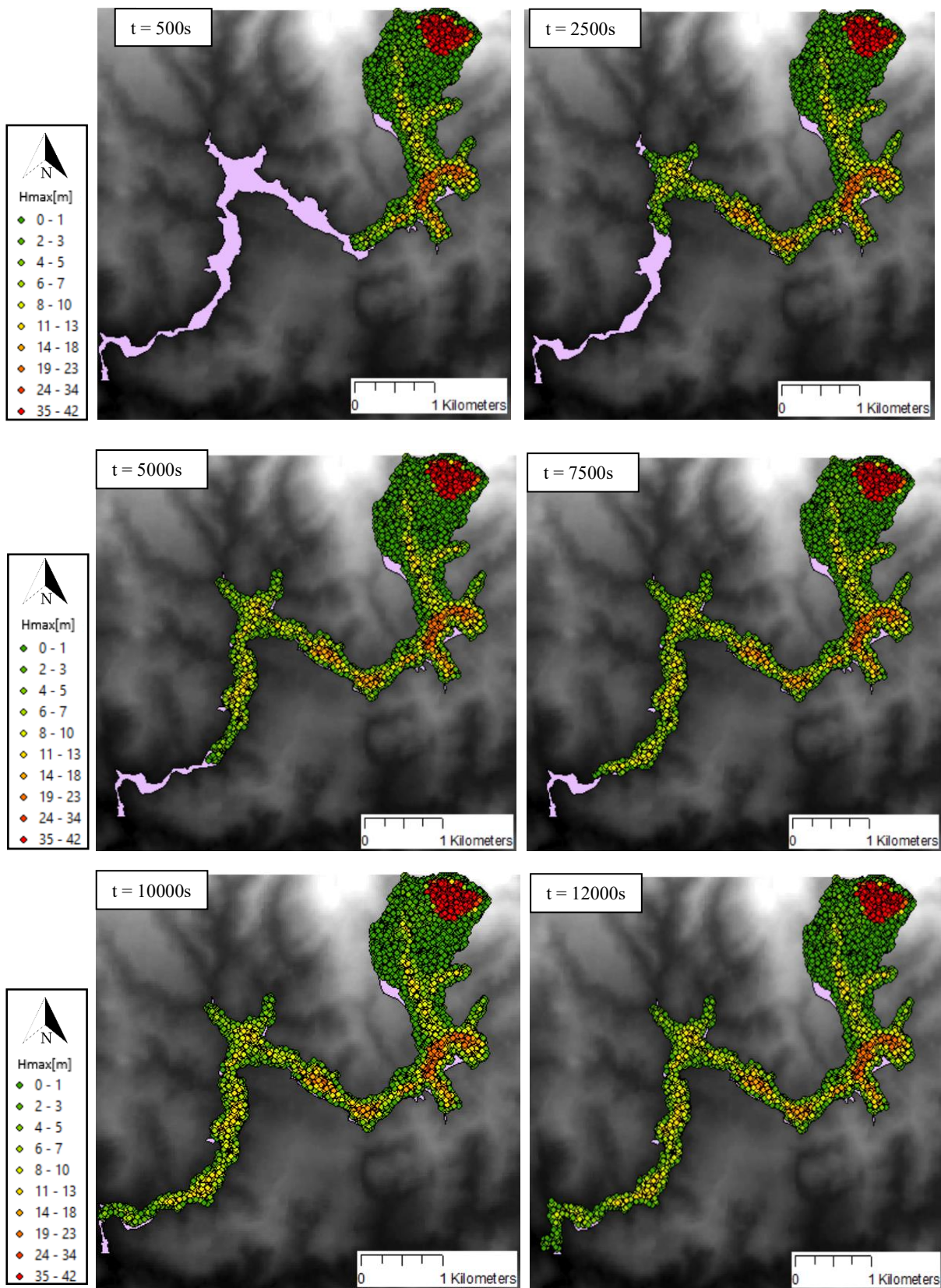


Figure 57 - Results of simulation with Bingham Rheology (method I), $\tau_y=50$ Pa and $\mu_0=250$ Pas.

In this simulation, the flow reaches the river Paraopeba at, approximately, $t:12000$ seconds, and as it was mentioned before, the initial area of the runout is larger in comparison to the other simulations, so there is a bigger spreading of the material, even in the opposite direction of the main flow, in the region surrounding the dam.

The remaining parts of the runout are similar to the other simulations in terms of shape, and there is no branch formed as in the Voellmy simulation. The maximum height of the flow along the path was about 25 m, in that region with the red colored points close to the first main curve.

In this case, the distance reached at each time step was smaller than in comparison with Voellmy. For example, the community of the city of Brumadinho was reached by the flow between $t:5000s$ and $t:7500s$, so there is no drastic reduction of the velocity, even if it decreases along the path.

Regarding the velocity map (Figure 58), it is observed a significative reduction of the maximum velocity, 6.1 m/s, in comparison to the value obtained for Voellmy in the first method, 14.5 m/s. In this way, in the Bingham rheology, the velocities are reduced a lot and most of the points reach a very small maximum velocity, below 1.5 m/s.

This high concentration of low velocities can be associated with the larger shape at the beginning since the spreading could cause the velocity profile reduction in that region close to the detachment. Nonetheless, despite this initial part, after the breaching, the flow channel is stretched and the velocities are increased, in a continuous region in the inner part of the path. After the last curve (pointed by the arrow), the velocities decrease again until the flow reaches the river.

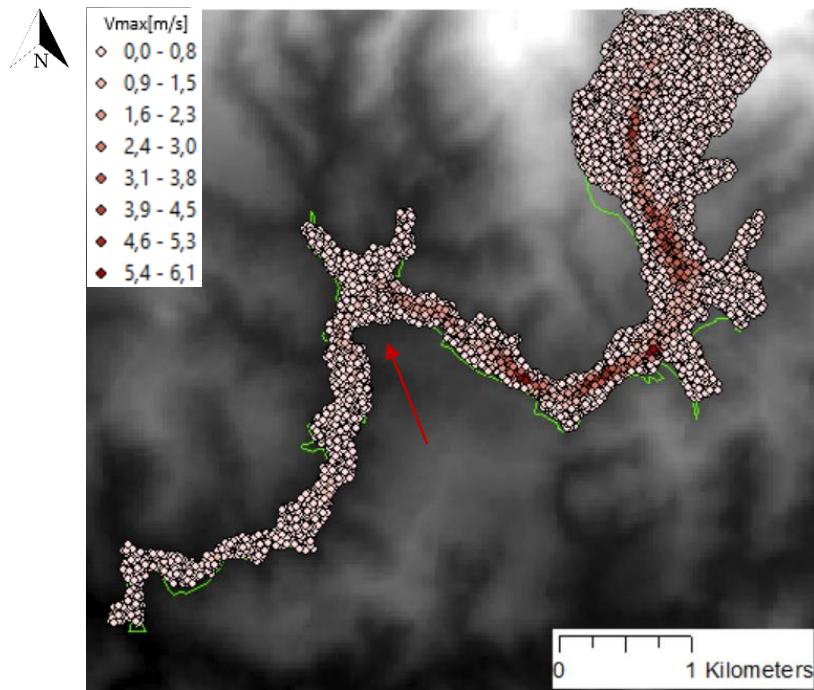


Figure 58 - Map of velocities with Bingham Rheology (method I), $\tau_y=50$ Pa and $\mu_0=250$ Pas, $t=12000s$.

IV. Bingham Rheology: Method II – Slip Surface Analysis

The calibration process was done once more, and it was observed that for the same values used for the parameters in the previous simulation, the distance reached by the flow was too short, as it happened in the Voellmy simulations. In this case, the values that would make the flow to reach its final position were very different, with a significant reduction of both yield stress and plastic viscosity. Therefore, it would be meaningless to use these values, and it was preferred to present the results in terms of the same parameters used for the first method, analyzing the runout until the final position it reaches. The results are shown in Figure 59.

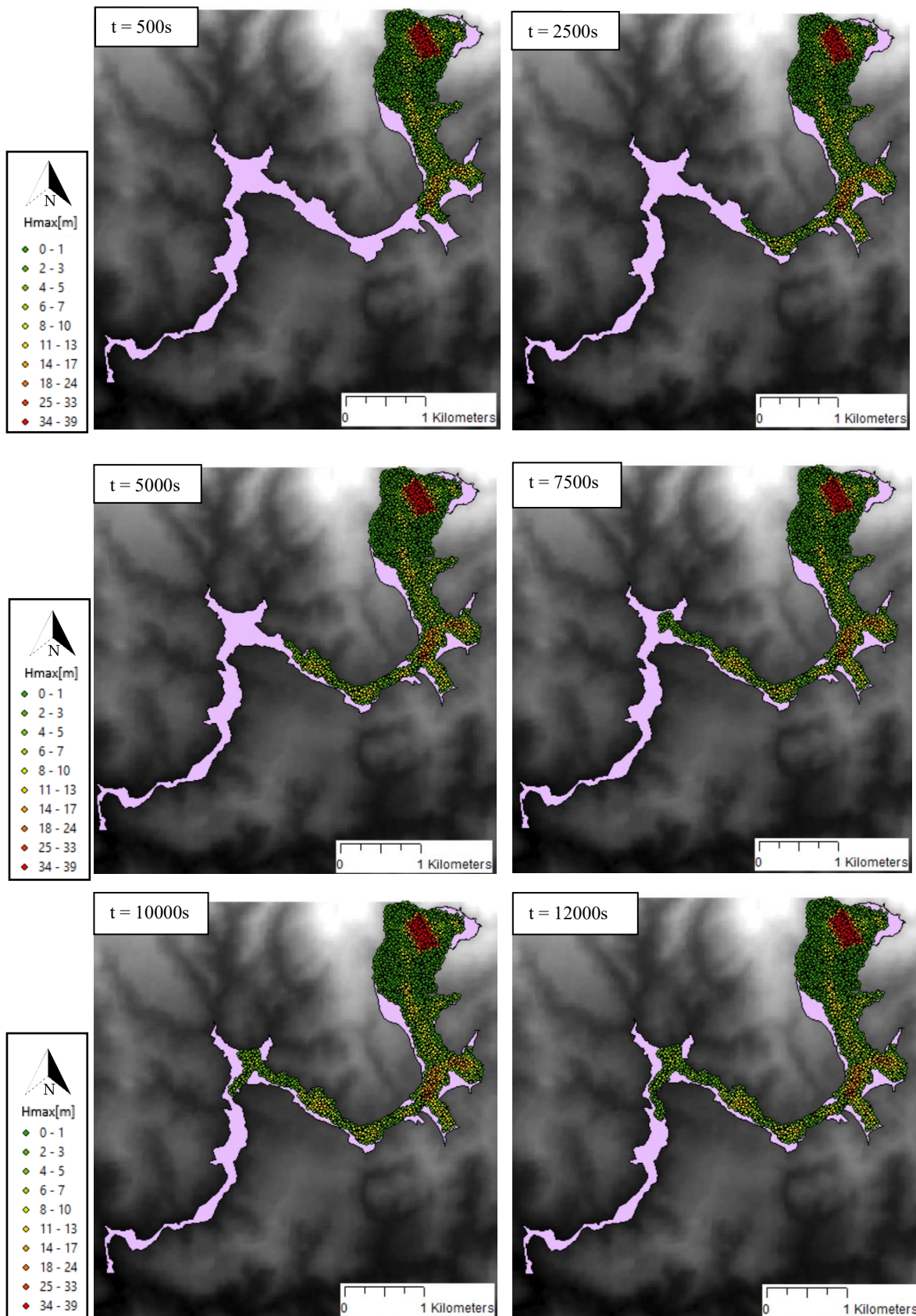


Figure 59 - Results of simulation with Bingham Rheology (method II), $\tau_y=50$ Pa and $\mu_0=250$ Pas.

In terms of shape, as in the simulation of method I, the beginning of the flow has a thick cross-section, with a bigger spreading of the material, and for the same interval of time, the distances

reached are smaller, as expected due to the reduction of volume and velocity, as is possible to see in Figure 60.

Looking at the velocity distribution, there is a particular region (pointed by the arrow), where the values are increased, after the detachment, when the flow path is stretched. After that, the velocities are more homogeneous with smaller values until the flow stops.

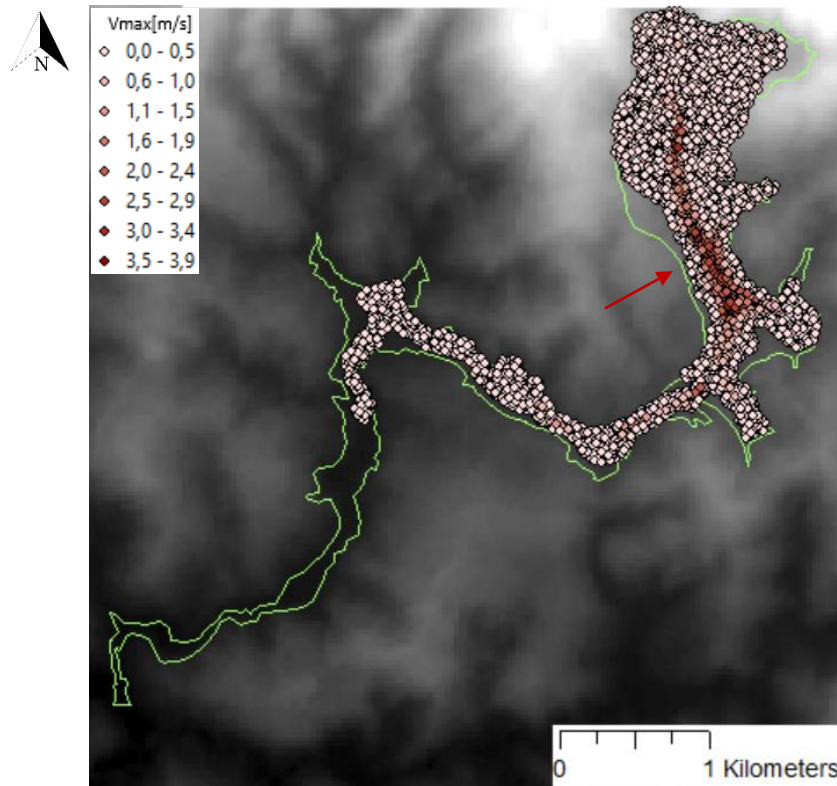


Figure 60 - Map of velocities with Bingham Rheology (method II), $\tau_y=50$ Pa and $\mu_0=250$ Pas, $t=12000s$.

V. Summary of the Results and Further Analyses

In Figure 61, it is possible to observe the result of all the simulations performed and discussed before, in terms of shape and maximum height, and in Figure 62, in terms of velocity. In terms of shape, there is a portion of the runout that is not covered by the points since it was established a threshold of 0.01 m for the maximum height values.

It is interesting to note that with the same values of parameters, even if the detachment area is modified regarding the area, position, and values of height, the results are quite similar both for Voellmy and Bingham. Additionally, these simulations are consistent with the shape of the real phenomenon, which makes these values of parameters reliable.

The differences between the rheologies are observed mainly in the shape close to the detachment area, which is more spread in the Bingham. It can be pointed out that the threshold chosen influenced the shape observed, since these areas not covered in Voellmy may be occupied by points with a height smaller than 1 cm. Nonetheless, for the rest of the movement, the shape of the flow is almost identical, which makes less relevant this initial difference in shape.

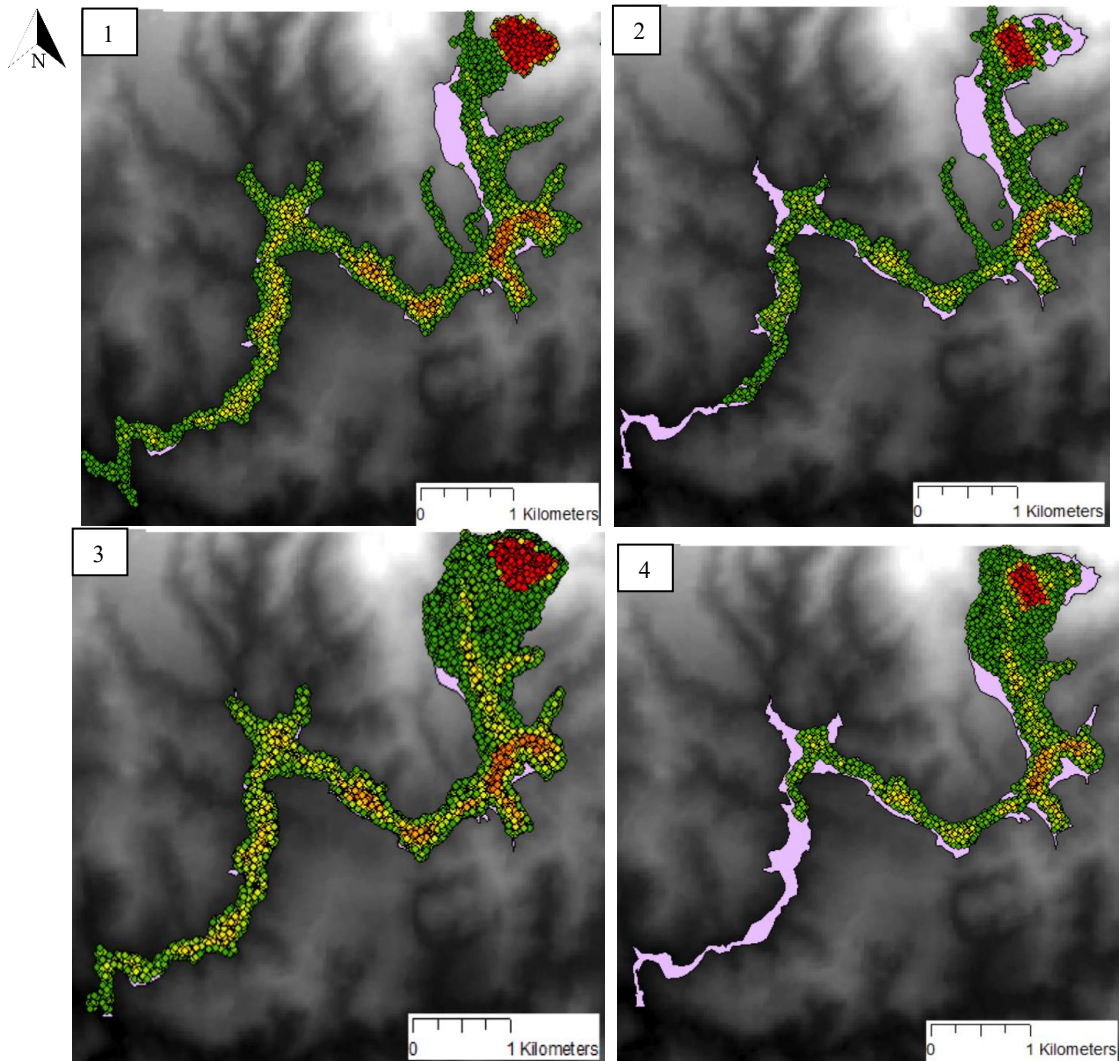


Figure 61 - Comparison between the different simulations in terms of shape and maximum height (m), 1- Voellmy (method I), 2 – Voellmy (method II), 3 – Bingham (method I), 4 – Bingham (method II).

Regarding velocity, for the same rheology, the results are very similar, differing only in the values, which are bigger in the first method. On the other hand, the results have more differences when comparing Voellmy and Bingham. For Voellmy, there are isolated zones of higher velocities, meanwhile, for Bingham, there is a continuous zone inside the path with higher velocities. Since there are no data available about the velocities profile, it not possible to affirm which between them better represents the occurrence.

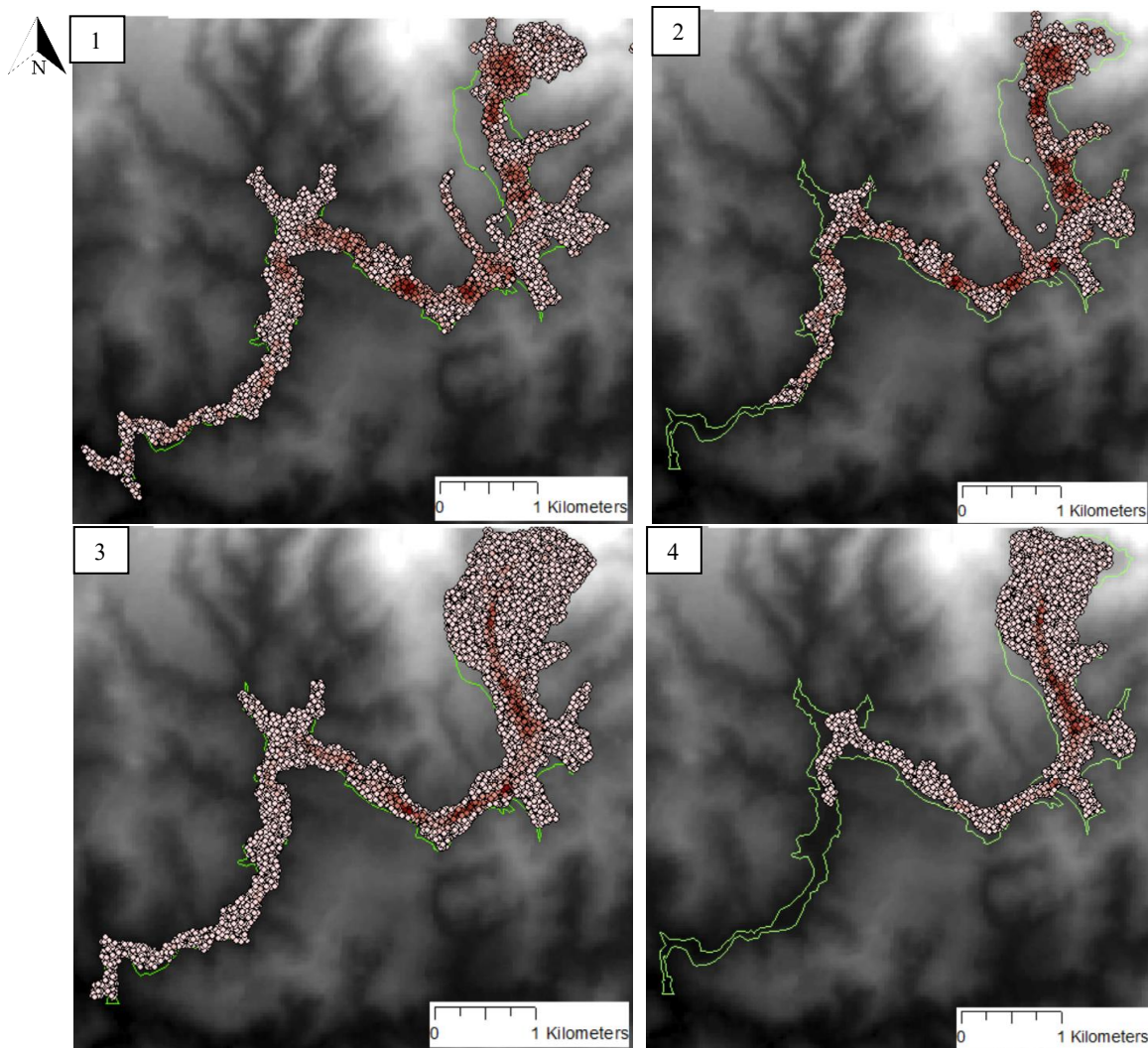


Figure 62 - Comparison between the different simulations in terms of velocity (m/s), 1- Voellmy (method I), 2 – Voellmy (method II), 3 – Bingham (method I), 4 – Bingham (method II).

Moreover, there are some differences in terms of shape found in the simulations (Figure 61), concerning the pre-determined path. For example, in the Bingham simulation, the points overcome the boundaries, flowing over the detachment area, and in Voellmy, some branches are formed outside the runout path.

Even if these distortions did not occur, they can be analyzed to verify how the code interpreted the movement of the material, and to check if it is reasonable. This can be done by studying the 3D distribution of the points representing the terrain and the flow, through the software Arcscene. Each of these discrepancies is discussed below.

- Case I: branches

The mentioned branches are highlighted in Figure 63.

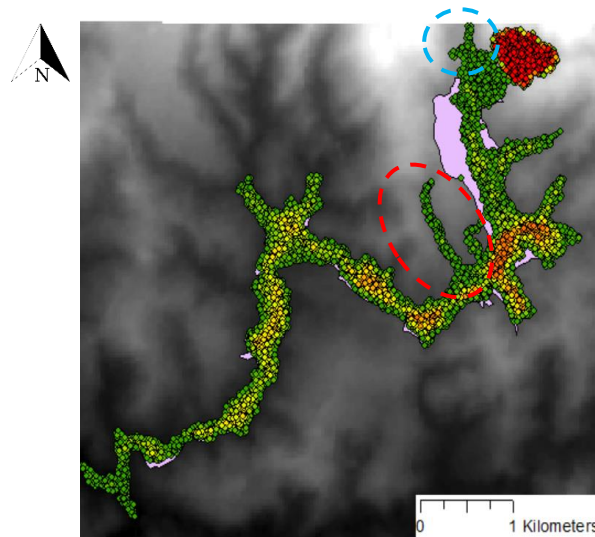


Figure 63 - Voellmy branches.

The first branch analyzed is the one highlighted by the blue circle in the figure above, and described in Figure 64, where the green points correspond to the terrain, the yellow ones to the detachment area, and the blue ones to the Voellmy flow, both for the first method. It can be noted that this branch is formed due to a valley formation in the terrain, indicated by the arrow. In this way, part of the material flows around a region with greater elevation and goes down directly to this gully, forming a branch.

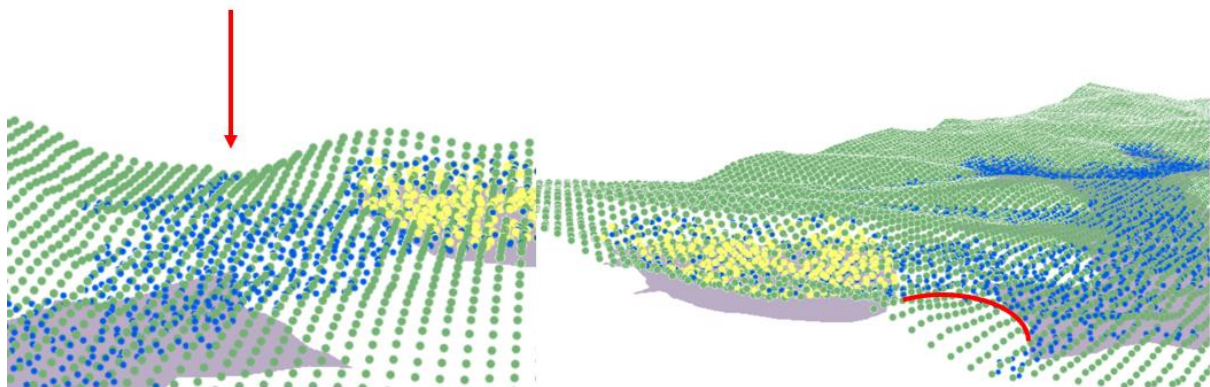


Figure 64 - Analysis of Voellmy branch I.

The second branch, highlighted by the red circle (Figure 63), is also related to a gully formation in the region, as shown in Figure 65, and indicated by the arrows. For the Voellmy simulation, this extra path is connected to points with a maximum height below the threshold in the analysis, then, they are not visible in the maps (Figure 66). However, in the gully, the width of the flow channel is reduced and, consequently, the height increases, making the points in the branch to overcome the threshold.

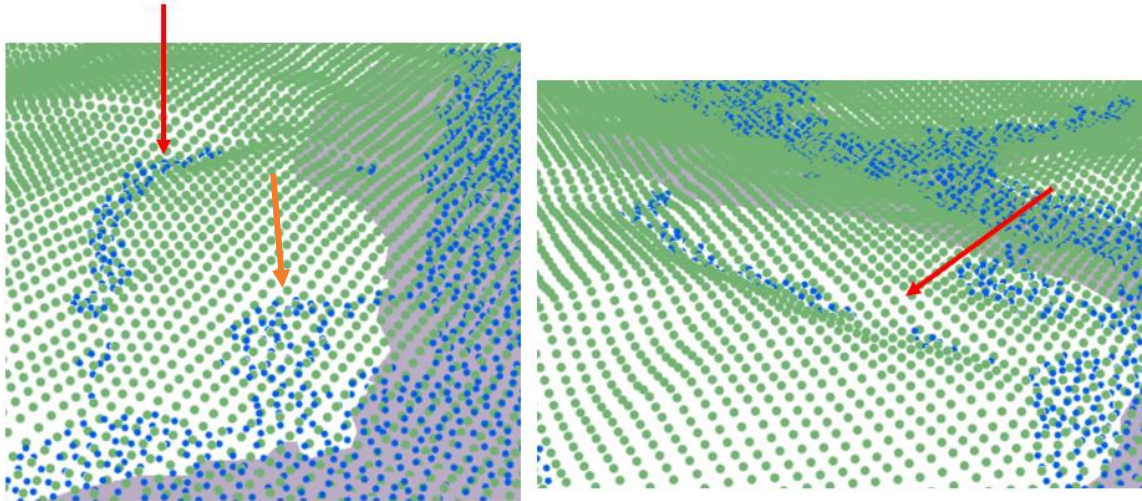


Figure 65 – Analysis of Voellmy branch II.

There is also an extra material indicated by the orange arrow in Figure 65, which is connected to the main mass by points not shown in the representation (Figure 66). Analyzing the 3D representation of the terrain, it is concluded that these points overcome the threshold due to a reduction of the terrain elevation in that region, which increases their maximum height (Figure 67).

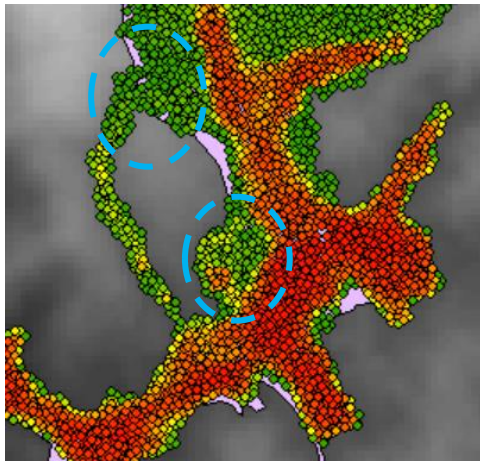


Figure 66 - Representation of the points below the threshold for Voellmy simulation.

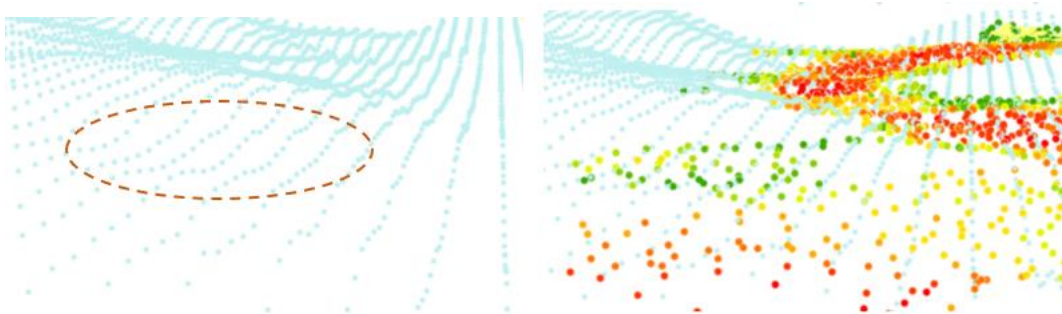


Figure 67 - Analysis of Voellmy extra points.

- Case II: Bingham overflow

The shape of the flow at the beginning of the runout is shown in Figure 68, where is possible to observe that the material spreads to the surrounding of the detachment area and the proximities.

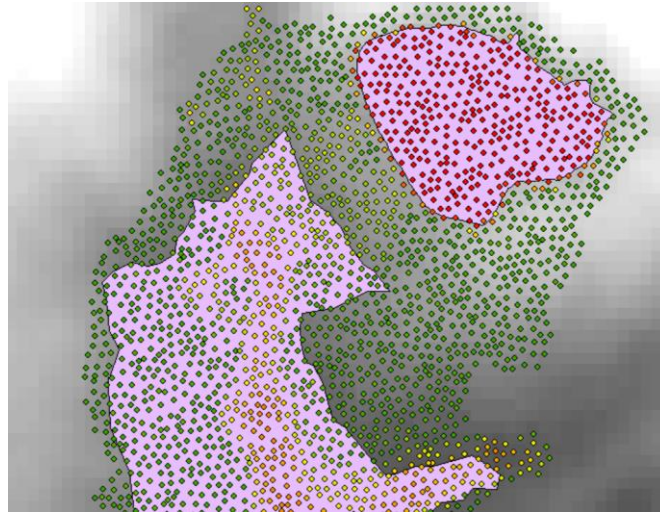


Figure 68 - Bingham overflow.

Looking at Figure 69, it can be noted that the flow (represented by red points) spreads from the detachment area to all the surrounding directions and has reached portions of the terrain with higher elevation with respect to the top of the dam. These elevated regions are pointed by the arrows in the image, and this indicates an upwards motion even if the velocity obtained is lower. In the other simulations, this type of movement does not occur, and the material just flows in the lower parts.

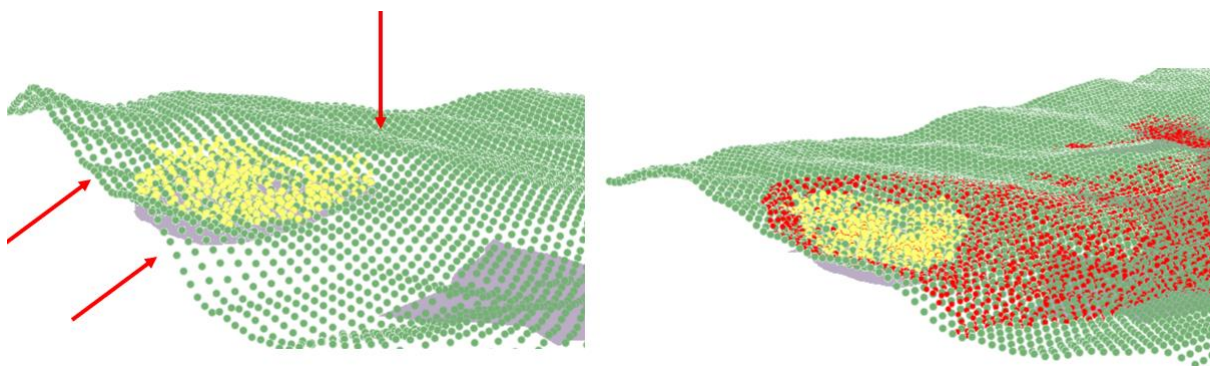


Figure 69 - Analysis of Bingham overflow.

The Voellmy (blue points) and Bingham (red points) flows are superposed for the sake of comparison (Figure 70) and it is possible to better visualize the areas where Bingham overflow occurs. This phenomenon does not represent the real situation, and the main consequence of

this spreading is the reduction of velocity at the beginning of the flow, as shown in Figure 71. As discussed before, this can be a consequence of the code itself, and how it distributes the moving points along the terrain analyzed, tending to enlarge the flow with low height points.

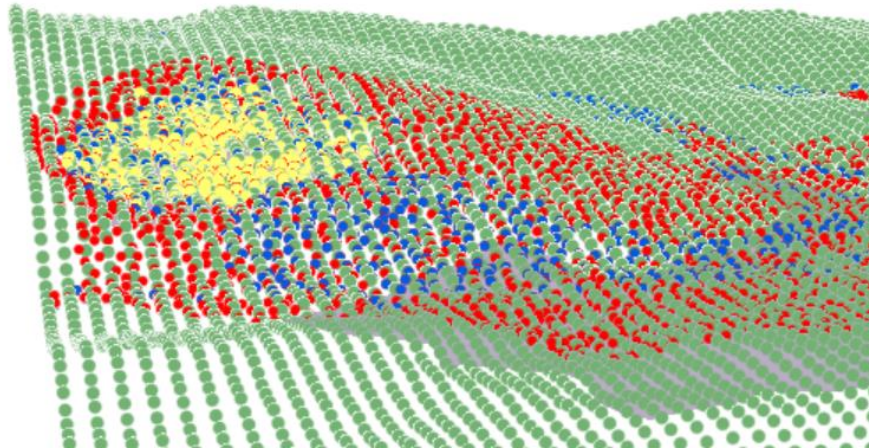


Figure 70 - Comparison between Voellmy and Bingham flows in 3D, for the first method.

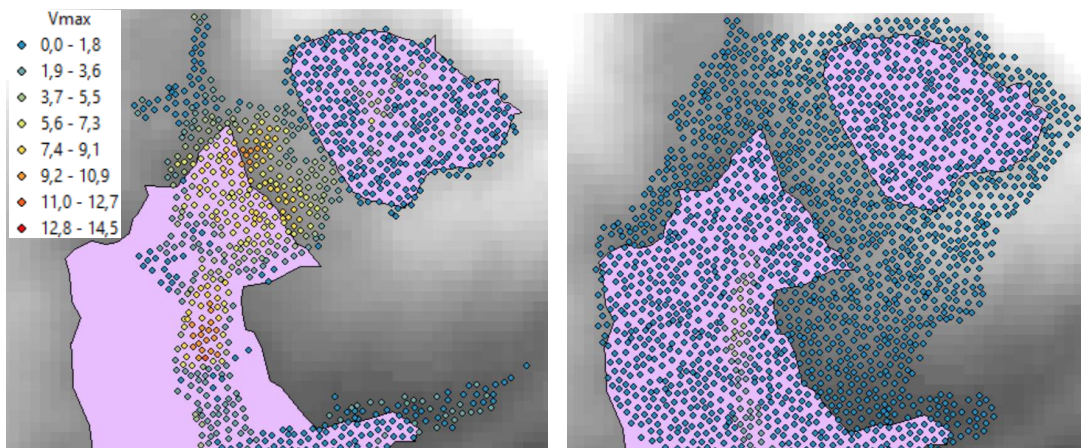


Figure 71 - Comparison between Voellmy and Bingham velocities, for the first method.

However, the remaining part of the runout follows a similar path in all the simulations, and observing the 3D representation is possible to conclude that the resultant shape is coherent to the terrain elevations. This verification is illustrated in the following figures, where the Voellmy runout for the first method is used (as said before, besides the beginning, the rest of the Bingham flow follows a very similar path, so there is no necessity to evaluate both of them).

Observing the figures below, it is noted that the material flows above a valley formation in the terrain, where it may have existed a water branch from the river Paraopeba. Moreover, it can be verified that the terrain has very low elevations where the runout passes.

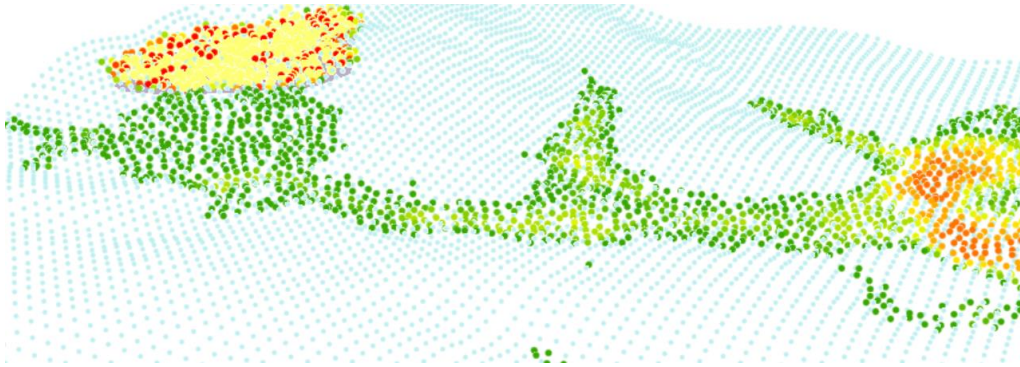


Figure 72 - 3D representation of the runout I.

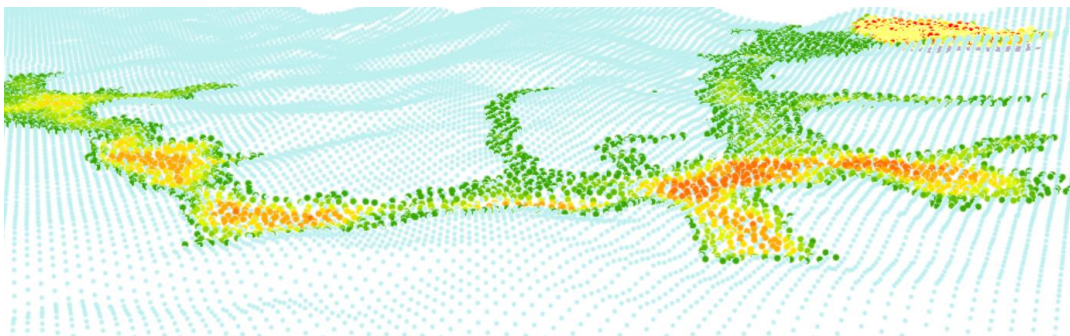


Figure 73 - 3D representation of the runout II.

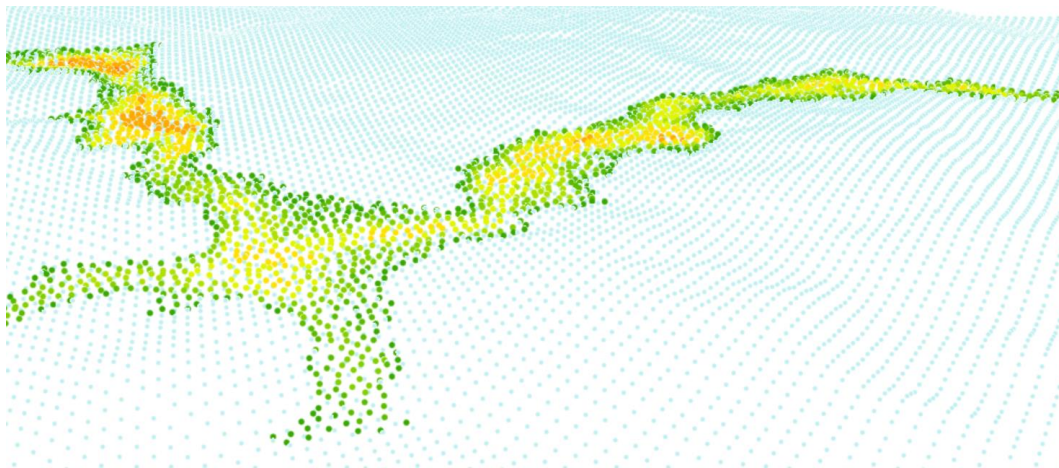


Figure 74 - 3D representation of the runout III.

Finally, it is possible to draw the final shape of the flows, resultant from the simulations, and to plot them over the aerial image, on Google Earth, of 3 days after the collapse. In this way, is possible to compare the shapes with the stain left by the real flow. Observing Figure 76, the Bingham flow, after the enlarged detachment zone, reproduces almost exactly the real phenomenon. On the other hand, Voellmy flow (Figure 75) better reproduces the beginning of the movement, close to the detachment, and for the rest of the path, despite the branches, the simulation is also quite good.

As said before, the runout is not necessarily described by only one rheology since its behavior can vary along its path. In this way, it is possible to state that at the beginning of the phenomenon, the flow behaved more like a landslide, and for that reason, Voellmy better matched this part. Nonetheless, after some time, the flow became more fluid-like, so Bingham rheology better described the occurrence.



Figure 75 - Final shape of Voellmy (method I) simulation plotted on Google Earth.



Figure 76 - Final shape of Bingham (method I) simulation plotted on Google Earth.

Regarding the second method used in this analysis, the simulations result in a path like the real phenomenon, but less similar than what is was observed in the first method. As discussed before, there is an underestimation of the volume released, which can be associated with the secondary instabilities that occur in tailings collapse, not detected on Slide analysis presented here. Nonetheless, the resultant impact caused by the outflow can not be neglected.



Figure 77 - Final shape of Voellmy (method II) simulation plotted on Google Earth.



Figure 78 - Final shape of Bingham (method II) simulation plotted on Google Earth.

Figure 79 shows the Voellmy detachment area for the first (pink) and the second (green) methods. Comparing the aerial image with the contour of the simulations, it is observed that the second method better reproduces the possible crest of the rupture, meanwhile, the first method embraces all the area of the dam.



Figure 79 - Comparison between the detachment area and the Voellmy simulations.

5. Conclusions

Even if the study presented here was a post-failure analysis of the collapse of the Brumadinho tailings dam, the main purpose was to evaluate the techniques that could be used to assess the probability of failure of the tailings dam and the damage it could cause. In this case, there was a lack of information about the rupture surfaces, the height of the flow, and the velocity profile, as it would happen in a monitoring analysis of any similar structure.

Because of this, two different approaches were used to estimate the detachment of the material in the rupture, which originated the outflow analyzed by the RASH 3D code. In the first method, more conservative, the whole area of the dam was considered to detach, and it was used the known volume released. For predictive analysis, this quantity is unknown, so the entire volume of the dam should be used, in favor of security and due to the progressive instabilities that occur in tailings rupture due to liquefaction.

On the other hand, the second method uses numerical analysis to estimate the slip surface with the lowest safety factor, which is most probably related to the real surface detaching when the rupture happens. Even if using a software for numerical analysis is more robust than just assume the total area and volume of the dam, the results can underestimate the damage caused by the failure of the tailings. This because the results only account for the first detachment, but not the progressive failures that can occur.

Therefore, in monitoring studies, it could be relevant to perform a numerical analysis to verify the potential of a rupture of the dam due to the results in terms of safety factor, together with control of the efficiency of the drainage system, of the correct material deposition and of the water level inside the dam. Then, to complement this verification and to assess the potential damage related to a possible failure of the structure, it is recommended to perform an analysis of the outflow that would be formed after the collapse, using the total volume reserved and the total area of the dam to obtain the material released that originates the runout.

The tailings can be treated using rheological descriptions, characterized by some different laws, such as the ones discussed here: Voellmy and Bingham. For the case of Brumadinho, both after calibration provided satisfactory results, however, since, in predictive analysis, the damage extent is not known, Voellmy could underestimate the potential damage.

As seen before, if a basal friction angle with a value greater than one was applied, the runout would not reach the expected final position. In this way, if, based on literature and comparison

with other occurrences, higher values of the Coulomb friction angle are used, the results may not match the real damage potential of the material flow. This can probably happen in tailings dam rupture due to liquefaction, where the outflow is almost liquid and friction is barely mobilized, as occurred in the Brumadinho case.

Thus, the Bingham method is more suitable since it is a more robust law to model the runout behavior, which presented very good results in terms of reproducing the damage extent. It is important to test different values of parameters to analyze the damage potential, comparing with known values of similar phenomena occurred and understanding their effect on the flow behavior. In this case, it is appropriate to verify the worst, but reasonable, scenario that could happen due to the failure of the tailings dam.

These analyses should be done together with other monitoring activities to estimate the damage extent, and then, to verify who and what is at risk if a possible failure of a tailings dam occurs. In this way, these tools can provide information for effective emergency plans that must be performed to protect who and what is downstream the dam: mine workers, inhabitants of the region, native vegetation, animals, water sources and rivers, constructions, i.e. everything that was affected by the Brumadinho tragedy as seen before.

6. Bibliography

- Agam, M. W., Hashim, M. H. M., Murad, M. I., & Zabidi, H. (2016). Slope Sensitivity Analysis Using Spencer's Method in Comparison with General Limit Equilibrium Method. *Procedia Chemistry*, 19, 651–658. <https://doi.org/10.1016/j.proche.2016.03.066>
- ANA - Agência Nacional das Águas. (2016). *Manual do Empreendedor sobre Segurança de Barragens Volume VIII-Guia Prático de Pequenas Barragens Manual do Empreendedor sobre Segurança de Barragens VIII Volume*.
- Andrade, S. B. de, Vale, V. L. do, Saliba, A. P. M., & Nascimento, N. de O. (2019). Avaliação da concentração de sólidos totais na bacia do Rio Paraopeba após ruptura da Barragem I - Brumadinho. *Revista Augustus*, 24(49), 100–112.
- Araujo, W., & Ledezma, C. (2020). Factors that affect liquefaction-Induced lateral spreading in large subduction earthquakes. In *Applied Sciences (Switzerland)* (Vol. 10, Issue 18). <https://doi.org/10.3390/APP10186359>
- Bonato, I. (2019). *SOLUÇÕES CONSTRUTIVAS PARA ESTABILIZAÇÃO DE BARRAGENS DE REJEITOS ALTEADAS A MONTANTE: UM ESTUDO DE CASO DE BRUMADINHO*. Universidade Federal do Paraná.
- BRUMADINHO ENGINEERING HISTORY – World Mine Tailings Failures - from 1915*. (n.d.). Retrieved April 11, 2020, from <https://worldminetailingsfailures.org/corrego-do-feijao-tailings-failure-1-25-2019/>
- Comissão Parlamentar de Inquérito: Rompimento da Barragem de Brumadinho*. (2019). <https://politica.estadao.com.br/blogs/fausto-macedo/wp-content/uploads/sites/41/2019/11/RELATÓRIO-CPI-BRUMADINHO.pdf>
- Dreno Horizontal Profundo - Drilling*. (n.d.). Retrieved April 11, 2020, from <https://drilling.com.br/servicos/dreno-horizontal-profundo/>
- Dutto, P., Stickle, M. M., Pastor, M., Manzanal, D., Yague, A., Tayyebi, S. M., Lin, C., & Elizalde, M. D. (2017). Modelling of fluidised geomaterials: The case of the aberfan and the Gypsum tailings impoundment flowslides. In *Materials* (Vol. 10, Issue 5). <https://doi.org/10.3390/ma10050562>
- Fei, M., Sun, Q., Zhong, D., & Zhou, G. G. D. (2012). Simulations of granular flow along an

- inclined plane using the Savage-Hutter model. *Particuology*, 10(2), 236–241.
<https://doi.org/10.1016/j.partic.2011.11.007>
- Fleurisson, J., & Cojean, R. (2016). *Error Reduction in Slope Stability Assessment*. February.
https://www.researchgate.net/publication/281919014_Error_Reduction_in_Slope_Stability_Assessment
- Fraccarollo, L., & Papa, M. (2000). Numerical simulation of real debris-flow events. *Physics and Chemistry of the Earth, Part B: Hydrology, Oceans and Atmosphere*, 25(9), 757–763. [https://doi.org/10.1016/S1464-1909\(00\)00098-8](https://doi.org/10.1016/S1464-1909(00)00098-8)
- G1. (2019). *Estudo contratado pela Vale confirma que barragem em Brumadinho se rompeu por liquefação*. <https://g1.globo.com/mg/minas-gerais/noticia/2019/12/12/estudo-contratado-pela-vale-diz-que-barragem-em-brumadinho-se-rompeu-por-liquefacao.ghtml>
- HuffPost Brasil. (2019). *Barragem da Vale em Brumadinho se rompeu por liquefação, dizem especialistas*. https://www.huffpostbrasil.com/entry/liquefacao-brumadinho_br_5df26d19e4b00c6926df0e4b?guccounter=1&guce_referrer=aHR0cHM6Ly93d3cuZ29vZ2xlLmNvbS8&guce_referrer_sig=AQAAADq6VOC5SG1tORxsP7a-MRt8n5fxIA29o6exWOpFPfiWGYAg0uSuJKKkxkzTFWFyE3zanDzqVrIbm81E1A40yaK
- Hungr, O. (1995). A model for the runout analysis of rapid flow slides, debris flows, and avalanches. *Canadian Geotechnical Journal*, 32(4), 610–623.
<https://doi.org/10.1139/t95-063>
- Hungr, O., Evans, S. G., Bovis, M. J., & Hutchinson, J. N. (2001). A Review of the Classification of Landslides of the Flow Type. *Environmental & Engineering Geoscience*, VII, 221–238.
- Illipronti Laurino, B., De Jesus Oliveira Preto, C. T., & Do Prado Ferreira Junior, C. (2020). *Análise acidente em brumadinho - Minas Gerais - utilização de rejeitos de barragens na construção civil*. 3, 231–238. <http://www.bjns.com.br/index.php/BJNS/article/view/86>
- Jeyapalan, J. K., Duncan, J. M., & Seed, H. B. (1983). Investigation of flow failures of tailings dams. *Journal of Geotechnical Engineering*, 109(2), 172–189.
[https://doi.org/10.1061/\(ASCE\)0733-9410\(1983\)109:2\(172\)](https://doi.org/10.1061/(ASCE)0733-9410(1983)109:2(172))

- Jornal Estado de Minas Gerais, & Parreiras, M. (2019). *Atividades de mina da Vale em Brumadinho deviam ter parado em 2016, diz inquérito*.
https://www.em.com.br/app/noticia/gerais/2019/09/25/interna_gerais,1087875/atividade-s-de-mina-da-vale-em-brumadinho-deviam-ter-parado-em-2016.shtml
- Kossoff, D., Dubbin, W. E., Alfredsson, M., Edwards, S. J., Macklin, M. G., & Hudson-edwards, K. A. (2014). Mine tailings dams : Characteristics , failure , environmental impacts , and remediation. *Applied Geochemistry*, 51, 229–245.
<https://doi.org/10.1016/j.apgeochem.2014.09.010>
- Kritikos, T., & Davies, T. (2015). Assessment of rainfall-generated shallow landslide/debris-flow susceptibility and runout using a GIS-based approach: application to western Southern Alps of New Zealand. *Landslides*, 12(6), 1051–1075.
<https://doi.org/10.1007/s10346-014-0533-6>
- Lan, Y., Ashrafiyanfar, N., & Paffenholz, J. (2019). *Landsat-8 data for Soil Moisture Mapping to Investigate the Tailing Dam Failure in Brumadinho , Brazil*. Usgs, 2019.
https://dokumente.ub.tu-clausthal.de/servlets/MCRFileNodeServlet/clausthal_derivate_00000995/lan_et_al_Landsat-8dataSoilMoistureMappingInvestigateTailingDamFailure.pdf
- Leonardi, A. (2015). *Numerical simulation of debris flow and interaction between flow and obstacle via DEM*. ETH Zurich.
- Lima Bevilaqua, J. F. (2019). *ANÁLISE MULTICRITÉRIO PARA DETERMINAÇÃO DAS POSSÍVEIS CAUSAS DO ROMPIMENTO DA BARRAGEM DE BRUMADINHO*. 2001, 5–10.
- Lumbroso, D., Davison, M., Body, R., & Petkovšek, G. (2020). Modelling the Brumadinho tailings dam failure, the subsequent loss of life and how it could have been reduced. *Natural Hazards and Earth System Sciences*, 2010(June), 1–24.
- M. Donnelly, D., & L. Barger, R. (1977). Weight Scaling for Southwestern Ponderosa Pine. *USDA Forest Service Research Paper RM*.
- Mangeney, A., Heinrich, P., & Roche, R. (2000). Analytical solution for testing debris avalanche numerical models. *Pure and Applied Geophysics*, 157(6–8), 1081–1096.
<https://doi.org/10.1007/s000240050018>

- Martin, T. E. (2002). *Some considerations in the stability analysis of upstream tailings dams*. 1–17.
- McDougall, S., Pirulli, M., Hungr, O., & Scavia, C. (2008). Advances in landslide continuum dynamic modelling. In *Landslides and Engineered Slopes* (pp. 145–157).
- Notícias UOL. (2020). *Brumadinho: Um ano após tragédia, rio Paraopeba ainda não se recuperou da lama*. <https://noticias.uol.com.br/ultimas-noticias/agencia-estado/2020/01/24/um-ano-depois-rio-paraopeba-ainda-nao-se-recuperou-da-lama.htm>
- Pastor, M., Quecedo, M., González, E., Herreros, M. I., Merodo, J. A. F., Fernández, J. A., & Mira, P. (2004). Simple approximation to bottom friction for Bingham fluid depth integrated models. *Journal of Hydraulic Engineering*, *130*(2), 149–155. [https://doi.org/10.1061/\(ASCE\)0733-9429\(2004\)130:2\(149\)](https://doi.org/10.1061/(ASCE)0733-9429(2004)130:2(149))
- Pereira, D. M., Cabral, S. M. de F., Guimarães, H. O. R., & Mângia, A. A. M. (2019). *Brumadinho: muito mais do que um desastre tecnológico*. *March*, 12. <https://doi.org/10.13140/RG.2.2.23813.60643>
- Pereira, L. F., Barros Cruz, G. De, & Morato Fiúza Guimarães, R. (2019). Impacts from the tailings dam rupture of Brumadinho, Brazil: an analysis based on land cover changes. *Journal of Environmental Analysis and Progress*, *04*(02), 122–129.
- Pirulli, M. (2005). Numerical Modelling of Landslides RunOut. *PhD Thesis*.
- Pirulli, M. (2010). On the use of the calibration-based approach for debris-flow forward-analyses. *Natural Hazards and Earth System Science*, *10*(5), 1009–1019. <https://doi.org/10.5194/nhess-10-1009-2010>
- Pirulli, M., Barbero, M., Marchelli, M., & Scavia, C. (2017). The failure of the Stava Valley tailings dams (Northern Italy): numerical analysis of the flow dynamics and rheological properties. *Geoenvironmental Disasters*, *4*(1). <https://doi.org/10.1186/s40677-016-0066-5>
- Quan Luna, B., Cepeda, J., Stumpf, A., van Westen, C. J., Remaître, A., Malet, J. P., & van Asch, T. W. J. (2013). Analysis and Uncertainty Quantification of Dynamic Run-out Model Parameters for Landslides. In *Landslide Science and Practice: Volume 3: Spatial Analysis and Modelling*.
- Remaître, A., Malet, J. P., Maquaire, O., Ancy, C., & Locat, J. (2005). Flow behaviour and

- runout modelling of a complex debris flow in a clay-shale basin. *Earth Surface Processes and Landforms*, 30(4), 479–488. <https://doi.org/10.1002/esp.1162>
- Rico, M., Benito, G., Salgueiro, A. R., & Pereira, H. G. (2008). Reported tailings dam failures A review of the European incidents in the worldwide context. *Journal of Hazardous Materials*, 152(March 2006), 846–852. <https://doi.org/10.1016/j.jhazmat.2007.07.050>
- RocScience. (2016). *Critical Slip Surface Search Methods in Slide 7.0*. https://www.rocscience.com/help/slide2/pdf_files/developer_tips/Slide_Search_Methods.pdf
- Rodríguez Pacheco, R. L. (2019). *Static liquefaction in tailings dam and flow failure*. February. https://www.researchgate.net/publication/331277260_STATIC_LIQUEFACTION_IN_TAILINGS_DAM_AND_FLOW_FAILURE
- Romão, A., Froes, C., Barcellos, C., Silva, D. X., Saldanha, R., Gracie, R., & Pascoal, V. (2019). Avaliação preliminar dos impactos sobre a saúde do desastre da mineração da Vale (Brumadinho, MG). *Desastre Da Vale Em Brumadinho – Impactos Sobre a Saúde e Desafios Para a Gestão de Riscos*, 16. <https://www.arca.fiocruz.br/handle/icict/32268>
- Sauthier, C., Pirulli, M., Pisani, G., Scavia, C., & Labiouse, V. (2015). Numerical modelling of gravel unconstrained flow experiments with the DAN3D and RASH3D codes. *Computers and Geosciences*, 85, 81–90. <https://doi.org/10.1016/j.cageo.2015.09.008>
- Schnaid, F., Poulos, H. G., Hudson, J. A., Marinos, P., Mitchell, J. K., Persson, L., Olalla, C., Baynes, F., Bérest, P., & Rowe, R. K. (2013). *Soils and Rocks, An International Journal of Geotechnical and Geoenvironmental Engineering*. 36(April). <http://www.soilsandrocks.com.br/soils-androcks/Soils36-1Baixa.pdf>
- Silva, W. P. da. (2010). *Estudo do potencial de liquefação estática de uma barragem de rejeito alteada para montante aplicando a metodologia de Olson (2001)* [Escola de Minas - UFOP]. <https://docplayer.com.br/61493841-Dissertacao-de-mestrado.html>
- Soares, A. F. S., Diniz, P. S., & Silva, L. F. de M. (2019). Valoração Dos Danos Aos Recursos Hídricos Decorrentes Dos Resíduos Da Barragem De Mineração Em Brumadinho-Mg. *Congresso Sul-Americano de Resíduos Sólidos e Sustentabilidade*, 2,

1–10. <https://www.ibeas.org.br/conresol/conresol2019/VII-063.pdf>

Takahashi, T. (2014). *Debris Flow: Mechanics, Prediction and Countermeasures* (2nd Editio).

Thomé, R., & Passini, M. L. (2018). *MINING TAILINGS DAMS : CHARACTERISTICS OF THE UPSTREAM HEIGHTENING METHOD THAT SUBSTANTIATED THE SUSPENSION OF IT ' S USE IN MINAS GERAIS*. 49–65.

<http://saber.unioeste.br/index.php/csaemrevista/article/view/19480/12650>

Vale, & TUV SUD. (2018). *Relatório De Auditoria Técnica de Segurança de Barragem - Complexo Paraopeba - Mina Córrego do Feijão - Barragem I*.

<https://worldminetailingsfailures.org/wp-content/uploads/2019/02/TUV-SUD-2018-Relatório-estabilidade.pdf>

Zhu, D. (2008). Investigations on the accuracy of the simplified Bishop method. *Landslides and Engineered Slopes. From the Past to the Future*, 1055–1057.

<https://doi.org/10.1201/9780203885284-c138>